FIREURISK - DEVELOPING A HOLISTIC, RISK-WISE STRATEGY FOR EUROPEAN WILDFIRE MANAGEMENT

Grant Agreement Number: 101003890 **Call identifier:** H2020-LC-CLA-2018-2019-2020	
Topic:	LC-CLA-15-2020 Forest Fires risk reduction: towards an integrated fire management approach in the E.U.
Instrument:	RIA

D4.6 – Report on Cascading effects

Deliverable Identifier:	D4.6
Deliverable Due Date:	31/03/2024
Deliverable Submission Date:	11/11/2024
Deliverable Version:	v.1.0
Lead partner:	GMV, TUD, FESB, SU, UAVR, REEFMC, SIA, AUTH
Authors:	Marta Gómez-Giménez, Antonio Franco-Nieto, Ángel Fernández-Carrillo, María Julia Yagüe-Ballester, Sylwester Zaprzala (GMV), Christopher Marrs, Kristina Beetz, Johanna Kranz, Matthias Forkel (TUD) Marin Bugarić, Darko Stipaničev (FESB), Carmen Sánchez-García, J. Neris, Stefan Doerr (SU), Ana I. Miranda, Diogo Lopes, Isilda Menezes (UAVR), Sergiy Zibtsev, V. Kashparov, Viktor Myroniuk, Dmytro Holiaka, Vadim Bogomolov (REEFMC), Giovanni Laneve (SIA), George Eftychidis, and Ioannis Gitas (AUTh).
Work Package:	WP4 Multi-level integration
Task:	Task 4.2.3 Cascading effects and interactions with other risks
Dissemination Level:	☒ PU: Public ☐ CO: Confidential, only for members of the Consortium (including the Commission Services)

This project has received funding from the European Union's Horizon 2020 research and innovation programme under grant agreement No 101003890.

Revision History

Version	Date	Edited by	Description
v.0.1	31/10/2023	Marta Gómez-Giménez (GMV)	Document Content outline / structure
v.0.2	21/02/2024	All authors	Final draft version v2.0
v.0.3	14/03/2024	Marta Gómez-Giménez (GMV)	Complete draft version formatted according to template
v.0.4	24/05/2024	Ana Miranda (UAVR)	Human health effects of smoke included in the deliverable
v.0.5	15/07/2024	Marta Gómez-Giménez (GMV)	Complete draft reviewed by A4.23 leader
v.0.6	17/09/2024	Marta Gómez-Giménez (GMV), Giovanni Laneve (SIA), George Eftychidis (AUTH), Carmen Sánchez-García (SU), Ana Miranda (UAVR)	Internal review of v0.5. Several sections were updated and improved
v.0.7	25/09/2024	Marta Gómez-Giménez (GMV)	Final consolidated version 0.7
v.0.8	08/10/2024	Stefan Doerr (SU),	Internal Review and additional Annex
v.0.9	08/11/2024	Marta Gómez-Giménez (GMV)	Final version updated: Executive summary and Annex were updated
v.1.0	11/11/2024	Marta Gómez-Giménez (GMV)	Final version submitted

Quality Control

Type	Date	Reviewed by	Approved/Comment
Internal and Peer Review	23/07/2024	Christopher Marrs	Minor changes suggested
Internal and Peer Review	22/08/2024	Emilio Chuvieco	Minor Changes suggested
Internal Review	8/10/2024	Vasileios Kazoukas	Security Officer: approved
Internal Review	11/11/2024	Stefan Doerr	QRB manager: approved

Copyright © FirEURisk Consortium. All rights reserved.

Executive Summary

This report includes several assessments related to potential compound hazards or cascading effects derived from wildfires and other non-fire hazards such as landslides and floods. Our case studies consider the definition of cascading effects coined by the Sendai Framework for Disaster Risk Reduction 2015-2030 i.e., disasters, which are magnified by multiple, sequential, and interconnected hazards. In some cases, it can be clearly noted that specific environmental factors amplify the negative impacts of natural hazards in a certain region. For example, in Central Europe (Pilot Site 2), we have analysed the factors that predispose forests to a bark beetle attack before the occurrence of a large wildfire; the effects of bark beetle disturbance and fuel types on fire radiative power and burn severity in the Bohemian-Saxon Switzerland National Park; the simulated behaviour and propagation potential of wildfires in areas previously affected by bark beetle infestations; and the post-fire soil erosion and water contamination risk after a wildfire in the Bohemian-Saxon Switzerland National Park. In Central Portugal (Pilot Site 3), we assessed the short-term impacts on human health resulting from the smoke from Portuguese extreme wildfire events. In the Chornobyl Exclusion Zone, we estimated the effects of air pollution through the emissions of nuclear smoke in the Chornobyl Exclusion Zone during wildfires. In Italy, we mapped the susceptibility to landslides after a fire event, specific examples are shown in Stromboli Island and Lazio region (Italy). Finally, we showcased the effects of postfire floods in the Region of Thessaly in Central Greece. Specific conclusions and recommendations are provided at the end of each section.

Dissemination

The results of this deliverable have been published in three scientific papers (sections: 2.1, 2.2, 4.1) and another paper is preparation (section 7).

Objectives not achieved

The lack of concurrent triggering events as well as in-situ information to establish a cause / effect relationship have hindered the implementation of a comprehensive and integrated analysis of the final damage produced by a cascading effect. Nevertheless, in this report, we showcase how events occurring at the same location and happening within a short time frame play a role in pre-disaster, disaster, and post-disaster phases as well as in the environmental impacts derived from them.

Key take away messages



WILDFIRES: The combination of open geospatial datasets with machine learning techniques is relevant in predicting factors that predispose forest to a bark beetle outbreak, which increases dead wood. Predictive modelling enhances the understanding of wildfire propagation potential and behaviour. Moreover, post-fire soil erosion simulations at high resolution can help us prioritise areas for on-ground monitoring and the implementation of operational mitigation measures, anticipate the risk of water contamination, and identify areas with high susceptibility of ash and sediment transport. Section 2.



AIR POLLUTION: Smoke from wildfires can affect the health of exposed citizens. This is particularly worrying in areas affected by radioactive contamination. Recommendations to prevent diseases include public health alert systems, public awareness and education campaigns, international collaboration radiation safety, and rapid wildfire detection and suppression. Sections 3.1 and 4.1.



FLOODS AND LANDSLIDES: Wildfires contribute to reducing vegetation cover, increasing erosion, and altering soil moisture retention capacities. As a result, the risk of flash floods and landslides increases during subsequent severe storms. Section 4.2 and 4.3.

Copyright © FirEUrisk Consortium. All rights reserved.

Disclaimer

The content of the publication herein is the sole responsibility of the publishers, and it does not necessarily represent the views expressed by the European Commission or its services.

While the information contained in the documents is believed to be accurate, the authors(s) or any other participant in the FirEURisk consortium make no warranty of any kind with regard to this material including, but not limited to the implied warranties of merchantability and fitness for a particular purpose.

Neither the FirEURisk Consortium nor any of its members, their officers, employees or agents shall be responsible or liable in negligence or otherwise howsoever in respect of any inaccuracy or omission herein.

Without derogating from the generality of the foregoing neither the FirEURisk Consortium nor any of its members, their officers, employees or agents shall be liable for any direct or indirect or consequential loss or damage caused by or arising from any information advice or inaccuracy or omission herein.

Copyright message

© FirEURisk Consortium, 2021-2025. This deliverable contains original unpublished work except where clearly indicated otherwise. Acknowledgement of previously published material and of the work of others has been made through appropriate citation, quotation or both. Reproduction is authorised provided the source is acknowledged.

Table of Contents

Executive Summary 3
1 Introduction 11
1.1 Purpose of the document 11
1.2 Structure of the Document 12
2 Case studies developed in a cross-border region in Central Europe (FirEUrisk Pilot Site #2) 12
2.1 Analysis of factors that predispose forest to a bark beetle outbreak 13
2.2 Effects of bark beetle disturbance and fuel types on fire radiative power and burn severity in the Bohemian-Saxon Switzerland 21
2.3 Fire behaviour and propagation potential in areas affected by bark beetle infestation 33
2.4 Predicting post-fire soil erosion and water contamination risk after the 2022 fire in the Bohemian and Saxon Switzerland National Parks 41
3 Case study developed in Central Portugal (Pilot Site #3) 51
3.1 Short-term human health impacts resulting from smoke from an extreme wildfire in Central Portugal 51
4 Case studies in Demonstration areas 62
4.1 Effects of air pollution through the emissions of nuclear smoke in the Chornobyl Exclusion Zone during wildfires 62
4.2 Post-fire landslides: Landslide susceptibility and related cascading effects after a fire event 75
4.3 Post-fire floods: impacts of two storms in Greece 86
5 Main Conclusions 96
5.1 Wildfires 96
5.2 Air pollution 97
5.3 Post-fire landslides 97
5.4 Post-fire floods 97
6 Appendix A: Section 4.1 99
7 Appendix B: Section 2.4 102

Copyright © FirEUrisk Consortium. All rights reserved.

List of Figures

Figure 2.1 Overarching workflow of the methodology. 15
Figure 2.2 Bark beetle damage map. 17
Figure 2.3 Bark beetle predictive model map. 18
Figure 2.4 Bark beetle attack predictive model vs Bark beetle damage map. 18
Figure 2.5 Example of spruce stand affected by bark beetle with standing and prone deadwood. 24
Figure 2.6 Forest fire statistics for Saxony 2008-2020 (source: Sachsenforst). 25
Figure 2.7 Composite Burn Index Results for the 21 Sites Recorded (Beetz, 2022) 26
Figure 2.8 Composite Burn Index Values for tall trees >20m 26
Figure 2.9 Beech trees severely affected by the flames rising up the slope (image: Christopher Marrs) 28
Figure 2.10 Incomplete combustion of large prone deadwood (image: Christopher Marrs). 28
Figure 2.11 Sequence of images taken by wildlife camera trap, before, during and after the fire (images: Courtesy of Saxon Switzerland National Park Administration) 29
Figure 2.12 FlamMap input layers for the propagation potential. 35
Figure 2.13 Layer containing estimated bark beetle damage. 36
Figure 2.14 Official 100m resolution FirEUrisk fuel map for the region. 37
Figure 2.15 Adjusted 100m resolution FirEUrisk fuel map for the region with integrated bark beetle damage. 37
Figure 2.16 Stage 1 summary table for PS2 Central-Eastern Europe. 37
Figure 2.17 Basic FlamMap results for official FirEUrisk fuel map. 38
Figure 2.18 Fireline intensity result for official FirEUrisk fuel map. 39
Figure 2.19 Basic FlamMap results for bark beetle infested fuel map. 39
Figure 2.20 Fireline intensity for bark beetle infested fuel map. 40
Figure 2.21 Fireline intensity difference. 40
Figure 2.22 Flame length difference 40
Figure 2.23 Rate of spread difference 41
Figure 2.24 Ground surface images after the 2022 fire in the Saxon Switzerland National Park showing the: organic soil layer with charred surface material (left), highly erodible mineral soil below a distinct ash layer (centre), and partially charred logs from trees downed prior to the fire (right) (Images: TU Dresden) 42
Figure 2.25 Soil erosion and ash transport hotspots for the area burnt by the 2022 fire in Bohemian and Saxon Switzerland NP, predicted by WEPPcloud-EU-WATAR (low: < 1 kg ha^{-1} of ash, intermediate: 1 – 4,400 kg ha^{-1} of ash, high: > 4,400 kg ha^{-1} of ash). 44
Figure 2.26 Sediment yield (kg ha^{-1}) before (left) and after (right) the 2022 fire in Bohemian and Saxon Switzerland National Parks predicted by WEPPcloud-EU-WATAR. 45
Figure 2.27 Ash transport (kg ha^{-1}) for the first year following the 2022 fire in the Bohemian and Saxon Switzerland National Parks estimated by WEPPcloud-EU-WATAR. 46
Figure 2.28 Post-fire images of the 2022 fire in the Saxon Switzerland National Park showing downed trees on the ground as a result of the Bark Beetle infestation and the fire. Images: TU Dresden. 47

Copyright © FirEUrisk Consortium. All rights reserved.

Figure 2.29 (Top, a) Hillslope delineation for the area contributing to the Hřensko gauging station (location represented by the blue pin). The orange area represents the area burnt by the 2022 fire. (Bottom, b) Streamflow comparison between observed (dotted black line) and predicted (orange line) monthly data. 49
Figure 3.1 Location of the areas affected by the EWE on October 15 and 16, 2017. 52
Figure 3.2 Spatial distribution of the PM2.5 concentrations between October 15th and 16th, 2017. 55
Figure 3.3 Spatial distribution of the hospital admissions, in Portugal, for respiratory (a) and cardiovascular (b) diseases due to PM2.5 levels caused by the 2017 October EWE. 56
Figure 4.1 Spatial distribution of areas affected by "big" wildfires (>100 ha) during April 2020: fires that were mostly localised in the ChEZ are marked in yellow; fires outside the ChEZ are marked in red 63
Figure 4.2 Simulated wildfire dynamic: start time – 2020-04-03 T 08:00:00 68
Figure 4.3 Landscape spatial distribution before wildfires in 2020 based on Sentinel-1 and 2 images as of 2019: 1 – meadow or fallow, 2 – swamp, 3 – single or groups of bushes and trees, 4 – coniferous forest, 5 – deciduous forest; 5 – dead stand after fire damage, 7 – dead stand 69
Figure 4.4 Fire outline. Areas affected by fire located in radioactivity land and destroyed forest stands 69
Figure 4.5 Dynamics of burnt areas and combusted materials during the 2020 wildfires in April using a 6-h time lags. 72
Figure 4.6 Time series of RNs emissions during the Chornobyl wildfires in April 2020. 72
Figure 4.7 Distribution of areas subjected to landslide in Italy (source: ISPRA). 82
Figure 4.8 (left) Planescope RGB image acquired on 01/06/2022. Red circles represent the hot spots observed at 13:15 (MODIS and VIIRS) of the 25 May. (right) Normalized Burn Ratio (NBR) map computed by using a Sentinel 2 image of 01/06/2022, whit superimposed the shapefile of the burnt area. 83
Figure 4.9 Image of the impact of the mud avalanche due to the heavy rain occurred some months after a disastrous wildfire in Stromboli (from La Repubblica newspaper). 83
Figure 4.10 Distribution of the landslide risk for the Stromboli Island, ...84
Figure 4.11 Formia town area. Distribution of landslide risk, from ISPRA dataset, before 2022 fire event. The blue polygon shows the area burnt by a fire between July 30th and August 3rd, 2022. In pink the area from where the debris flow originated. The inset on upper left shows the DEM in the area with superimposed, in white, the polygon of the origin of the debris flow. 84
Figure 4.12 Main basins potentially affected by the flood peaks. 88
Figure 4.13 Visual Analysis of Thessaly Flood Impact (Source: NoA left and Copernicus right) 89
Figure 4.14 Comprehensive rainfall distribution map during Storm Daniel in Greece, detailing record-breaking precipitation across various regions, with an emphasis on Thessaly's most affected areas. (Source: Weatherzone left and NoA right). 90
Figure 4.15 Rainfall data from the National Observatory of Athens. 91

Figure A 6.1 The speed of fire spread at the time of wildfires in the areas. 99
Figure A 6.2 The direction of fire spread at the time of the wildfires in the area. 99
Figure A 6.3 Spatial distribution of heat of combustion for combustible materials per unit surface area 99
Figure A 6.4 – Spatial distribution of fireline intensity during wildfires in April 2020. 99
Figure A 6.5 Spatial distribution of Byram's flame length during wildfires in April 2020. 100

Copyright © FirEUrisk Consortium. All rights reserved.

Figure A 6.6 The contamination density of soil with Sr-90 in fire-affected areas in April 2020 in the 100
Figure A 6.7 The contamination density of soil with Cs-137 in fire-affected areas in April 2020 100
Figure A 6.8 The contamination density of soil with Pu-238-240 in fire-affected areas in April 2020 in the Chornobyl Exclusion Zone and adjacent territories as of April 15, 2020. 100
Figure A 6.9 The contamination density of soil with Am-241 in fire-affected areas in April 2020 in the Chornobyl Exclusion Zone and adjacent territories as of April 15, 2020. 100
Figure A 6.10 The density of Sr-90 activity emission into atmosphere air from a unit of the surface area during the Chornobyl wildfire in April 2020. 100
Figure A 6.11 The density of Cs-137 activity emission into atmosphere air from a unit of the surface area 101
Figure A 6.12 The density of Pu-238-240 activity emission into atmosphere air from a unit of the 101
Figure A 6.13 The density of Am-241 activity emission into atmosphere air from a unit of the surface area 101

Copyright © FirEUrisk Consortium. All rights reserved.

List of tables

Table 2.1 Burn severity levels identified using the dNBR for both National Parks (Beetz, 2022) 27
Table 2.2 Burnt Area by Forest Type Saxon Switzerland (Beetz, 2022) 27
Table 2.3 Predictions of eroded soil, ash, and carbon and nitrogen reaching the river during the first year after the fire. 45
Table 2.4 Return period analysis and probability of occurrence of runoff, sediment and ash transport events in the first year after the fire.....46
Table 2.5 Streamflow model results before and after the 2022 fire in the SSNP for annual (A), monthly (M) and daily (D) streamflow averages. 48
Table 3.1 Hospital admissions estimated in this study (between 15 and 16 October 2017) and reported by the NHS (October 2017). 55
Table 4.1 Combustible biomass and radioecological parameters for 2020 Fire (Beresford et al., 2018; IAEA, 2010; Kashparov et al., 2020; Holiaka et al., 2020a,b) 64
Table 4.2 Areas and RNs emissions during the Chornobyl wildfires in Red Forest (2016) and in the ChEZ and adjacent territories (April, 2020). 72
Table 4.3 List of information layers used to identify the landslide susceptibility. 80

Copyright © FirEUrisk Consortium. All rights reserved.

List of Acronyms

List of Acronyms	
PS	Pilot Site
BLT	Black leaves torch
BSI	Bare Soil Index
CAS	Czech Academy of Sciences
CBH	Canopy Base Height
CC	Canopy Cover
CBD	Canopy Bulk Density
CH	Canopy Height
ChEZ	Chornobyl Exclusion Zone
CLMS	Copernicus Land Monitoring Service
CM	Canopy mortality
CLRE	Red-edge-band Chlorophyll Index
Composite Burn Index	CBI
DFI	Dead Fuel Index
dNBR	Difference Normalised Burn Ratio
EC	European Commission
ECMWF	European Centre for Medium-Range Weather Forecasts
EVI	Enhanced Vegetation Index
EU-DEM	European Digital Elevation Model
FM	Fuel Model
JRC	Joint Research Centre
LAI	Leaf area index
LCL	Leaf Cover Loss
MBI	Modified Bare Soil Index
MAE	Mean Absolute Error
MSAVI2	Modified Soil Adjusted Vegetation Index 2
NBR	Normalised Burn Ratio
NDMI	Normalized Difference Moisture Index
NDREI1	Normalized Difference Red Edge Index 1
NDREI2	Normalized Difference Red Edge Index 2
NDVI	Normalized Difference Vegetation Index
NFI	National Forest Inventory
NHS	National Health Service
OLS	Ordinary Least Squares
RMSE	Root Mean Square Error
RN	Radionuclides
RRTMG	Rapid Radiative Transfer Model short- and long-wave radiation model
SVR	Support Vector Regression
TUD	Technische Universität Dresden
WUI	Wildland Urban Interface

Copyright © FirEURisk Consortium. All rights reserved.

1 Introduction

1.1 Purpose of the document

Within the Sendai Framework for Disaster Risk Reduction 2015-2030, cascading disasters are defined as "disasters, which are magnified by multiple, sequential, and interconnected hazards" (UNISDR, 2015). In FirEUrisk, cascading effects refer to the combination of fires with other natural hazards, which may potentially increase negative fire impacts (Chuvieco et al., 2023). Those events can occur in a stepwise or parallel manner (Garcia-Aristizabal et al., 2014). Marzocchi et al. (2012) has proposed a methodology for assessing the impact of cascading effects on the affected area and the implementation of a Decision Support System, which has been implemented in the EU FP-7 SNOWBALL project. In that case, a cascading effect is "the overall hazard/impact scenario timeline, including the chain of events (cascading events) and damage caused by cascading events on elements at risk assumed in the evaluation (i.e. people, buildings, infrastructures, economy, etc.)" (Zuccaro et al., 2018).

The FirEUrisk project is geared to integrate wildfire risk components such as danger, exposure, and vulnerability (Chuvieco et al., 2023). The occurrence of fire and non-fire hazards have been analysed according to the conditions of specific regions. The lack of concurrent triggering events as well as in-situ information to establish a cause / effect relationship have hindered the implementation of a comprehensive and integrated analysis of the final damage produced by a cascading effect. Nevertheless, in this report, we showcase how events occurring at the same location and happening within a short time frame play a role in pre-disaster, disaster, and post-disaster phases as well as in the environmental impacts derived from them. For example, higher deadwood amounts alter fire spread and behaviour; fire smoke contributes to air pollution and dispersing radionuclides; and post-fire conditions together with severe rainfalls contribute to soil erosion, floodings, and landslides. The temporal scale of the case studies presented in this report was selected according to the occurrence of a particular hazard. Some products that inform about factors that predispose to a cascading effect could be produced in a regular basis according to input data limitations.

This activity was expected to be implemented in Central Europe (Pilot Site 2, PS-2) and other Demonstration Areas in Italy and Ukraine. In addition, we have also included an analysis in Central Portugal (PS-3). Especially, in Central Europe, we analysed the factors that predispose forests to a bark beetle attack, the effects of bark beetle disturbance and fuel types on fire radiative power and burn severity in the Bohemian and Saxon Switzerland National Parks, the fire behaviour and propagation potential in areas affected by bark beetle infestations, and the post-fire soil erosion and water contamination risk after a wildfire in the Bohemian and Saxon Switzerland National Parks. In Central Portugal, we assessed the short-term human health impacts resulting from smoke from an extreme wildfire event. In the Chornobyl Exclusion Zone, we estimated the effects of air pollution through the emissions of nuclear smoke in the Chornobyl Exclusion Zone during wildfires. In Italy, we mapped the susceptibility to landslides after a fire event, specific examples are shown in Stromboli Island and Lazio region (Italy). Finally, we showcased the effects of post-fire floods in the Region of Thessaly in Central Greece.[1]

[1] https://fireurisk.eu/pilot-sites/

Copyright © FirEUrisk Consortium. All rights reserved.

1.2 Structure of the Document

This section briefly presents the contents of the document. The case studies included in this report include:

- Case studies developed in a cross-border region in Central Europe (FirEUrisk Pilot Site #2).
    - Analysis of factors that predispose forest to a bark beetle outbreak in Central Europe.
- Effects of bark beetle disturbance and fuel types on fire radiative power and burn severity in the Bohemian and Saxon Switzerland National Parks
    - Fire behaviour and propagation potential in areas affected by bark beetle infestation
    - Predicting post-fire soil erosion and water contamination risk after the 2022 fire in the Saxon Switzerland National Park
  - Case study developed in Central Portugal
    - Short-term human health impacts resulting from smoke from an extreme wildfire in Central Portugal
  - Case studies in Demonstration Areas
    - Effects of air pollution through the emissions of nuclear smoke in the Chornobyl Exclusion Zone during wildfires
    - Landslides susceptibility and related cascading effects after fire events in Stromboli Island and Formia
    - Impacts of post-fire floods in Central Greece

2 Case studies developed in a cross-border region in Central Europe (FirEUrisk Pilot Site #2)

The FirEUrisk Central Europe Pilot Site is located in a transboundary area in Southern Brandenburg and Eastern Saxony, Germany; North Bohemia, Czechia; and Lower Silesia, Poland. The Pilot Site spans approximately 32,777 km², encompassing lowlands, mountains, and urban areas from the Ore Mountains in the West to the Sudetes Mountains in the East, and from the North German Plain to the Bohemian Elbe lowland river. The River Elbe, originating in the Giant Mountains, flows northwest through Bohemia and Saxony, while the Lower Silesia area is drained by the River Oder. About a third of the area is forested (11,819 km²), with coniferous forests covering 24.5%, dominated by Norway spruce and Scots pine. Mixed and broadleaved forests account for 7.25% and 4.2%, respectively, with oak, ash, birch, rowan, and sycamore maple as prominent species. The region includes four national parks, forming two protected areas across the German-Czech and Polish-Czech borders. Notable parks are Saxon Switzerland and Bohemian Switzerland in the Elbe Sandstone Mountains, Karkonosze in Lower Silesia, and Krkonoše in North Bohemia, with high woodland cover percentages (e.g. Saxon Switzerland boasts 94% forest cover).

In 2022, a human-caused fire started in the Bohemian Switzerland National Park in the Czech Republic, quickly spreading and crossing the border into the Saxon Switzerland National Park in Germany. This event is considered the largest fire that has occurred in the Czech Republic in modern history (Boháč & Drápela, 2023). The complex topography and access to some places made the fire suppression activities more complicated in a region highly impacted by an infestation of bark beetle (Boháč & Drápela, 2023; DW, 2022). Initial estimations of the affected area reported 16 km^2 after the intervention of emergency workers (Berčák et al., 2023; Boháč & Drápela, 2023; DW, 2022). Recent studies

Copyright © FirEUrisk Consortium. All rights reserved.

carried out in collaboration with the National Parks have reported that the final total affected area covered 12 km^2 (c.f. 2.2)[2,3].

The interconnection of biotic and abiotic factors influences wildfire risk dynamics, which involve a multi-phase continuum:

1. **Pre-disaster**: factors that predispose forests to bark beetle outbreaks can act as triggers or promoters for high-intensity fires. Large-scale bark beetle outbreaks contribute to changes in forest fuels by enhancing their susceptibility to ignition.
2. **Disaster**: biotic and abiotic disturbances effects concerning change in stands and forest mortality increase fire hazard and potential fire behaviour. Bark beetle-caused tree mortality enlarges the quantity of surface fuel load, the quantity of ladder fuels, and fuel flammability leading to heightened fire propagation. Changes in fuels affect the frequency and severity of fires due to the influence of the structure and composition of stands, where large, dead, woody fuels and live surface fuels dominate. Although fire-related disturbances are infrequent in Central Europe, wildfires have begun to pose an emerging threat.
3. **Post-disaster**: marked by the aftermath, including challenges such as soil erosion due to increased runoff and, thus, vulnerability and apparition of new natural hazards.

In the following sections, we showcase several analyses related to the fire occurred in the Bohemian and Saxon Switzerland National Parks in 2022 within the FirEUrisk Central Europe Pilot Site #2. For example, we assessed the factors that predispose forests to a bark beetle attack, which could increase deadwood and impact negatively on wildfire dynamics; the characterisation of the wildfire in terms of fuel types and bark beetle disturbance, the fire behaviour and propagation in areas affected by bark beetle infestation, and the potential post-fire soil erosion and water contamination after the 2022 fire in the Saxon Switzerland National Park.

2.1 Analysis of factors that predispose forest to a bark beetle outbreak

The methods and results of this section has been published as Fernández-Carrillo, Á., Franco-Nieto, A., Yagüe-Ballester, M. J., & Gómez-Giménez, M. (2024). Predictive Model for Bark Beetle Outbreaks in European Forests. Forests, 15(7). https://doi.org/10.3390/f15071114

Introduction

Climate change and socio-economic pressures have contributed to increasing disturbance regimes of fires, drought, and insect outbreaks at the global scale in the last decade. In addition, accounting for intertwined effects among disturbance drivers that can either amplify or dampen their effects is challenging because of non-linearity and complex interactions (Seidl et al., 2017). The occurrence of such extreme events alters the resistance and resilience of ecosystems, which impact on their strength to avoid a hazard, survive it, and recover from it (Buma, 2015).

[2] https://www.nationalpark-saechsische-schweiz.de/wp-content/uploads/2022/10/FAQ-Waldbrand-2022.pdf
[3] https://emergency.copernicus.eu/mapping/list-of-components/EMSR610

Copyright © FirEUrisk Consortium. All rights reserved.

In the last years, European forest have been affected by multiple hazards particularly severe such as droughts, biotic damages, and heatwaves increasing forest mortality. Moreover, increasing deadwood and changing climate conditions bring along a higher risk of wildfires (Chuvieco et al., 2023). In this case study, we monitored *Picea abies* (Norway spruce), which is the main host of bark beetle (*Ips typographus*). We also analysed factors that predisposed forest to a bark beetle outbreak that could potentially increase the negative effects of wildfires. Previous results allowed us to build a bark beetle prediction map to estimate the probability of future outbreaks in spruce European forests (Fernández-Carrillo et al., 2024). The study area of this analysis is the FirEurisk Pilot Site Central Europe, which covers a cross-border region including small areas in Germany, Poland, and Czech Republic. It is important to note that Central Europe is the name of the Pilot Site in FirEUrisk, but strictly speaking, this term refers to a larger area including other countries. Therefore, we referred to European forests because we worked in some regions of three countries located in Europe and faor consistency with the published paper, we are using the same terminology.

Data

Preprocessing and processing of multitemporal Sentinel satellite composite images were used to classify *Picea abies*. Monthly Sentinel-2 composites of 2019, 2020, and 2021 were produced by selectively incorporating only those images featuring cloud coverage below 60%, utilising the FMASK algorithm (Frantz et al., 2018). In the following list, we enumerate the data sources utilised to investigate factors that predispose forests to bark beetle infestations:

- National Forest Inventory, NFI. Three forest inventories were collected: Lower-Silesian Forest data, Brandenburg Forest data, and Saxony forest; whose reference year is 2021. Susceptibility of Norway spruce stands to attack by bark beetle is highly correlated to abundance of its prime host tree, stand age, and high canopy cover.
- Copernicus Land Monitoring Service, CLMS produces land reference geospatial datasets, in particular, two datasets have been used: CLC+ Backbone for training areas of *Picea abies* classification (class non-picea); and European Digital Elevation Model (EU-DEM) for characterising the topography i.e. elevation, slope and aspect. Exposed *Picea* stands on ridges, hilltops, or upper slopes are particularly susceptible to bark beetle attacks. High solar irradiation triggers propagation of beetle, thus any structural trait leading to increased insolation and temperature conditions in the stand favours the development of bark beetle. Exposure to solar irradiation was derived from terrain features. The relevance of including further information about climate variables has been discussed in Fernández et. al (2024).
- Joint Research Centre, JRC is a source of European Forest Insect & Disease Disturbances (DEFID2) which was used for validation of bark beetle damage output in the Czech area of pilot site.
- Saxon Switzerland National Park bark beetle data, between 1990 to 2021, derived from field work and provided by the National Park. This data was used for validating the bark beetle predictive model.

Methods

The methodology was divided into four phases: image preprocessing, spruce classification, bark beetle damage, and bark beetle attack predictive model (Figure 2.1). The first two are explained in *Analysis of the health status of Picea abies and bark beetle damage map*., and the last one in *Analysis of factors that predispose forests to a bark beetle outbreak*.

Copyright © FirEUrisk Consortium. All rights reserved.

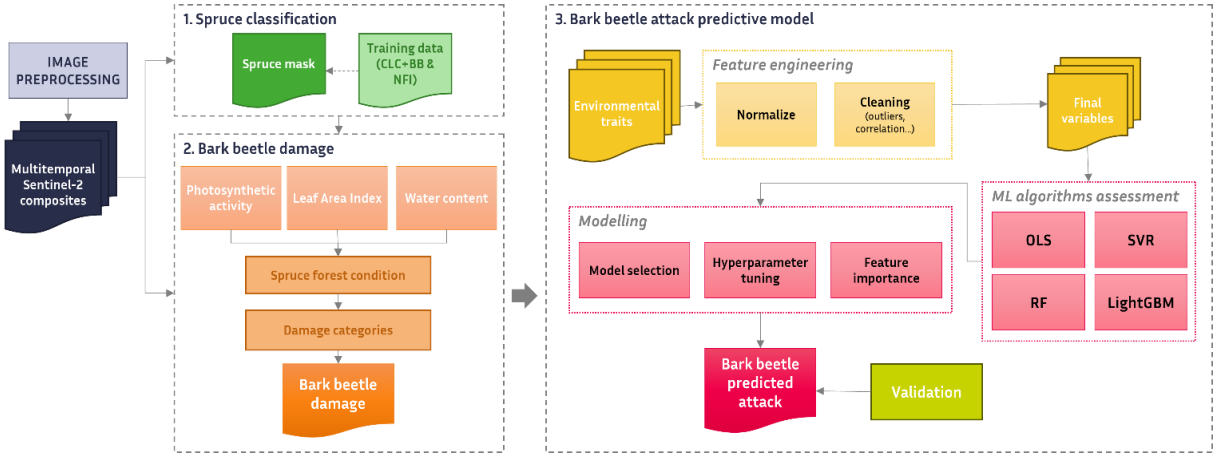


Figure 2.1 Overarching workflow of the methodology.

Analysis of the health status of *Picea abies and* bark beetle damage map

The *Picea abies* classification provides a binary spruce-non spruce mask in September 2020 for the PS. This product is the basis for the methodology of vegetation stress monitoring and bark beetle damage during of 2021. Spruce samples were obtained through systematic sampling within spruce stands from NFI datasets and non-spruce samples were assigned based on the CLC + Backbone product. Different spectral indices were selected based on their proven ability to discriminate areas dominated by *Picea abies* based on a scientific review (Bonannella et al., 2022; Candotti et al., 2022; Dalponte et al., 2022). These are: Bare Soil Index (BSI), Red-edge-band Chlorophyll Index (CLRE), Dead Fuel Index (DFI), Enhanced Vegetation Index (EVI), Modified Bare Soil Index (MBI), Modified Soil Adjusted Vegetation Index 2 (MSAVI2), Normalized Difference Moisture Index (NDMI), Normalized Difference Red Edge Index 1 (NDREI1), Normalized Difference Red Edge Index 2 (NDREI2), and Normalized Difference Vegetation Index (NDVI). Then proceeded to Pairwise Pearson correlation analysis of vegetation indices, reducing dimensionality by checking and minimising collinearity and redundancy. The indices with lower Pearson coefficients were selected: EVI, MBI, MSAVI2, and NDVI.

For stress assessment, a spruce condition baseline is needed as reference line of tree health of the *Picea* stands from the spectral analysis of the biophysical characteristics of the vegetation: photosynthetic activity, leaf area index, and water content. Based on the literature review about the effects of bark beetle (Candotti et al., 2022; Dalponte et al., 2022), the following vegetation indices were computed for each date: NDVI, MSAVI2, NDMI and Leaf Area index green (LAIgreen). NDVI and Soil Adjusted Vegetation Index (SAVI) are direct indicators of plant greenness and photosynthetic activity, NDMI is an indicator of vegetation water content, and LAIgreen is an estimate of the proportion of green leaves per area. As defoliation is one of the main effects caused by bark beetles, LAI has been considered as one of the key variables in this study. Anomalies in vegetation condition during this timeframe were estimated using three indices. Each index was computed and a multitemporal linear regression was individually adjusted for each index. The regression modelled vegetation changes, considering minimal disturbance to spruce pixels, focusing on trends and seasonal alterations between phenological moments. Following the adjustment of the linear regression model, the error for each pixel, representing the distance from the real value of the index to the estimate, was computed to generate images depicting anomalies in vegetation indices. The mean of all standardised errors served as a direct

Copyright © FirEURisk Consortium. All rights reserved.

indicator of vegetation status. Negative anomalies were categorised into distinct damage classes (Fernandez-Carrillo et al., 2020): [1] No damage: pixels with an error above -1 standard deviation from the mean. [2] Minor damage: pixels with an error between -1 and -2 standard deviations, indicating mild bark beetle-induced effects like partial discoloration or defoliation. [3] Moderate damage: pixels with an error between -2 and -3 standard deviations. [4] Severe damage: pixels with an error below -3 standard deviations, signifying extensive damage, including complete death of most spruce trees. A lack of accurate reference datasets for bark beetle damage impeded validation, but records from the FirEUrisk project for Saxon Switzerland National Park were used. For more details see Fernández-Carrillo et al. (2024).

Analysis of factors that predispose forests to a bark beetle outbreak

European Commission (EC) (Turbé et al., 2012), identified **environmental traits** that predisposed forests to a bark beetle outbreak. The study aimed to predict areas at higher risk of bark beetle attacks between September 2020 and October 2021 by integrating spatial information on key environmental traits associated with bark beetle development. Each trait was selected based on its relevance and availability. Some environmental traits were excluded from the analysis due to challenges related to accurate data sources, suitable spatial resolution for the analysis or proxies derived from remote sensing data. The complete list of factors that predispose forest to a bark beetle attack considered in this analysis can be read in Fernández-Carrillo et al. (2024). The integration of appropriate environmental traits into the predictive model ensures a comprehensive and data-driven approach to predicting bark beetle attacks in the study area.

We carried out a **feature engineering** process before training the bark beetle predictive model. The first step was to transform the input variables for the model. The technique-maintained interpretability and aided in exploring patterns within the data, preserving essential information. Pearson correlation coefficients were computed, leading to the exclusion of highly correlated variables to enhance training efficiency and avoid collinearity. After dimensionality reduction, the final variables selected to build the model were:

1. Spruce density
2. Stand density
3. Elevation
4. Slope
5. Aspect Sin
6. Aspect Cos
7. Potential solar irradiation
8. Bark beetle density 200 m
9. Bark beetle density 1 km,
10. Bark beetle density 10 km
11. Bark beetle density 25 km
12. Bark beetle distance

To predict bark beetle attacks, bark beetle damage estimates for 2021 were used as the target variable, creating a binary map of damage and no-damage categories resampled to 50 m. To avoid bias towards spruce presence, a per-pixel spruce proportion map was derived, and the attack proportion was multiplied by the spruce proportion to create the final target. This continuous variable ranged from 0 to 1, representing the proportion of spruce damaged by bark beetles in each 50 x 50 m pixel. The dataset was split into train (80%) and test (20%) subsets for model adjustment and performance evaluation.

The **model selection and hyperparameter tuning** involved a systematic strategy with a broad random search followed by a more precise grid search. This optimization aimed to enhance model accuracy, efficiency, and generalisation. Evaluation metrics such as r^2, mean absolute error (MAE), and root mean square error (RMSE) were computed for each

Copyright © FirEUrisk Consortium. All rights reserved.

configuration. Following the adjustment of hyperparameters for all tested models, including Ordinary Least Squares (OLS), Random Forest regression (RF), Support Vector Regression (SVR), XGBoost, and LightGBM. **Feature importance** was determined using Gini impurity decrease for the Random Forest model. **Inference and postprocessing** involved predicting the spruce attack probability in each pixel, considering the known spruce proportion in September 2020. **Validation** utilised ground truth data from Saxon Switzerland National Park, with damaged areas in 2021 considered as ground truth. The predictive bark beetle attack product was binarised at different probability thresholds, and performance metrics were computed. The validation results might be biased due to possible damage between September and December 2020 and areas damaged between November and December 2021.

Results

The spruce classification output was a binary spruce/non-spruce map of the study area at 10 m spatial resolution. The performance metrics demonstrated strong values with an overall accuracy of 91% and an F1-score of 86%, however, a relatively elevated omission error of 21% due to underestimation of the spruce area. The bark beetle damage map (Figure 2.2) boasts a spatial resolution of 10 m. Confusion matrices and performance metrics were computed to validate damage estimates derived from EO data. Performance metrics illustrate the model's proficiency in mapping bark beetle damage, showcasing notable values for overall accuracy at 82% and an F1-score of 85%.

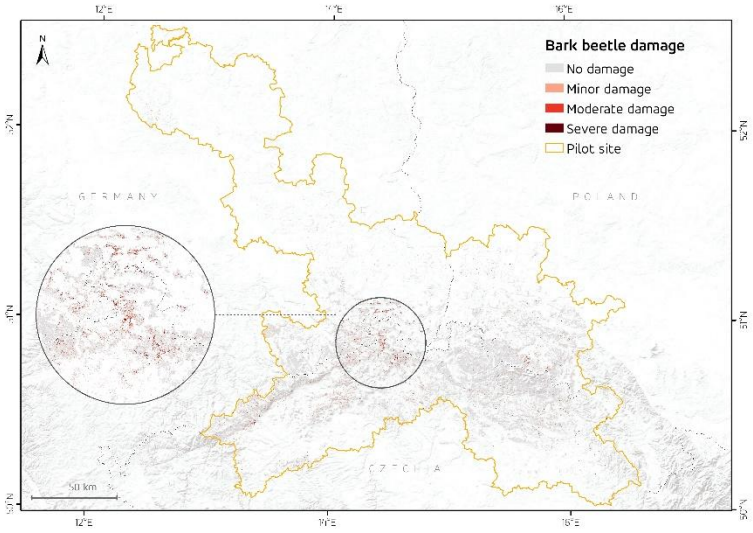


Figure 2.2 Bark beetle damage map.

The best model was selected to produce a raster showing the predicted bark beetle damage. RF model is the top-performer, delivering the most favorable outcomes, as evidenced by the metrics computed over a 20% test set of the data, with a RMSE of 0.03 and a MAE of 0.11. Geospatial results will help managers optimise their resources and mitigate the negative effects of plagues and wildfires. The output is a map showing predicted bark beetle attack probability from 0 to 100. Bark beetle attack predictive model map (Figure 2.3).

Copyright © FirEUrisk Consortium. All rights reserved.

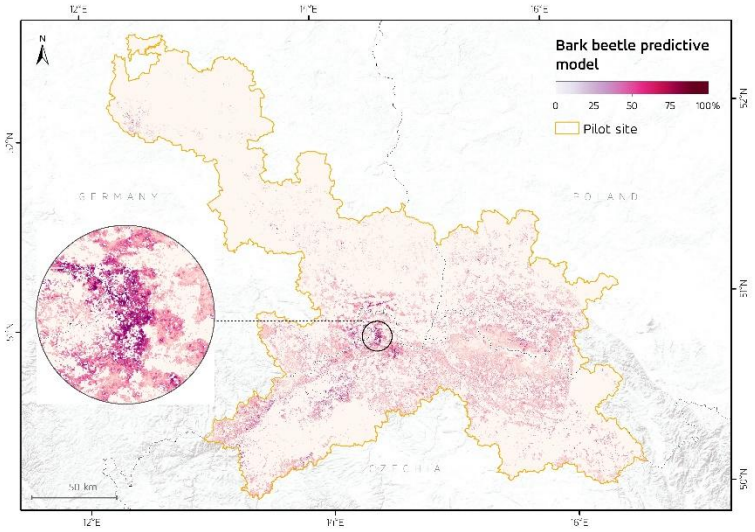


Figure 2.3 Bark beetle predictive model map.

The bark beetle predictive model achieved an accuracy of 92.3%, an F1-score of 78.0%, a commission error of 31.2%, an omission error of 46.4%, and a relative bias of -22.2%.

In Figure 2.4, a visual analysis of the correspondence between products Bark beetle predictive model map and Bark beetle damage map is presented, allowing for a detailed examination of their interrelationships. This representation facilitates a thorough exploration of the associations and comparisons between the two products.

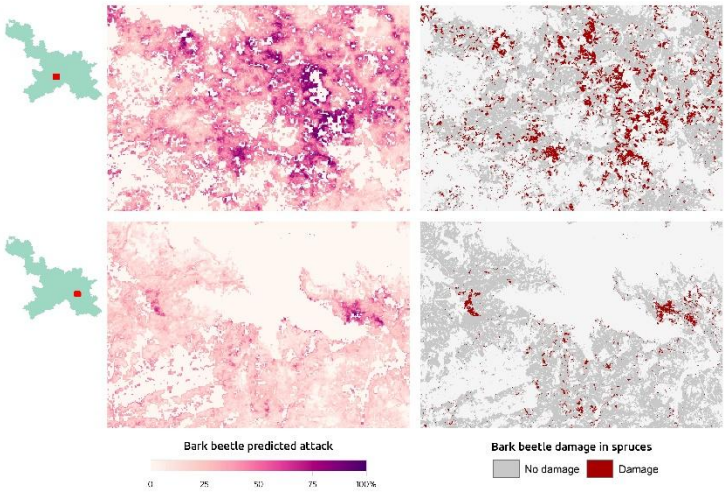


Figure 2.4 Bark beetle attack predictive model vs Bark beetle damage map.

Conclusions

This study proposes a novel and integrated methodological framework by combining different open geospatial datasets with ML techniques to create a predictive model of spruce bark beetle attack. The time frame of the analysis was selected to understand the environmental conditions of a wildfire that occurred in PS2 - Central Europe in 2022. Several factors that predispose forest to a bark beetle attack were considered to predict a potential outbreak in spruce forest,

Copyright © FirEUrisk Consortium. All rights reserved.

which is the main host. Bark beetle dynamics play a relevant role in ecological process, especially, in areas affected by wildfires because they increase the amount of deadwood. Deadwood directly influences how wildfires behave and their impact on ecological processes. The results of this analysis leverage on scalable methodologies and open data sources that can be replicated and implemented in other European forests. The importance of predisposing factors may vary from region to region for different reasons such as data availability and the objectives of the study. Nevertheless, we recommend considering all the factors recommended by the European Commission in the first place to try to build comparable studies among regions. As presented by Fernández-Carrillo et al. (2024), the approach of our analysis to monitor bark beetle outbreaks was designed and implemented to be scalable to other locations across Europe and other continents. Specific improvements should be addressed regarding the assimilation of more input variables into the model such as forest age, climate, and using a larger dataset to validate the damage prediction maps.

Policy recommendations

Advanced forest management practices and refined monitoring tools are necessary for the implementation of effective mitigation and adaptation strategies. Hlàsny et al. (2019) has proposed a suite of policy recommendations for Europe's forests grouped by three main lines of action: i) establish management objectives at local level; ii) strengthen the coordination at European level, and iii) adopt a holistic, landscape-scale approach. Specific measures should include further research on the social aspects of bark beetle outbreaks and improved education and communication; cross-cutting management plans including different sectors (forestry, environment, finance, transportation, and public safety sectors); and an integrated management framework including monitoring, sanitation, silviculture, and non-intervention.

In Central Europe countries including Poland, Czech Republic, Germany, Austria, and Slovakia, should consider implementing or developing of fire danger monitoring systems, restricting forest access, assessing communication signal coverage, creating additional firebreaks, notifying competent fire units, reevaluating technical means for fire protection, providing maps or GIS data, and exploring aerial firefighting. Moreover, beyond applied management, forest owners should collaborate with local fire brigades for example, regular ground and aerial fire patrols during timber processing are ideal for comprehensive fire prevention. A better planification may also include a thorough knowledge of the region and understand the historical wildfire context of the region (Berčák et al., 2023).

In the Czech Republic (where the wildfire considered in our study started), Hlàsny et al. (2021) has proposed a forest management approach based on a multi-scale perspective to avoid a decrease in forest resilience. Actions dedicated to the regeneration of post-outbreak sites and preventative measures in areas that have not yet been affected (e.g., premature harvesting, the preventative sanitation removal of infested trees, etc.) should be prioritised instead of outbreak suppression. Therefore, the importance of measures that increase forest resilience and that reduce outbreaks have been highlighted to mitigate the impacts of bark beetle.

In line with previous recommendations and the results of our case study in Central Europe, we emphasise that a landscape perspective is crucial to a comprehensive and integrated forest management strategy in European forests. It is imperative to establish collaboration among institutions across different regions to deal with cascading and compound effects. Finally, efforts should be made to collect and harmonise geospatial datasets at high spatial resolution required to monitor ecological processed. Especially, information about environmental factors that

Copyright © FirEUrisk Consortium. All rights reserved.

predispose forest to a bark beetle outbreak. Further recommendations and necessary efforts have been included in Fernández-Carrillo et al. (2024), in particular, in the Strength, Weaknesses, Opportunities and Threats analysis.

References

Berčák, R., Holuša, J., Kaczmarowski, J., Tyburski, Ł., Szczygieł, R., Held, A., Vacik, H., Slivinský, J., & Chromek, I. (2023). Fire Protection Principles and Recommendations in Disturbed Forest Areas in Central Europe: A Review. *Fire*, *6*(8). https://doi.org/10.3390/fire6080310

Boháč, A., & Drápela, E. (2023). Present Climate Change as a Threat to Geoheritage: The Wildfire in Bohemian Switzerland National Park and Its Use in Place-Based Learning. *Geosciences (Switzerland)*, *13*(12). https://doi.org/10.3390/geosciences13120383

Bonannella, C., Hengl, T., Heisig, J., Parente, L., Wright, M., Herold, M., & de Bruin, S. (2022). Forest tree species distribution for Europe 2000-2020: mapping potential and realized distributions using spatiotemporal machine learning. *PeerJ*. https://doi.org/10.7717/peerj.13728

Buma, B. (2015). Disturbance interactions: characterization, prediction, and the potential for cascading effects. *Ecosphere*, *6*(4), art70. https://doi.org/https://doi.org/10.1890/ES15-00058.1

Candotti, A., De Giglio, M., Dubbini, M., & Tomelleri, E. (2022). A Sentinel-2 Based Multi-Temporal Monitoring Framework for Wind and Bark Beetle Detection and Damage Mapping. *Remote Sensing*, *14*(23), 1–29. https://doi.org/10.3390/rs14236105

Chuvieco, E., Yebra, M., Martino, S., Thonicke, K., Gómez-Giménez, M., San-Miguel, J., Oom, D., Velea, R., Mouillot, F., Molina, J. R., Miranda, A. I., Lopes, D., Salis, M., Bugaric, M., Sofiev, M., Kadantsev, E., Gitas, I. Z., Stavrakoudis, D., Eftychidis, G., … Viegas, D. (2023). Towards an Integrated Approach to Wildfire Risk Assessment: When, Where, What and How May the Landscapes Burn. In *Fire* (Vol. 6, Issue 5). https://doi.org/10.3390/fire6050215

Dalponte, M., Solano-Correa, Y. T., Frizzera, L., & Gianelle, D. (2022). Mapping a European Spruce Bark Beetle Outbreak Using Sentinel-2 Remote Sensing Data. In *Remote Sensing* (Vol. 14, Issue 13). https://doi.org/10.3390/rs14133135

DW. (2022). *Fires "under control" in Saxony and Brandenburg*. DW [Last Access 21/08/2024]. https://www.dw.com/en/wildfires-in-saxony-and-brandenburg-under-control/a-62613303

Fernández-Carrillo, Á., Franco-Nieto, A., Yagüe-Ballester, M. J., & Gómez-Giménez, M. (2024). Predictive Model for Bark Beetle Outbreaks in European Forests. *Forests*, *15*(7). https://doi.org/10.3390/f15071114

Fernandez-Carrillo, A., Patočka, Z., Dobrovolný, L., Franco-Nieto, A., & Revilla-Romero, B. (2020). Monitoring Bark Beetle Forest Damage in Central Europe. A Remote Sensing Approach Validated with Field Data. *Remote Sensing*, *12*(21), 3634.

Frantz, D., Haß, E., Uhl, A., Stoffels, J., & Hill, J. (2018). Improvement of the Fmask algorithm for Sentinel-2 images: Separating clouds from bright surfaces based on parallax effects. *Remote Sensing of Environment*, *215*, 471–481. https://doi.org/https://doi.org/10.1016/j.rse.2018.04.046

Garcia-Aristizabal, A., Almeida, M., Aubrecht, C., Polese, M., Ribeiro, L. M., Viegas, D., & Zuccaro, G. (2014). Assessment and management of cascading effects triggering forest fires. In *Advances in forest fire research* (pp. 1073–1085). Imprensa da Universidade de Coimbra. https://doi.org/10.14195/978-989-26-0884-6_117

Copyright © FirEUrisk Consortium. All rights reserved.

Hlásny, T. , Liebhold, A. , Montagné-Huck, C. , Müller, J. , Qin, H. , Raffa, K. , Schelhaas, M.-J. , Seidl, R. , Svoboda, M. , & Viiri, H. ,. (2019). *Living with bark beetles: impacts, outlook and management options*. Science to Policy 8. European Forest Institute. https://doi.org/https://doi.org/10.36333/fs08

Hlásny, T., Zimová, S., Merganičová, K., Štěpánek, P., Modlinger, R., & Turčáni, M. (2021). Devastating outbreak of bark beetles in the Czech Republic: Drivers, impacts, and management implications. *Forest Ecology and Management*, *490*, 119075. https://doi.org/https://doi.org/10.1016/j.foreco.2021.119075

Marzocchi, W., Garcia-Aristizabal, A., Gasparini, P., Mastellone, M. L., & Di Ruocco, A. (2012). Basic principles of multi-risk assessment: a case study in Italy. *Natural Hazards*, *62*(2), 551–573. https://doi.org/10.1007/s11069-012-0092-x

Seidl, R., Thom, D., Kautz, M., Martin-Benito, D., Peltoniemi, M., Vacchiano, G., Wild, J., Ascoli, D., Petr, M., Honkaniemi, J., Lexer, M. J., Trotsiuk, V., Mairota, P., Svoboda, M., Fabrika, M., Nagel, T. A., & Reyer, C. P. O. (2017). Forest disturbances under climate change. *Nature Climate Change*, *7*, 395–402. https://doi.org/10.1038/nclimate3303

Turbé, A., Jana, U., Toni, A., Woodward, S., Schopf, A., Netherer, S., Angelstam, P., Mudgal, S., & Sonigo, P. (2012). Disturbances of EU forests caused by biotic agents: final report. In *European Commision* (Vol. 270).

UNISDR. (2015). *Reading the Sendai Framework for Disaster Risk Reduction 2015 - 2030*.

Zuccaro, G., De Gregorio, D., & Leone, M. F. (2018). Theoretical model for cascading effects analyses. *International Journal of Disaster Risk Reduction*, *30*, 199–215. https://doi.org/10.1016/j.ijdrr.2018.04.019

2.2 Effects of bark beetle disturbance and fuel types on fire radiative power and burn severity in the Bohemian-Saxon Switzerland

Marrs, Christopher; Beetz, Kristina; Kranz, Johanna; Forkel, Matthias, Technische Universität Dresden,

(This section has been partially published as Kristina Beetz, Christopher Marrs, Annika Busse, Markéta Poděbradská, Daniel Kinalczyk, Johanna Kranz, Matthias Forkel, Effects of bark beetle disturbance and fuel types on fire radiative power and burn severity in the Bohemian-Saxon Switzerland, Forestry: An International Journal of Forest Research, 2024;, cpae024, https://doi.org/10.1093/forestry/cpae024).

Introduction

Since 2017, the Saxon Switzerland National Park in Saxony, Germany and its counterpart on the Czech side of the border, Bohemian Switzerland, have suffered a catastrophic outbreak of bark beetle (*Ips typographus*), the so-called epidemic phase (Hlásny et al., 2021). This has resulted in large swathes of Norway spruce (*Picea abies* (L.) Karst.) being killed off and large amounts of standing and fallen/prone deadwood of various sizes. As a result of the outbreak, 34% of the Saxon Switzerland National Park has dead, dying or affected trees. Bark beetle infestations are part of the natural functioning of forest ecosystems; however, climate-related factors have increased the vulnerability of tree to attack. There are two main climate-related factors associated with bark beetle outbreaks that increase this vulnerability.

Firstly, drought has a detrimental effect on trees, in the summer droughts of 2018 in central Europe severely affected European beech (*Fagus sylvatica*), Scot's pine (*Pinus sylvestris*) and the spruce (Schuldt et al., 2020). This weakened the trees, leading to early leaf senescence and deterioration of needles, respectively. The accelerated rate at which

Copyright © FirEURisk Consortium. All rights reserved.

nutrients are exported from dying tissue during senescence and subsequent benefits for organisms feeding upon the cambium has been hypothesised as one reason for the increase in vitality and survivability of bark beetle larvae (White, 2015).

Secondly, milder winters mean bark beetle are active for longer. This can mean more than one brood per year with obvious consequences for the trees. Weakened or damaged (Gilbert et al., 2005) trees, favoured by the bark beetle, and an increased number of beetles and longer periods of warm weather when the beetles start to swarm or spread out have affected much of Saxony's spruce resource. The beetle usually attacks larger and older trees, meaning that trees destined for timber have been, and continue to be lost. A number of geographic factors can also influence the location of the outbreaks such as density of stand, age, species diversity, slope, aspect and elevation (Kamińska et al., 2021; Nardi et al., 2023; Netherer and Nopp-Mayr, 2005; Sproull et al., 2016). Biotic factors also play a role but are less understood (Biedermann et al., 2019).

Bark Beetle Disturbance and Conservation

In the Bohemian and Saxon Switzerland National Parks the extraction of trees for timber or other purposes is not practiced in Core Zone, except for public safety reasons such as close to footpaths. The number and density of dead trees has been found to be a factor in the spread of bark beetle (Stereńczak et al., 2020) and thus this practice of little or no intervention may have had influence on the scale and continuation of the outbreak. However, for understandable reasons related to biodiversity, the deadwood is left in place and not salvaged. In a study of regeneration following an outbreak in the Czech Republic in the 1990's it was found that spruce, Rowan (*Sorbus aucuparia*) and European beech (*Fagus sylvatica*) recovered better without intervention, whereas areas clear-felled were repopulated by pioneer species such as Downy birch (*Betula pubescens*) and Aspen (*Populus tremula*) (Jonášová and Prach, 2004). Another study from Slovakia highlights the importance of protected forests with complex structures, i.e. with infected trees left in the forest, for stability in a changing climate (Potterf et al., 2023). Depending on the specific biodiversity objectives of a National Park, both approaches can be valuable for biodiversity in terms of habitat structure and diversity across a landscape. Standing dead trees and deadwood left on the forest floor are a supporting factor in maintaining biodiversity in forest systems (Johansson et al., 2017; Jonsson et al., 2005; Kuuluvainen et al., 2017; Martin et al., 2021) and is declining worldwide (Löfroth et al., 2023), it should be kept in mind that the bark beetle is part of this biodiversity. However, the loss of canopy due to insect-damage is also likely to have an effect on the microclimate of the understorey with consequences for biodiversity and species composition (Greiser et al., 2024; Ram et al., 2020) and resilience of forests to climate change (Albrich et al., 2020) and as such current and future forest management inside and outside of the national parks should take this into account.

Bark Beetle Disturbances and the Economy

Outside of National Parks, trees are removed from the forests as soon as they show signs of bark beetle infestation. Forest owners/managers are required by law to prevent the spread of bark beetle (Sachsenforst, 2017). Much of Saxony's Forest resource are economic forests and managed to provide wood products for market, as well as supporting biodiversity and ecosystem services such as rainfall interception and retention and recreation. However, the potential economic losses that would be incurred by forest owners/managers have meant large areas of spruce have been clear-felled or salvaged and sent to market, before the bark beetle can reduce its value to that of firewood. However, in a local market, large-scale mass and synchronised oversupply (Hlásny et al., 2021) will ultimately lead to

Copyright © FirEUrisk Consortium. All rights reserved.

lower prices and further financial loss. In Germany, following wide-spread felling of spruce the log prices dropped by almost 50% between early 2018 and the end of 2019 (Taylor, 2020).

In the Saxon Switzerland National Park, the beetle epidemic and resulting landscape change has not had a recognisable economic impact in terms of loss of timber revenue. It has however, been the subject of much debate and has certainly has a social impact, especially in local communities close to the Wildland Urban Interface (WUI). Fear of increased risk of fire or intensity of fire as a result of the large amounts of dry deadwood has become a political issue. With local communities already at odds with the National Park regarding access and rights, the danger of fire, whether real or perceived, has only added to this discontent (mdr.de, 2023a).

Pre-fire conditions

In 1990, upon designation, the National Park inherited a cultural landscape consisting of monocultures of spruce, Scot's pine and larch (*Larix* sp.) alongside remnant patches of European beech woodland as well as mixed woodlands of oak (*Quercus* sp.), birch, ash (*Fraxinus excelsior*), rowan and others. These blocks of single tree species meant that when the bark beetle took hold, concentrations of deadwood increased both in terms of standing deadwood and prone trees lying on the ground, consisting of large tree trunks, coarse woody debris as well small diameter wood, so-called fine fuels from the canopy (Figure 2.5). These fine fuels can be potentially readily consumed by fire (Nolan et al., 2022).

Such tree mortality can change the composition and condition of the forest floor fauna, in areas where canopy cover is low the increased exposure to solar radiation can increase soil temperatures and soil moisture (Yamulki et al., 2021) allowing grasses and other plants to proliferate, with consequences for flammability and wildfire risk. In Poland, for example, an increase in grass cover due to canopy mortality has effectively lengthened the fire season, with more fires in the winter/spring months (Ubysz., 2003). Forest fire statistics from southwest Poland and Saxony (Figure 2.6) support this with high numbers of fires outside of the expected summer fire season. Research from the northwest Czech Republic also confirms peaks in vegetation fire danger in late April (Možný and Bareš, 2014).

Understorey vegetation types in the National Park naturally vary according to the forest type. Within the dense coniferous stands, it consists of little more than a bed of dead needles with very little, small diameter dead wood. The beech understorey is typical of its type, with a thick carpet of leaves, thinly spaced beech saplings and sparsely spread deadwood of all diameters. The other forest parcels including the Scot's pine and mixed woodlands have a more varied understorey with a mixture of grasses, and bilberry (*Vaccinium* sp.), where dead spruce is found in the mixed forest, there are areas with higher loads of dead wood on the ground, as well as standing deadwood. In the dead and moribund monoculture spruce stands the understorey contains a large amount of deadwood of varying sizes as mentioned above (Figure 2.5). However, dependant on the stage of beetle attack and thus canopy cover there can be saplings and herbaceous plants taking advantage of the increased light conditions.

The Fire in 2022

On the 24th of July 2022 following long periods of dry and hot weather, a fire was deliberately lit by an arsonist (mdr.de, 2023b) in the Bohemian Switzerland National Park on the Czech side of the border. It was first identified by rangers on the German side of the border on the morning of 24th. By the next day on 25th, the fire was considered to be out of control, the fire was officially declared extinct on the 12th of August. The fire affected around 1,173 ha of the two protected areas, 1,060 ha in the Czech Republic and 113 ha in the Federal State of Saxony, Germany and required an effort from over 2,000 emergency service personnel from across Europe. The terrain, limited water supply, sub-surface

Copyright © FirEUrisk Consortium. All rights reserved.

fires, weather conditions and less than ideal communications between Czech and Saxony all played a role in the length of time it took to gain control of the fire. Thankfully there was no loss of life, though some injuries were sustained by firefighters and a number of buildings in the Czech village of Mezná were lost as a result of embers igniting the buildings or vegetation close to them. Whilst the loss of the trees and other vegetation caused no discernible economic loss as a result of the non-harvesting policy of the National Park, the cost of fighting the fire and lost revenue for hotels and businesses in the vicinity, reliant on visitors to the park, was considerable. No known estimates of the loss of ecosystem services have been undertaken to date, though there has certainly been a change with bare soils less able to absorb rainfall, leading to run-off and a clear loss of habitats, though successional habitats are now developing.

Following the fire, with the help of the Saxon Switzerland National Park, the Technische Universität Dresden, Institute of Photogrammetry and Remote Sensing with support from the Global Change Research Institute (CzechGlobe) of the Czech Academy of Sciences (CAS) and Bohemian Switzerland National Park Administration undertook research into the pre- and post-fire conditions, fire behaviour and analysis of the types of vegetation burnt. A modelling study of this fire has been recently published by researchers from CzechGlobe (Kudláčková et al., 2023).



Figure 2.5 Example of spruce stand affected by bark beetle with standing and prone deadwood. (image: Christopher Marrs)

Copyright © FirEURisk Consortium. All rights reserved.

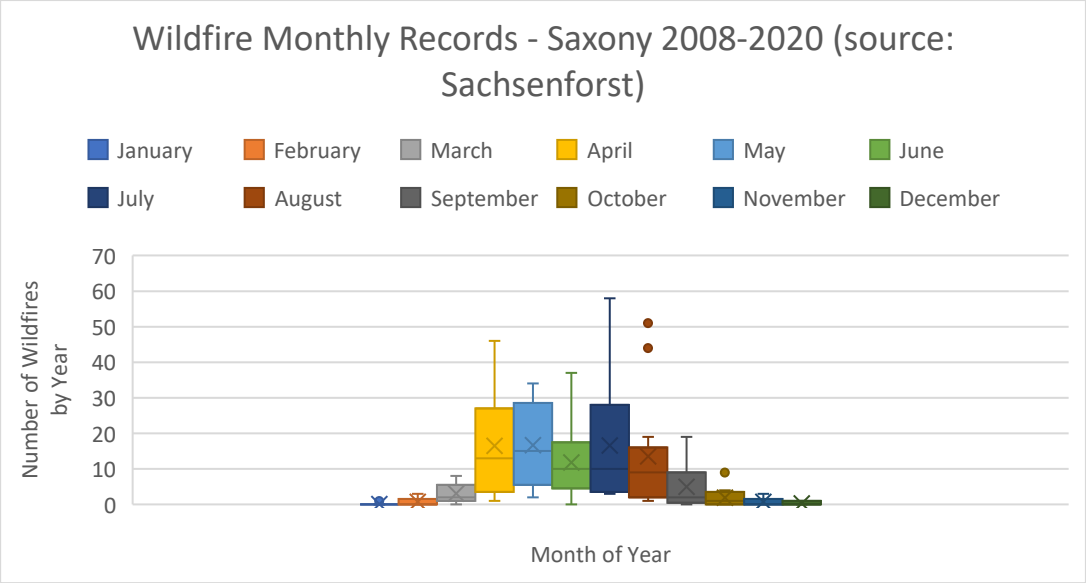


Figure 2.6 Forest fire statistics for Saxony 2008-2020 (source: Sachsenforst).

Weather conditions

In the weeks leading up to the fire the weather conditions favoured the outbreak of fire or rather the likelihood of propagation, with long periods of little or no rain and high temperatures. Night-time temperatures in the week leading up to the fire were on average 15° C, reducing moisture recovery. Despite the alignment of these factors for increased fire danger, the Saxon Fire Warning Level (*Waldbrandindex*) was level three (medium), on a scale of one to five, five being the highest. Dead fuel moisture levels (10-hour) recorded by a weather station destroyed by the fire were below 20% in the two weeks leading up to the ignition.

Analysis of the fire

Field Surveys

Following the fire in the autumn of 2022 researchers from TU Dresden undertook an extensive survey of the post-fire conditions across 21 sites in the burnt area (Beetz et al., 2024). This involved assessing the fire intensity through the application of a Composite Burn Index (CBI). The CBI used was a combination of GeoCBI (De Santis and Chuvieco, 2009) and the CBI of (Key and Benson, 2006) and took account of 5 stratum with the forests, pre-fire conditions, and where possible, post-fire conditions. Pre-fire condition variables included: litter cover, litter depth, duff depth, bare cover, main species, number of living trees, and numbers of dead. Post-fire condition variables included: area affected, duff consumed, litter consumed, fine/coarse woody debris consumed, soil colour change, black/brown leaves, living (surviving) vegetation, new growth, species, leaf cover loss, canopy mortality and char height.

The results of the field surveys revealed that in all sites the ground cover suffered a high severity of burning (Figure 2.7), in several site this included the combustion of the duff layer down to the clayey sub-soils. The combustion of the shrub layer was varied according to the forest type, in areas dominated by dead spruce this layer was lost. In others, where lying deadwood was not so concentrated, many trees suffered only leaf/needle loss, though whether the shrub will recover has yet to be determined.

Copyright © FirEUrisk Consortium. All rights reserved.

An indication of the intensity of the fire and flame length is given by the scorch height, which is how high up the tree stem evidence of burning can be seen. In the broadleaved woodlands, mostly beech, this was seldom more than a metre. In the mixed woodland it was higher, though mainly on the dead spruce stems within the mixed woodland. It is in the dead spruce stands where the highest charring took place, often visible above 6 metres. In the dead spruce stands the highest fire intensity was recorded and observed throughout the burnt area.

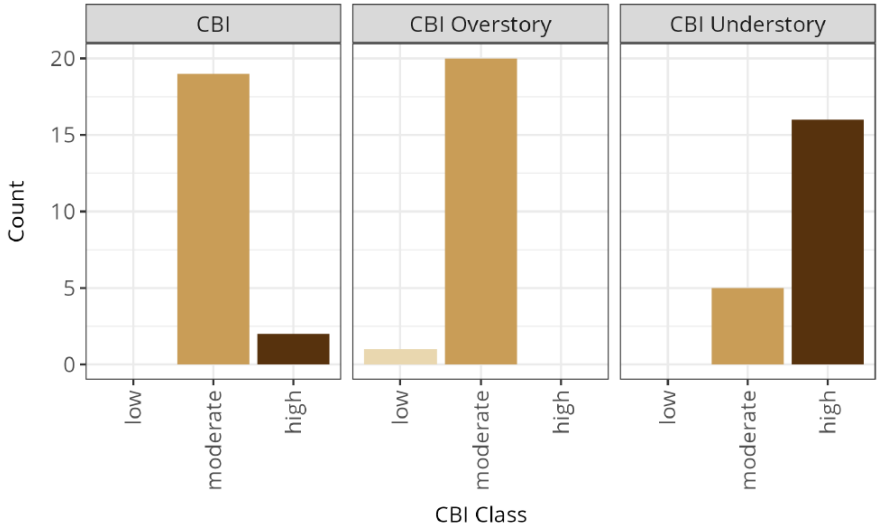


Figure 2.7 Composite Burn Index Results for the 21 Sites Recorded (Beetz, 2022)

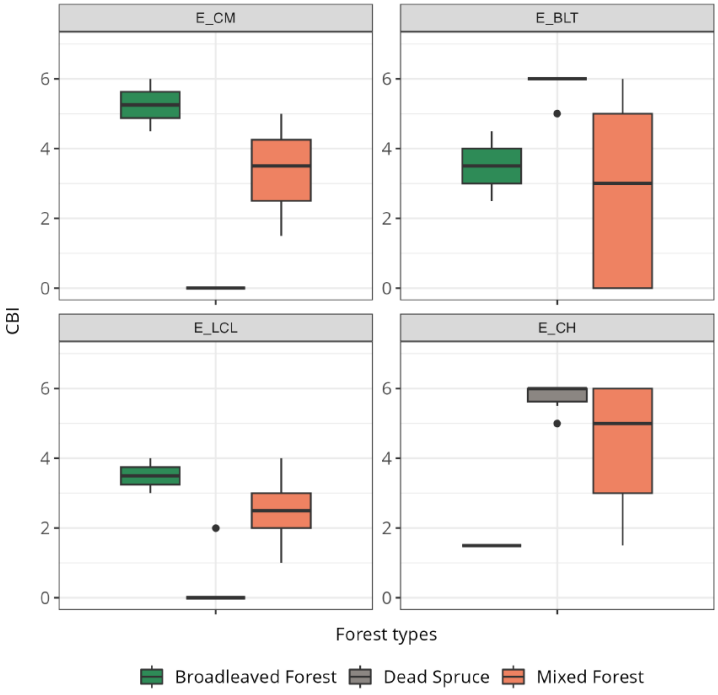


Figure 2.8 Composite Burn Index Values for tall trees >20m

Copyright © FirEURisk Consortium. All rights reserved.

(CM: canopy mortality, BLT: black leaves torch, LCL: leaf cover loss, CH: char height) (Beetz, 2022)

Use of satellite remote sensing

Additional research to understand the burn severity was carried out using satellite remote sensing images. Employing a combination of Sentinel-2A/2B and Landsat 8/9 images from August and September 2021 (year before the fire) and from the same months in 2022 (after the fire) the Normalised Burn Ratio (NBR) and Difference Normalised Burn Ratio (dNBR) indices could be calculated. The dNBR was then classified into seven severity levels according to (Key and Benson, 2006) ranging from High Severity to Enhanced Regrowth (Table 2.1).

Table 2.1 Burn severity levels identified using the dNBR for both National Parks (Beetz, 2022)

Severity Level	Area (ha)	Percentage of total burnt area* (%)
High severity	38.2	3.3
Moderate-high severity	302.4	25.8
Moderate-low severity	395.3	33.7
Low severity	297.8	25.4
Unburnt	116.7	9.9
Enhanced regrowth, low	23.6	2
Enhanced regrowth, high	0	0

*Note, burnt area refers to the area within the fire perimeter as identified by the National Parks, which contains some areas not affected by the fire

Table 2.2 Burnt Area by Forest Type Saxon Switzerland (Beetz, 2022)

Forest Type	Area (ha)
Bark beetle affected spruce stands	50
Sparsely vegetated rocky outcrops	15
Pine	13
Beech	6
Other hardwoods	2
Rest (including Includes spruce (live), birch, larch, mesic grassland, oak, shrub heathland, riverine, arable, peat land and seasonal wet grassland)	27

Whilst the table above indicates that bark beetle affected spruce stands make up a high percentage of the forest damaged by the fire, it should be noted that this is a reflection of amount of these stands in the Saxon Switzerland National Park and should not be understood as their flammability in this context.

Observational interpretation of the fire

During the 21 field visits to the burnt areas of the National Parks there were a number of observations of note and worth elaborating upon. It was clear that in the small valleys, and on the slopes the most severe and complete combustion took place. In such locations within the Bohemian Switzerland in Czechia there was almost total

Copyright © FirEURisk Consortium. All rights reserved.

combustion of the available fuels, both live and dead. This was due to their alignment with the prevailing wind, slope and available fuels. The calculation of the dNBR also supports this correlation between slope and high severity.

In the beech forests only the ground layer, consisting of dry leaves was partially consumed by the fire and scorching of the standing live trees was low, often less than a metre. The exception to this were the edges of the beech forest at the top of the slope, it was here where the highest mortality took place, with very large and old trees killed by the heat and flames travelling up the slopes (Figure 2.9).



Figure 2.9 Beech trees severely affected by the flames rising up the slope (image: Christopher Marrs)



Figure 2.10 Incomplete combustion of large prone deadwood (image: Christopher Marrs).

In the area which were predominately dead or dying spruce, the ground layer was totally consumed by the flames, yet the large dry logs lying on the ground burnt to a depth of no more that 1-2cm. It could be assumed that once the fast-burning mix of dry dead fuels and combustible live vegetation had been consumed and the fire had moved on that

Copyright © FirEUrisk Consortium. All rights reserved.

these large logs ceased to burn (Figure 2.10). Perhaps the most surprising fire behaviour was observed by a wildlife camera trap, which recorded the approach and passing of the fire front. Images taken by the camera show seemingly healthy green vegetation of grasses and bilberry being totally consumed by the fire (Figure 2.11). The camera trap images were time-stamped and from this and measurements in the field (forest) the rate of spread could be calculated and revealed a rate of around 1 metre per minute. With this information the fuel model type can be better identified and improve fire behaviour predictive modelling.



Figure 2.11 Sequence of images taken by wildlife camera trap, before, during and after the fire (images: Courtesy of Saxon Switzerland National Park Administration).

Other important field observations included the height at which the standing dead spruce burnt, in some areas this was over and above 6 m. At such heights it is likely that this contributed to spot fires, one of which was around 1.3 km downwind from the fire front.

Copyright © FirEUrisk Consortium. All rights reserved.

Finally, it is clear from the field visits that the fire fighters worked in very difficult conditions. The sheer amount of large prone spruce trees would have made for extremely slow progress on foot coupled with the burning standing trees, many of which fell during the fire, made this both a difficult and very dangerous fire to tackle and probably contributed towards the extended period required to extinguish the fire.

Discussion and Conclusions

The fire of 2022 in the Bohemian and Saxon Switzerland National Parks provides a remarkable example of transboundary compounding effects and their influence on fire risk. Neither the bark beetle infestation nor fire respect administrative boundaries. Areas within the fire perimeter containing standing and prone deadwood burnt with a high intensity. The intensity of the deadwood areas burning, and terrain ensured that adjacent, perhaps less-flammable, forest parcels were affected. The height at which the standing deadwood burnt most likely contributed to spot fires and the spread of the fire. Most of the small diameter woody debris in the dead stands affected by the fire were consumed, meaning that only emergent vegetation and large diameter logs remain. Dependant on the regenerated vegetation type(s) it could be said that chances of a high energy fire in these locations in the future is low. However, some stands affected by the fire have a new accumulation of fuels due to post-fire mortality or the remains of unburnt dead branches that fell after the fire. Large swathes of dead spruce stands remain in the Parks that were not affected by the fire, they remain in a highly combustible state and thus the danger remains. Should a fire *not* break out in the near future, this danger level could be expected to reduce as the small woody debris decomposes, leaving only the large diameter logs. The decomposition rate will be determined by the surrounding vegetation and weather conditions (Aakala, 2010; Herrmann and Bauhus, 2013), neither of which can be accurately predicted at this time. Other research indicates species and size (diameter) as important factors for decomposition (Herrmann et al., 2015).

Outside of the national parks, the clear-felling of spruce as a result of actual or expected bark beetle infestation has changed the landscape and fuel types. Increased light levels and pioneer species, as well young saplings (regeneration and afforested) will change the propagation characteristics (Kitzberger et al., 2012; Thompson et al., 2011; Philip J. Zylstra et al., 2022) with higher flame lengths and rate of spread due to grasses and lower canopy base height. This may or may not increase the likelihood of fire dependant on the prevailing weather conditions, but would certainly have an impact on the possibility of fires spreading to established forests.

There is an irony in the two approaches to dealing with the bark beetle outbreak inside and outside of the National Parks. Within the parks the dead spruce stands were left in situ for the sake of biodiversity enhancement, which, should a fire not happen, will eventually be the case. Outside of the park the trees were removed for economic reasons resulting in a habitat change, most likely an improvement on monoculture spruce forest, but in the short term the risk of fire or risk of fire spreading to established woodlands has most likely increased. The full ecological and fire danger-related effects of the mass outbreak of bark beetle both inside and outside the National Parks may yet lie ahead of us.

Copyright © FirEUrisk Consortium. All rights reserved.

References

Aakala, T., 2010. Coarse woody debris in late-successional Picea abies forests in northern Europe: Variability in quantities and models of decay class dynamics. For. Ecol. Manag. 260, 770–779. https://doi.org/10.1016/j.foreco.2010.05.035

Albrich, K., Rammer, W., Seidl, R., 2020. Climate change causes critical transitions and irreversible alterations of mountain forests. Glob. Change Biol. 26, 4013–4027. https://doi.org/10.1111/gcb.15118

Beetz, K., 2022. Forest fires in the Bohemian-Saxon Switzerland in 2022: Mapping and analysis of fuel types, fire dynamics and severity using remote sensing data, Masters Thesis.

Beetz, K., Marrs, C., Busse, A., Poděbradská, M., Kinalczyk, D., Kranz, J., 2024. Role of bark beetle disturbance and fuel types on fire radiative power and burn severity in the Bohemian-Saxon Switzerland. Forestry in review.

Biedermann, P.H.W., Müller, J., Grégoire, J.-C., Gruppe, A., Hagge, J., Hammerbacher, A., Hofstetter, R.W., Kandasamy, D., Kolarik, M., Kostovcik, M., Krokene, P., Sallé, A., Six, D.L., Turrini, T., Vanderpool, D., Wingfield, M.J., Bässler, C., 2019. Bark Beetle Population Dynamics in the Anthropocene: Challenges and Solutions. Trends Ecol. Evol. 34, 914–924. https://doi.org/10.1016/j.tree.2019.06.002

De Santis, A., Chuvieco, E., 2009. GeoCBI: A modified version of the Composite Burn Index for the initial assessment of the short-term burn severity from remotely sensed data. Remote Sens. Environ. 113, 554–562. https://doi.org/10.1016/j.rse.2008.10.011

Gilbert, M., Nageleisen, L.-M., Franklin, A., Gregoire, J.-C., 2005. Post-storm surveys reveal large-scale spatial patterns and influences of site factors, forest structure and diversity in endemic bark-beetle populations. Landsc. Ecol. 20, 35–49. https://doi.org/10.1007/s10980-004-0465-y

Greiser, C., Hederová, L., Vico, G., Wild, J., Macek, M., Kopecký, M., 2024. Higher soil moisture increases microclimate temperature buffering in temperate broadleaf forests. Agric. For. Meteorol. 345, 109828. https://doi.org/10.1016/j.agrformet.2023.109828

Herrmann, S., Bauhus, J., 2013. Effects of moisture, temperature and decomposition stage on respirational carbon loss from coarse woody debris (CWD) of important European tree species. Scand. J. For. Res. 28, 346–357. https://doi.org/10.1080/02827581.2012.747622

Herrmann, S., Kahl, T., Bauhus, J., 2015. Decomposition dynamics of coarse woody debris of three important central European tree species. For. Ecosyst. 2, 27. https://doi.org/10.1186/s40663-015-0052-5

Hlásny, T., König, L., Krokene, P., Lindner, M., Montagné-Huck, C., Müller, J., Qin, H., Raffa, K., Schelhaas, M.-J., Svoboda, M., Viiri, H., Seidl, R., 2021. Bark Beetle Outbreaks in Europe: State of Knowledge and Ways Forward for Management. Curr. For. Rep. 7, 1–28. https://doi.org/10.1007/s40725-021-00142-x

Johansson, T., Gibb, H., Hjältén, J., Dynesius, M., 2017. Soil humidity, potential solar radiation and altitude affect boreal beetle assemblages in dead wood. Biol. Conserv. 209, 107–118. https://doi.org/10.1016/j.biocon.2017.02.004

Jonášová, M., Prach, K., 2004. Central-European mountain spruce (Picea abies (L.) Karst.) forests: regeneration of tree species after a bark beetle outbreak. Ecol. Eng. 23, 15–27. https://doi.org/10.1016/j.ecoleng.2004.06.010

Jonsson, B.-G., Kruys, N., Ranius, T., 2005. Ecology of species living on dead wood - Lessons for dead wood management. Silva Fenn. 39, 289–309.

Kamińska, A., Lisiewicz, M., Kraszewski, B., Stereńczak, K., 2021. Mass outbreaks and factors related to the spatial dynamics of spruce bark beetle (Ips typographus) dieback considering diverse management regimes in the Białowieża forest. For. Ecol. Manag. 498, 119530. https://doi.org/10.1016/j.foreco.2021.119530

Copyright © FirEUrisk Consortium. All rights reserved.

Key, C., Benson, N., 2006. Landscape Assessment: Ground measure of severity, the Composite Burn Index; and Remote sensing of severity, the Normalized Burn Ratio., in: FIREMON: Fire Effects Monitoring and Inventory System. p. LA 1-51.

Kitzberger, T., Aráoz, E., Gowda, J.H., Mermoz, M., Morales, J.M., 2012. Decreases in Fire Spread Probability with Forest Age Promotes Alternative Community States, Reduced Resilience to Climate Variability and Large Fire Regime Shifts. Ecosystems 15, 97–112. https://doi.org/10.1007/s10021-011-9494-y

Kudláčková, L., Poděbradská, M., Bláhová, M., Cienciala, E., Beranová, J., McHugh, C., Finney, M., Novotný, J., Zahradníček, P., Štěpánek, P., Linda, R., Pikl, M., Vébrová, D., Možný, M., Surový, P., Žalud, Z., Trnka, M., 2023. Using FlamMap to assess wildfire behavior in Bohemian Switzerland National Park. Nat. Hazards. https://doi.org/10.1007/s11069-023-06361-8

Kuuluvainen, T., Aakala, T., Várkonyi, G., 2017. Dead standing pine trees in a boreal forest landscape in the Kalevala National Park, northern Fennoscandia: amount, population characteristics and spatial pattern. For. Ecosyst. 4, 12. https://doi.org/10.1186/s40663-017-0098-7

Löfroth, T., Birkemoe, T., Shorohova, E., Dynesius, M., Fenton, N.J., Drapeau, P., Tremblay, J.A., 2023. Deadwood Biodiversity, in: Girona, M.M., Morin, H., Gauthier, S., Bergeron, Y. (Eds.), Boreal Forests in the Face of Climate Change: Sustainable Management, Advances in Global Change Research. Springer International Publishing, Cham, pp. 167–189. https://doi.org/10.1007/978-3-031-15988-6_6

Martin, M., Tremblay, J.A., Ibarzabal, J., Morin, H., 2021. An indicator species highlights continuous deadwood supply is a key ecological attribute of boreal old-growth forests. Ecosphere 12, e03507. https://doi.org/10.1002/ecs2.3507

mdr.de, 2023a. Ein Jahr nach dem Waldbrand: Wie weiter in der Sächsischen Schweiz? | MDR.DE [WWW Document]. URL https://www.mdr.de/nachrichten/sachsen/dresden/freital-pirna/waldbrand-saechsische-schweiz-streit-nationalpark-100.html (accessed 2.26.24).

mdr.de, 2023b. Waldbrände 2022 in Nationalparks: Mutmaßlicher Brandstifter war vorbestraft | MDR.DE [WWW Document]. URL https://www.mdr.de/nachrichten/sachsen/dresden/freital-pirna/feuer-waldbrand-boehmische-schweiz-verdaechtiger-100.html (accessed 2.26.24).

Možný, M., Bareš, D., 2014. Forecast danger of vegetation fires in the open countryside in the Czech Republic.

Nardi, D., Jactel, H., Pagot, E., Samalens, J.-C., Marini, L., 2023. Drought and stand susceptibility to attacks by the European spruce bark beetle: A remote sensing approach. Agric. For. Entomol. 25, 119–129. https://doi.org/10.1111/afe.12536

Netherer, S., Nopp-Mayr, U., 2005. Predisposition assessment systems (PAS) as supportive tools in forest management—rating of site and stand-related hazards of bark beetle infestation in the High Tatra Mountains as an example for system application and verification. For. Ecol. Manag., Decision Support in Multi Purpose Forestry 207, 99–107. https://doi.org/10.1016/j.foreco.2004.10.020

Nolan, R.H., Price, O.F., Samson, S.A., Jenkins, M.E., Rahmani, S., Boer, M.M., 2022. Framework for assessing live fine fuel loads and biomass consumption during fire. For. Ecol. Manag. 504, 119830. https://doi.org/10.1016/j.foreco.2021.119830

Potterf, M., Svitok, M., Mezei, P., Jarčuška, B., Jakuš, R., Blaženec, M., Hlásny, T., 2023. Contrasting Norway spruce disturbance dynamics in managed forests and strict forest reserves in Slovakia. For. Int. J. For. Res. 96, 387–398. https://doi.org/10.1093/forestry/cpac045

Copyright © FirEUrisk Consortium. All rights reserved.

Ram, D., Lindström, Å., Pettersson, L.B., Caplat, P., 2020. Forest clear-cuts as habitat for farmland birds and butterflies. For. Ecol. Manag. 473, 118239. https://doi.org/10.1016/j.foreco.2020.118239

Sachsenforst, 2017. Borkenkäfer - Hinweise für Waldbesitzer.

Schuldt, B., Buras, A., Arend, M., Vitasse, Y., Beierkuhnlein, C., Damm, A., Gharun, M., Grams, T.E.E., Hauck, M., Hajek, P., Hartmann, H., Hiltbrunner, E., Hoch, G., Holloway-Phillips, M., Körner, C., Larysch, E., Lübbe, T., Nelson, D.B., Rammig, A., Rigling, A., Rose, L., Ruehr, N.K., Schumann, K., Weiser, F., Werner, C., Wohlgemuth, T., Zang, C.S., Kahmen, A., 2020. A first assessment of the impact of the extreme 2018 summer drought on Central European forests. Basic Appl. Ecol. 45, 86–103. https://doi.org/10.1016/j.baae.2020.04.003

Sproull, G.J., Adamus, M., Szewczyk, J., Kersten, G., Szwagrzyk, J., 2016. Fine-scale spruce mortality dynamics driven by bark beetle disturbance in Babia Góra National Park, Poland. Eur. J. For. Res. 135, 507–517. https://doi.org/10.1007/s10342-016-0949-8

Taylor, R., 2020. Spruce bark beetle and its impact on wood markets. Int. For. Ind. URL https://internationalforestindustries.com/2020/06/09/spruce-bark-beetle-impact-wood-markets/ (accessed 2.16.24).

Thompson, J.R., Spies, T.A., Olsen, K.A., 2011. Canopy damage to conifer plantations within a large mixed-severity wildfire varies with stand age. For. Ecol. Manag. 262, 355–360. https://doi.org/10.1016/j.foreco.2011.04.001

Ubysz., B., 2003. The influence factors on the forest fire danger in Poland [WWW Document]. URL https://www.fao.org/3/xii/0009-b3.htm (accessed 7.20.22).

White, T.C.R., 2015. Are outbreaks of cambium-feeding beetles generated by nutritionally enhanced phloem of drought-stressed trees? J. Appl. Entomol. 139, 567–578. https://doi.org/10.1111/jen.12195

Yamulki, S., Forster, J., Xenakis, G., Ash, A., Brunt, J., Perks, M., Morison, J.I.L., 2021. Effects of clear-fell harvesting on soil CO2, CH4, and N2O fluxes in an upland Sitka spruce stand in England. Biogeosciences 18, 4227–4241. https://doi.org/10.5194/bg-18-4227-2021

Zylstra, Philip J., Bradshaw, S.D., Lindenmayer, D.B., 2022. Self-thinning forest understoreys reduce wildfire risk, even in a warming climate. Environ. Res. Lett. 17, 044022. https://doi.org/10.1088/1748-9326/ac5c10

Zylstra, Philip J, Bradshaw, S.D., Lindenmayer, D.B., 2022. Self-thinning forest understoreys reduce wildfire risk, even in a warming climate. Env. Res Lett.

2.3 Fire behaviour and propagation potential in areas affected by bark beetle infestation

Bugarić, M., Stipaničev, D., Faculty of Electrical Engineering, Mechanical Engineering and Naval Architecture (FESB) and Gómez-Giménez, M, Zaprzala, S., Fernández-Carrillo, A., Franco-Nieto, A., and Julia Yagüe Ballester (GMV).

Introduction

The complexity of wildfire behaviour, influenced by a myriad of factors including vegetation type, climate conditions, and especially forest health issues such as bark beetle infestations, necessitates a detailed understanding and innovative approaches to wildfire management and mitigation strategies. This study focuses on Pilot Site 2, encompassing the Saxon Switzerland National Park and adjacent areas, which have recently experienced significant bark beetle outbreaks leading to altered forest fuel conditions and subsequently affecting wildfire propagation potential. The main objectives of this research are as follows:

Copyright © FirEUrisk Consortium. All rights reserved.

- To assess the impact of bark beetle infestations on forest fuel models and understand how these alterations influence the wildfire propagation potential in Pilot Site 2.
- To employ and evaluate advanced geospatial data processing and predictive modelling techniques to calculate wildfire propagation potential, incorporating updated fuel maps reflective of bark beetle damage.
- To provide insights into the implications of changed forest fuel conditions for wildfire behaviour and risk management in the affected area.
- Develop a proof of concept to integrate bark beetle damage into a fire behaviour analysis.

Methods: Overview of propagation potential

The concept of propagation potential is integral to wildfire risk management, representing the likelihood and potential intensity of wildfire spread under specific environmental conditions. Calculating this metric involves integrating various static and dynamic factors, including topography, vegetation (fuel models), and current weather conditions. This study utilises the FlamMap software, a fire behaviour prediction and analysis tool, to estimate the wildfire propagation potential across Pilot Site 2. The analysis is further enriched by incorporating bark beetle-induced alterations to the fuel models, reflecting the real-world condition of the forests more accurately.
In FirEURisk, we defined a Propagation potential - calculation methodology for Pilot Sites (PS), the overview of the procedure for propagation potential calculation using FlamMap is as follows:

- Preparation of static input data in FlamMap form for each PS that includes: Elevation, Slope, Aspect, Fuel model (FM), Canopy Cover [CC], Canopy Height (CH), Canopy Base Height (CBH) and Canopy Bulk Density (CBD) (Figure 2.12).
- Collection of essential weather data and fuel moisture data of past fires in PS territory during the last 20 years including estimation of all moisture parameters necessary for Initial Fuel Moisture (FMS file (Live Woody, Live Herbaceous, 1-h, 10-h and 10-h Dead Fuel Moisture) and wind data). Diving input weather and moisture data according to wind directions. Filtering the data and take only wind direction scenarios that are responsible for >10% historical fires. Calculating annually burnt area on average per wind direction scenarios. Calculating 95-percentile and 50-percentile values for: live woody fuel moisture content, wind speed (gust) and 1h dead fuel moisture for selected wind direction scenarios.
- Running FlamMap simulations for each combination of wind direction, wind speed and fuel moisture content. The last step is to combine all the results. For the basic FlamMap run, burnt area is used as a factor to combine the overall result. The procedure is to calculate the percentage of burnt area (from overall burnt area) that is happening for a certain combination of input data. It is important to know whether to assign the burnt area to extreme or average scenario (the 50-percentile and the 95-percentile) for that wind direction scenario.

Therefore, for this research, the following methodology was used:

- Data Acquisition: Collect comprehensive static (elevation, slope, aspect, and fuel models) and dynamic (weather conditions, vegetation health) data. Special attention is given to incorporating the latest satellite imagery and forest inventory data to map bark beetle damage.
- Fuel Model Updates: Utilise the Scott and Burgan fuel classification system as a basis but modify fuel models based on the severity of bark beetle infestation observed. This includes reclassifying areas with significant

Copyright © FirEURisk Consortium. All rights reserved.

deadwood accumulation as a result of beetle damage to more appropriate fuel models that reflect their increased fire risk.

- FlamMap Analysis: Input the updated fuel models into FlamMap, along with other necessary static and dynamic data, to simulate potential fire behaviour scenarios. The software provides outputs including fire spread direction, speed, and intensity, which are interpreted as the wildfire propagation potential.

The accurate calculation of wildfire propagation potential is crucial for effective pre-fire planning and real-time firefighting strategies. By integrating the effects of bark beetle damage into this calculation, this study aims to provide more nuanced insights into wildfire risks and behaviour, supporting informed decision-making for forest and wildfire management in Pilot Site 2.

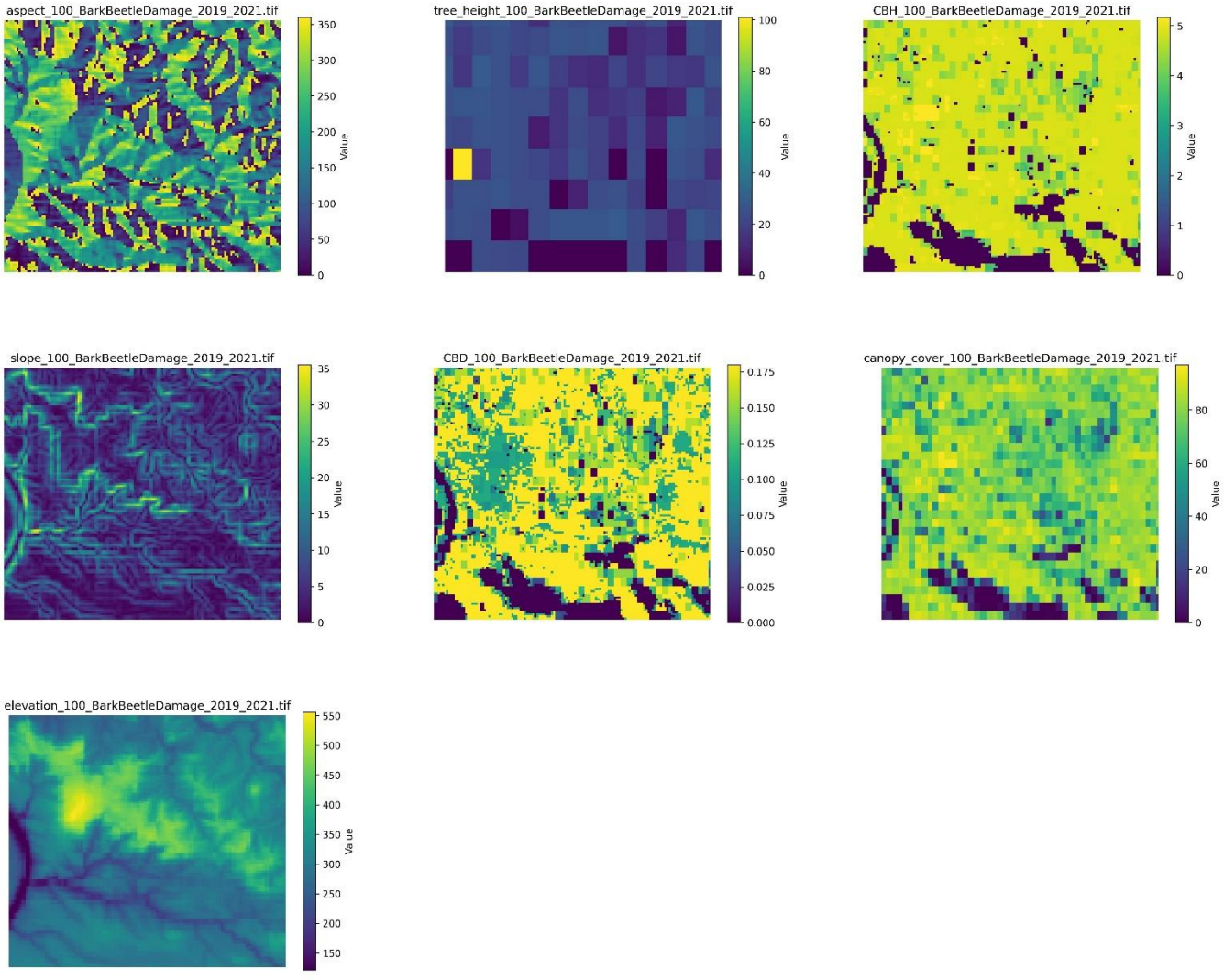


Figure 2.12 FlamMap input layers for the propagation potential.

Copyright © FirEURisk Consortium. All rights reserved.

Bark beetle infestation influence on fire behaviour

The FlamMap simulations were estimated using a layer containing the bark beetle damage between 2019 and 2021 (Fernández-Carrillo et al., 2024). The objective of this analysis was to capture through a modelling approach the influence of this biotic damage into the behaviour and spread of the fire occurred in the Bohemian and Saxon Switzerland National Parks in 2022. The bark beetle damage includes three categories i.e., 1= mild, 2= moderate, 3= severe (Figure 2.13). Those classes were associated with the Scott and Burgan categories considering the expected effect of the biotic damage on fuel types. For example, the Scott and Burgan TL5 category: *high load conifer litter; light slash or mortality fuel*. Spread rate low; flame length low) was associated with the bark beetle category 3: severe damage. The Scott and Burgan category TL3 category: *Moderate load conifer litter. Spread rate very low; flame length low* was associated with mild and moderate biotic damages. The suitability of this classification should be confirmed with in-situ data. Therefore, the results of this analysis are for testing purposes and to show a proof of concept.

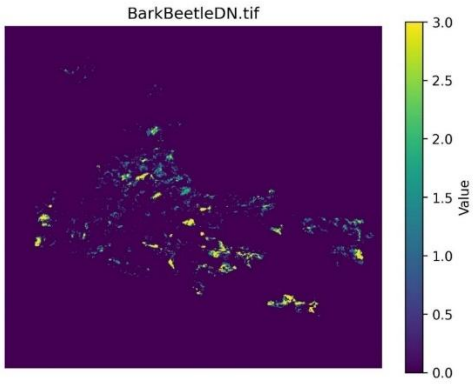


Figure 2.13 Layer containing estimated bark beetle damage.

- **Damage Severity Classification**:
  - The study commenced with the analysis of the provided bark beetle damage layer, which detailed the extent of infestation across various forest sections. This layer's classifications of damage severity allowed for a nuanced approach to updating the fuel models.
- **Fuel Model Adjustment:**
  - Leveraging the classifications within the bark beetle damage layer, adjustments were made to the official FirEUrisk Pilot site fuel models to reflect the current forest condition. This process involved mapping the severity of damage (mild, moderate, severe) to specific codes within the Scott and Burgan fuel model system, ensuring that the updated fuel models accurately represented the altered fuel conditions due to bark beetle damage.
- **Predictive Modelling Enhancement:**
  - With the adjusted fuel models, the study further applied predictive modelling tools to simulate potential fire behaviour under the updated forest conditions. This crucial step allowed for the evaluation of how changes in fuel, attributed to bark beetle damage, could potentially influence fire spread and intensity.

Copyright © FirEUrisk Consortium. All rights reserved.

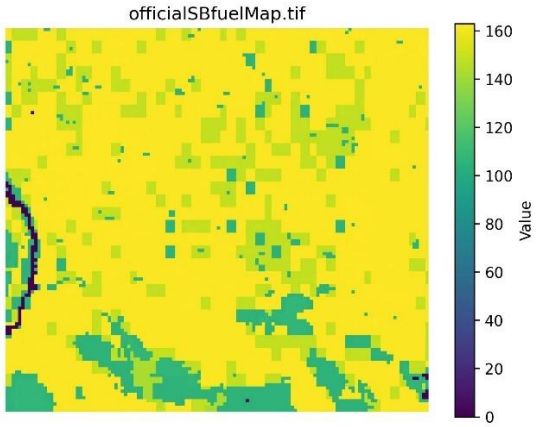


Figure 2.14 Official 100m resolution FirEURisk fuel map for the region.

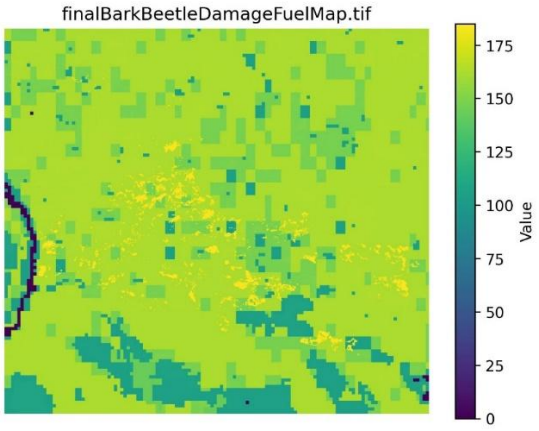


Figure 2.15 Adjusted 100m resolution FirEURisk fuel map for the region with integrated bark beetle damage.

The initial fuel map (Figure 2.14) serves as a baseline reference, illustrating the pre-adjustment forest conditions and fuel distributions across the Saxon Switzerland National Park. This visual comparison underscores the significance of incorporating ecological disturbances into fuel model adjustments. With the updated fuel models, FlamMap simulations were conducted for each weather scenario identified as relevant to PS2. These scenarios were designed to encompass a broad spectrum of conditions, from typical to extreme, thereby providing a comprehensive understanding of potential fire behaviour across different environmental contexts.

scenario	percentile	wind speed (gust)	li	1h dead fuel moisture	1h dfmc (72.5p)	burned area (sum)	burned a	number of fires	average fire size	fire size stdev
north	95 percentile	11.12280392646789	-	7.4308510568726405	13.618563500109339	211.11999999999998	1.44	59	3.58	4.41
north	50 percentile	6.224161148071289	-	17.39268589479297	13.618563500109339	281.8	1.93	159	1.77	1.55
northeast	95 percentile	11.586869239807127	-	6.985442484271598	11.626357505338246	588.489	4.03	60	9.81	34.78
northeast	50 percentile	6.747329711914063	-	15.87661454171587	11.626357505338246	482.9549999999999	3.31	161	3.0	7.95
east	95 percentile	13.0086669921875	-	7.126091371611988	11.781585026065862	971.4200000000001	6.65	140	6.94	22.88
east	50 percentile	8.581618309020996	-	15.101324192703864	11.781585026065862	1024.9100000000003	7.01	401	2.56	4.65
southeast	95 percentile	13.148336505889892	-	6.486067482933433	10.26912280973192	454.7	3.11	121	3.76	6.84
southeast	50 percentile	8.193625450134277	-	14.05491254059475	10.26912280973192	667.0613999999999	4.57	294	2.27	2.25
south	95 percentile	13.46990156173706	-	7.3891280288267644	12.592961236267858	2263.9130999999998	15.49	198	11.43	63.51
south	50 percentile	8.360235691070557	-	15.703340744910511	12.592961236267858	1569.8799999999999	10.74	558	2.81	10.84
southwest	95 percentile	13.695022010803225	-	7.978876244001514	11.98503687889402	1195.83	8.18	158	7.57	34.47
southwest	50 percentile	8.569026947021484	-	16.029643500424772	11.98503687889402	1031.0049999999999	7.06	451	2.29	2.19
west	95 percentile	16.648635864257812	-	8.201917119412414	13.070544630538151	1483.3154999999997	10.15	170	8.73	30.21
west	50 percentile	9.592805862426758	-	17.52028045039452	13.070544630538151	928.268	6.35	403	2.3	4.05
northwest	95 percentile	14.833181858062744	-	8.258991063094895	14.217311946533181	687.63	4.71	115	5.98	12.63
northwest	50 percentile	8.946209907531738	-	17.837377703424856	14.217311946533181	769.97	5.27	292	2.64	6.39

Figure 2.16 Stage 1 summary table for PS2 Central-Eastern Europe.

This project has received funding from the European Union's Horizon 2020 research and innovation programme under grant agreement No 101003890.

Following the initial assessment and classification of bark beetle damage, the next step was the geospatial analysis. This stage was crucial for translating the categorised damage severities into actionable data within the context of wildfire behaviour prediction and management. For every significant weather scenario, FlamMap simulations were carried out, for both original and bark beetle infected version of FlamMap landscape file.

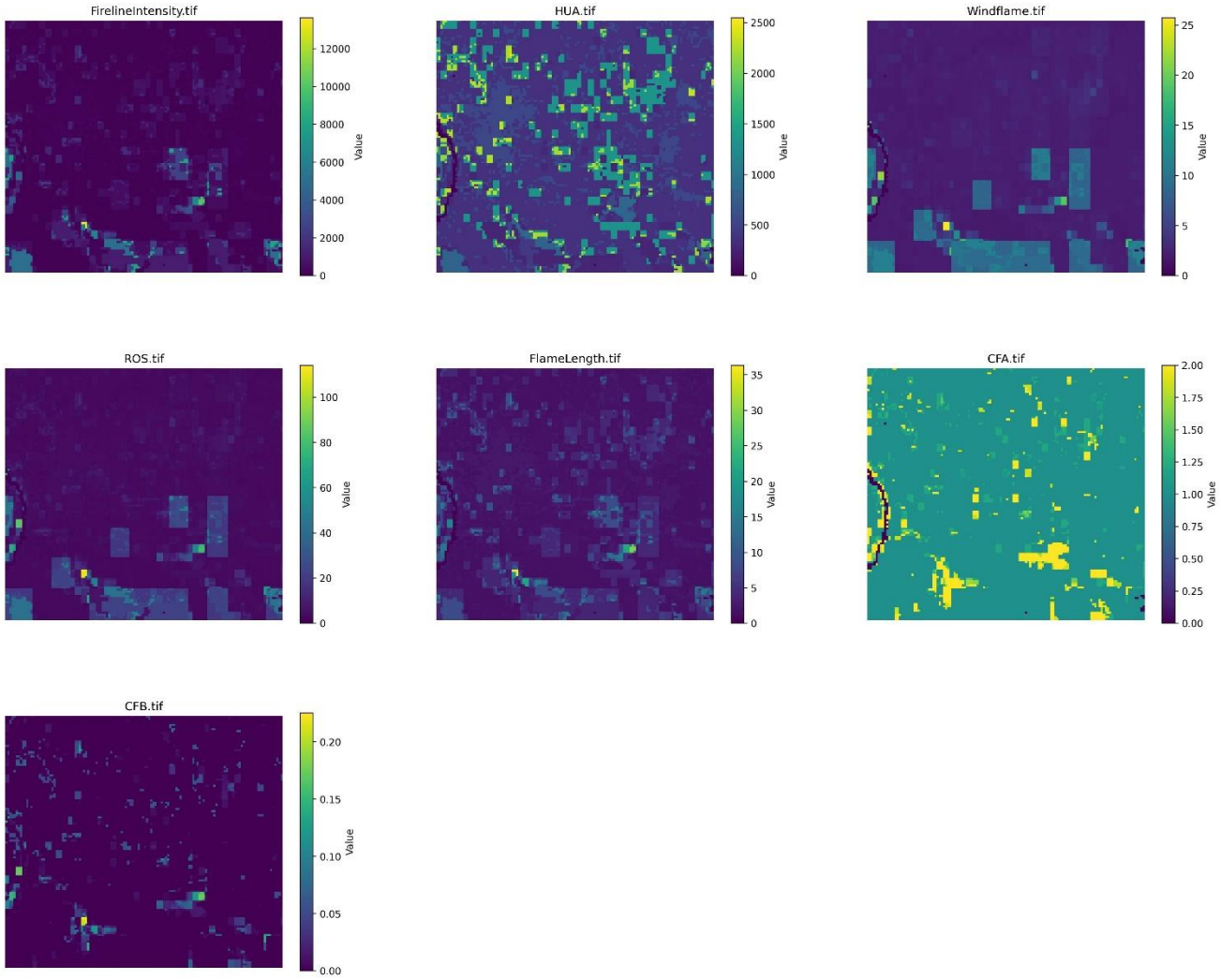


Figure 2.17 Basic FlamMap results for official FirEUrisk fuel map.

Results for all basic FlamMap outputs for official FirEUrisk fuel map are shown in Figure 2.17. Fireline intensity, as one of the most important indicators for fire behaviour is given in Figure 2.18.

Copyright © FirEUrisk Consortium. All rights reserved.

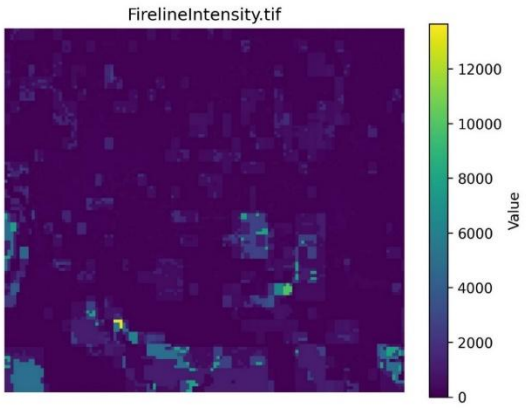


Figure 2.18 Fireline intensity result for official FirEUrisk fuel map.

As for bark beetle infested scenario, results are given in Figure 2.19 and Figure 2.20.

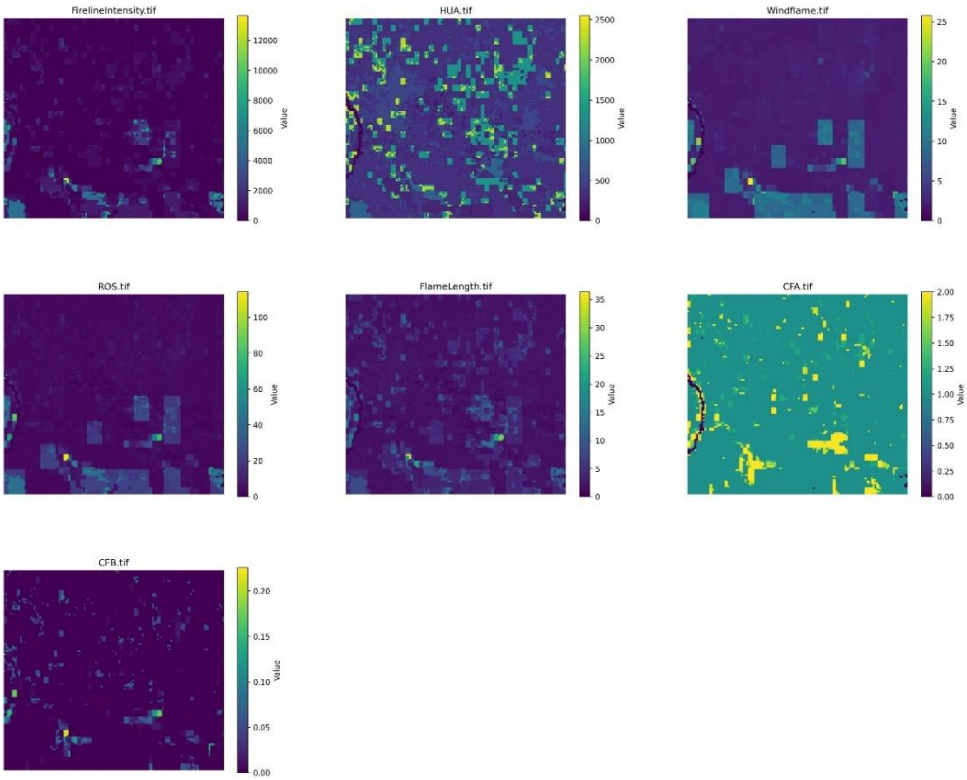


Figure 2.19 Basic FlamMap results for bark beetle infested fuel map.

Copyright © FirEUrisk Consortium. All rights reserved.

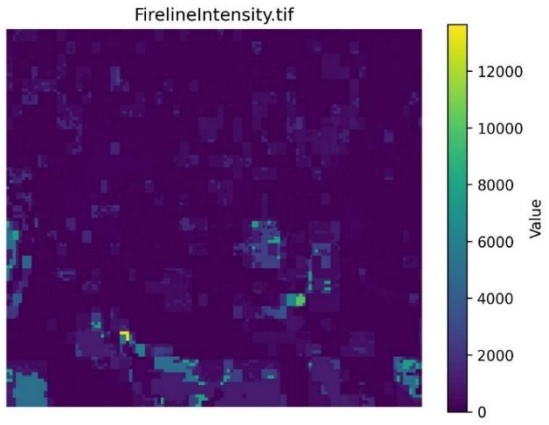


Figure 2.20 Fireline intensity for bark beetle infested fuel map.

Finally, differences in Fireline intensity, Rate of spread and flame length are given in following figures:

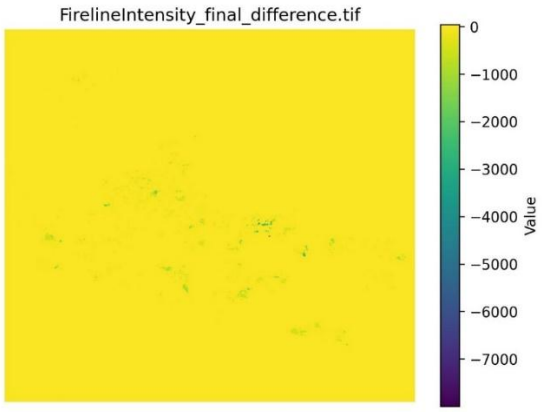


Figure 2.21 Fireline intensity difference.

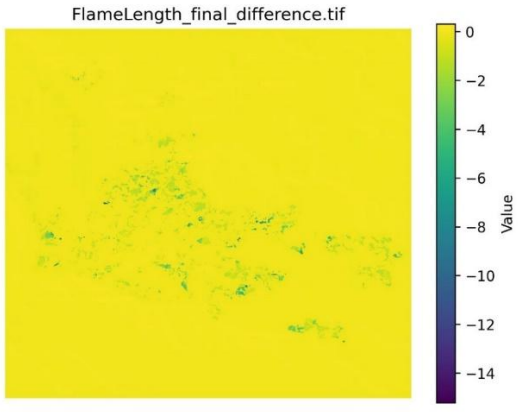


Figure 2.22 Flame length difference

Copyright © FirEUrisk Consortium. All rights reserved.

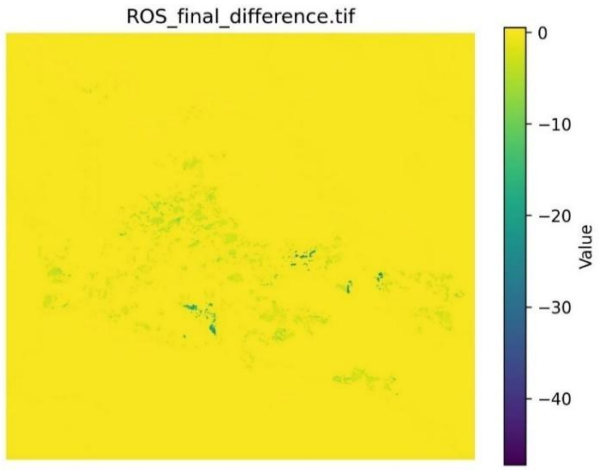


Figure 2.23 Rate of spread difference

Conclusions and policy recommendations

This study presents a methodological advancement in the integration of ecological disturbances, particularly bark beetle damage, into wildfire risk assessments. By applying advanced geospatial data processing and predictive modelling, it enhances the precision of wildfire propagation potential analysis in Pilot Site 2, reflecting altered forest conditions with updated fuel models.

This approach underscores the necessity of incorporating real-world ecological changes into wildfire behaviour predictions, ensuring that risk assessments are both accurate and relevant to current forest health statuses. Nevertheless, since the study could not be calibrated and validated with in-situ data. Further analyses will be necessary to derive conclusions.

2.4 Predicting post-fire soil erosion and water contamination risk after the 2022 fire in the Bohemian and Saxon Switzerland National Parks

Sánchez-García, C., Neris, J., Doerr, S.H., Swansea University, SU (more information available in Section 7, publication in preparation)

Introduction

Soil and ash are key sources of sediment, carbon, nitrogen, and associated pollutant movement following a fire. Their transport into freshwater systems can pose severe environmental and socio-economic implications including impacts on water quality, disruptions to drinking water supply and high remediation costs, as well as the depletion of carbon and nutrients from areas affected by erosion (Gustine et al., 2022; Robinne et al., 2021). With increases in extreme fire weather forecasted for many regions of Europe (Jones et al., 2022), assessing and predicting wildfire risks to water supply as well as landscape carbon and nutrient dynamics is fundamental to inform decision-making at different levels, from rapid assessments by land and water quality managers to longer-term policy decisions.

This project has received funding from the European Union's Horizon 2020 research and innovation programme under grant agreement No 101003890.

We used the WEPPcloud-EU-WATAR product (see Methods) developed in other activities of the project across the 2022 fire in the Bohemian and Saxon Switzerland National Parks, We (i) identified the hillslopes that are likely to be the main sources of soil erosion and ash transport (hotspots), and (ii) estimated the potential post-fire soil erosion, ash transport and carbon (C) and nitrogen (N) losses. Post-fire soil erosion and ash transport can be highly localised.



Figure 2.24 Ground surface images after the 2022 fire in the Saxon Switzerland National Park showing the: organic soil layer with charred surface material (left), highly erodible mineral soil below a distinct ash layer (centre), and partially charred logs from trees downed prior to the fire (right) (Images: TU Dresden).

Methods

The WEPPcloud-EU-WATAR tool

WEPPcloud-EU-WATAR is a physically-based, probabilistic runoff and erosion model designed for quantification of post-fire soil, ash, water, nutrient and pollutant transport from burnt hillslopes into water bodies for a given burn area and fire severity. WEPPcloud-EU-WATAR was developed on the basis of the well-established Water Erosion Prediction Project model (WEPP; Flanagan et al., 1995; Laflen et al., 1997), which has been used routinely for several decades by federal agencies for the evaluation of natural resources issues throughout the USA and in over 15 other countries. The model operates at the hillslope and catchment scales and can be applied to actual or potential fires to predict erosion risk and efficacy of mitigation actions, such as fuel reduction or hillslope erosion prevention treatments. WEPPcloud-EU-WATAR can be accessed here: https://wepp.cloud/weppcloud/ and then clicking on 'Start EU WEPPcloud-Disturbed Run'. The tool is open-access, end-user friendly and available with limited input requirement from the end-user, maximising its accessibility and usability.

When compared with other soil erosion models, like the Revised Universal Soil Loss Equation (RUSLE, Renard et al., 1997), WEPPcloud-EU-WATAR provides a more comprehensive probabilistic and spatially distributed predictions, plus

Copyright © FirEURisk Consortium. All rights reserved.

the capability of predicting transport of nutrients (e.g., carbon, nitrogen), and potential contaminants (e.g., Pb, Zn, As, Cd and Hg) in sediments and ash from hillslopes to water bodies to assess post-fire risks to water quality.

Input datasets

We used topographic information to delineate the structure of the burnt area and identify hillslopes and channels. The topographic information is extracted from the European Digital Elevation Model (EU-DEM; Copernicus Land Monitoring Service) which has a resolution of 25 m. For soils we used the European Soil Database (Panagos et al., 2022) sourced from the European Soils Data Centre (ESDAC; Joint Research Centre), and for land cover we used CORINE 2018 (EEA, 2018). Climate data comprising 10-minute precipitation (mm), daily temperature (° C), wind speed (m $^{-1}$) and direction (deg.), and solar radiation (Langleys d^{-1}) was sourced from the nearest weather station (Tokan, lat: 50.8753, long: 14.4158, 403 m.a.s.l.) provided by the Global Change Research Institute of the Czech Academy of Sciences (GCRI). The climate file was created using the WEPPCLIFF tool (McGehee, et al., 2020). WEPPcloud-EU-WATAR then utilises this climate data with a point-scale stochastic weather generator (CLIGEN) to develop daily weather simulations (Nicks et al., 1995; Lew et al., 2022).

To simulate burnt area and severity we used a soil burn severity map provided by TU Dresden (Beetz et al., 2024). Wildfire ash is one of the main sources of nutrient and potential contaminants to water bodies following a fire (e.g., Gomez-Isaza et al., 2022; Santín et al., 2015; Smith et al., 2011) with ash loads mainly depending on fuel loads and burn severity. To estimate ash loads across the burnt area, ash depths of 5 mm for low and moderate severity areas and of 10 mm for high severity areas were selected based on field observations from similar ecosystems (Neris, *pers. comm.*). Nutrient and pollutant concentrations in wildfire ash have been sourced from a comprehensive global dataset of wildfire ash chemical composition from the *Centre for Wildfire Research* at Swansea University (Sánchez-García et al., 2023).

Probabilistic and return period analysis

Return period analysis and probability of occurrence determine the likelyhood of certain runoff, sediment and ash transport events to occur the first year after the fire and are useful for forest manager decision-makers to determine post-fire risks including risk to water quality. The probability of occurrence estimates for sediment and ash transport by water within 1 year after the fire were calculated as follows: p(N) = 1 1(1-p)^N; where p = 1 / recurrence interval, N is the period of interest.

Results

Predicted post-fire soil erosion, ash, carbon and nitrogen losses

Our spatial predictions displayed the distribution of hillslopes that could be the main sources of eroded soil and ash and, thus, potential pollutants (Figure 2.25). The identification of these hotspots is key to prioritize areas for stabilization treatments such as mulching, seeding or logging, and exclude stable hillslopes.

Copyright © FirEUrisk Consortium. All rights reserved.

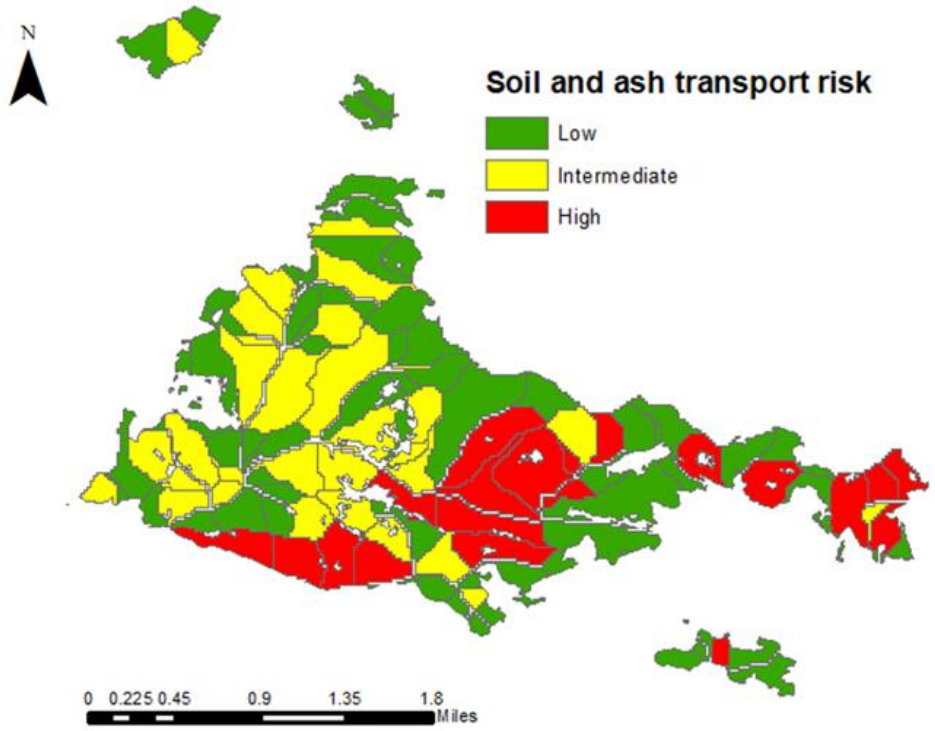


Figure 2.25 Soil erosion and ash transport hotspots for the area burnt by the 2022 fire in Bohemian and Saxon Switzerland NP, predicted by WEPPcloud-EU-WATAR (low: < 1 kg ha^{-1} of ash, intermediate: 1 – 4,400 kg ha^{-1} of ash, high: > 4,400 kg ha^{-1} of ash).

In most hillslopes producing erosion after the fire, erosion rates are estimated to have varied between 1 and 1,500 kg ha^{-1}, with a minority of hillslopes producing sediment yields > 1,500 kg ha^{-1} located in the southern area (Figure 2.26). These erosion rates represent an increase of 2 to 3 orders of magnitude with respect to pre-fire conditions, reaching up to 4 orders of magnitude in the southern slopes (in dark orange) and coincide mostly with areas burnt at higher severity. For the first year after the fire, the model predicted an increase in average annual erosion of 20 tonne more than before the fire as simulated using pre-fire conditions.

Field data on actual erosion rates was not available for this study site and hence we could only test model performance for runoff and not for sediment yield (see Section 4). Nevertheless, our annual sediment yield estimates for unburnt conditions were, on average, an order of magnitude lower than the sediment yields for European catchments of similar water discharge (Matthews et al., 2023). However, some of these catchments had higher proportions of agricultural land use (~75%) than the catchment considered in this study (~12%), which might partly explain the difference in the modelled sediment yields.

Copyright © FirEUrisk Consortium. All rights reserved.

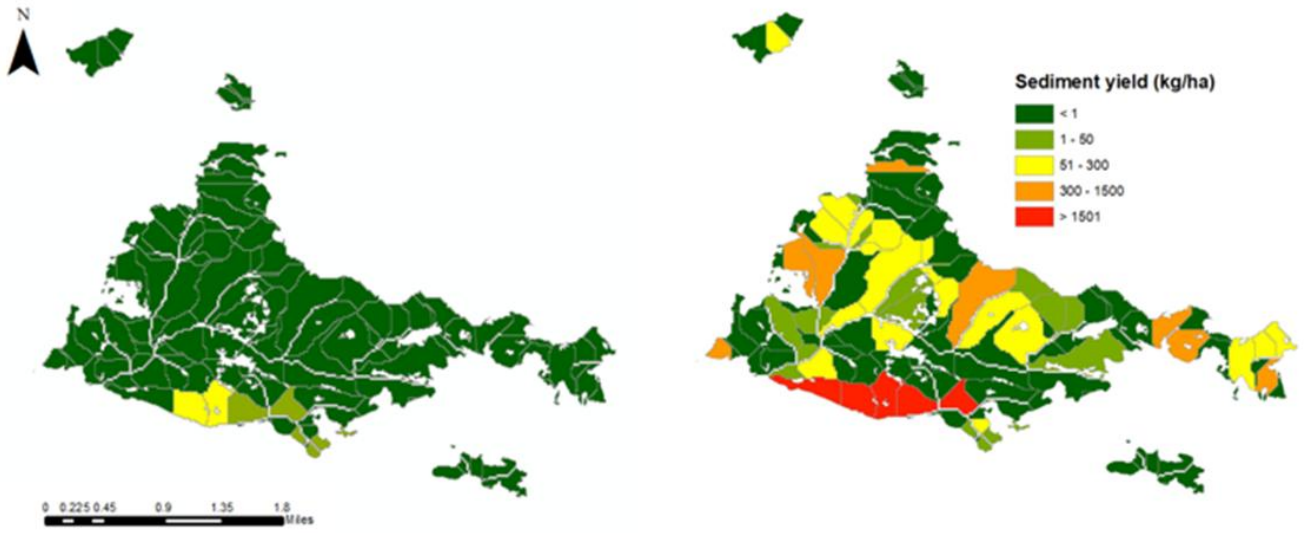


Figure 2.26 Sediment yield (kg ha^{-1}) before (left) and after (right) the 2022 fire in Bohemian and Saxon Switzerland National Parks predicted by WEPPcloud-EU-WATAR.

In addition to sediment and runoff, WEPPcloud-EU-WATAR represents the main processes affecting ash transport to stream network, i.e., ash production during the fire, ash decay, ash incorporation into the soil, wind redistribution and ash transport by water (Neris et al., *in prep*). Water transport (runoff) is the main process controlling ash transport into streams and freshwater bodies. To calculate ash transport by water, the model uses the adjusted runoff and erosion predictions provided by WEPP to incorporate the effect of ash water retention on runoff production (Cerdá and Doerr, 2008).

Table 2.3 Predictions of eroded soil, ash, and carbon and nitrogen reaching the river during the first year after the fire.

Soil		Ash		C		N	
T	T ha^{-1}	T	T ha^{-1}	T	kg ha^{-1}	T	kg ha^{-1}
20	0.02	3174.9	2.6	944.9	787.4	36.1	30.1

An estimated 3,175 tonnes of ash (2.6 tonne ha^{-1}), and 945 and 36 tonnes of carbon and nitrogen have been transported on average into the stream network during the first year after the fire (Table 2.4). Our return period analysis estimated a 50% and 20% probability that approximately 780 and 1,200 tonnes of ash, respectively, would be transported into the water network during the first post-fire year (Table 2.5). It has not been possible, however, to validate the model for erosion and ash transport estimates given the absence of observed data from the burnt area. It is, therefore, important

Copyright © FirEUrisk Consortium. All rights reserved.

to highlight that these values are unvalidated simulations and, ideally, should have been coupled with exploratory field surveys.

Table 2.4 Return period analysis and probability of occurrence of runoff, sediment and ash transport events in the first year after the fire.

Probability	Recurrence interval	Precipitation depth	Runoff	Sediment yield	Ash transport
(%)	years	mm	mm	T	T
20%	5	48	14	80	1200
50%	2	39	8.7	22	780

Additional factors that might have affected post-fire erosion and ash transport and which are not captured by the current version of WEPPcloud-EU-WATAR model include a) the effect of vegetation recovery during the first year after the fire on hydrology and erosion, and b) the effect of the downed wood from bark beetle infestation in the burnt area. It is difficult to estimate the effect of dead wood on post-fire hydrology and erosion without a hillslope-scale monitoring study. While logs placed along the contour might have reduced runoff speed, and thus, erosion, those placed across the contour (i.e. downhill) might have had the opposite effect (Figure 2.28).

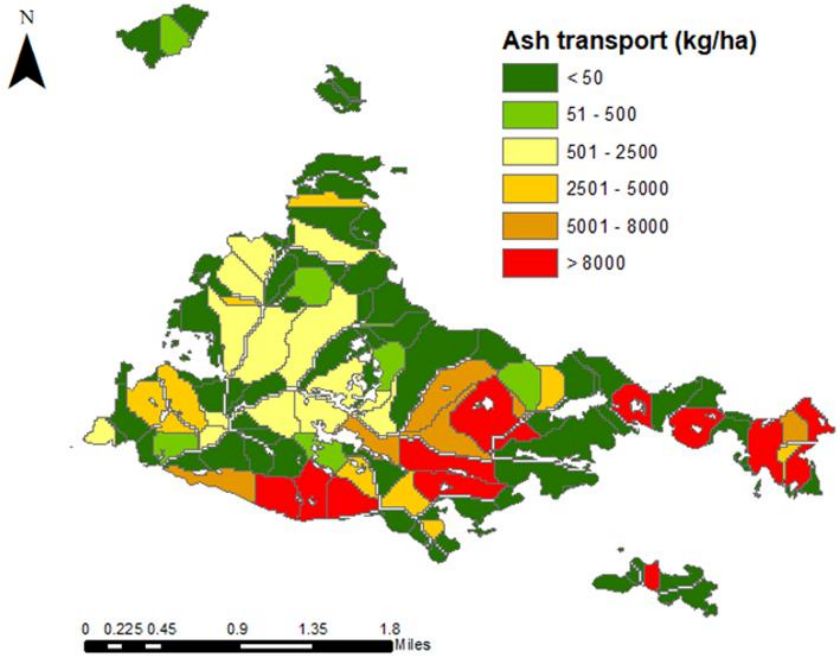


Figure 2.27 Ash transport (kg ha^{-1}) for the first year following the 2022 fire in the Bohemian and Saxon Switzerland National Parks estimated by WEPPcloud-EU-WATAR.

Copyright © FirEURisk Consortium. All rights reserved.



Figure 2.28 Post-fire images of the 2022 fire in the Saxon Switzerland National Park showing downed trees on the ground as a result of the Bark Beetle infestation and the fire. Images: TU Dresden.

Model performance and adequacy of WEPPcloud - EU-WATAR to large catchments

We tested the model performance for runoff using streamflow data from the Hřensko gauging station (Czech Republic) (lat: 50.87375, long: 14.23652) located upstream of the confluence of the Kamenice River with the Elbe River given the lack of hillslope runoff and erosion data from the burnt area. The contributing catchment to this gauging station is around 21,000 ha and comprises most of the burnt area (around 5% of the total catchment) (Figure 2.29). This is so far the largest catchment that WEPPcloud-EU-WATAR has been applied to and provided an opportunity to test the adequacy of this tool for large European catchments.

Since WEPPcloud-EU-WATAR is not designed to account for groundwater contributions to baseflow, we partitioned observed streamflow into the runoff and baseflow components using a hydrograph separation tool, (SepHydro, *Danielescu et al., 2018*). We then compared the runoff component of the separated streamflow with simulated streamflow. We ran WEPPcloud-EU-WATAR with default parameters, modifying only the saturated hydraulic conductivity of the bedrock (from 5.7 to 0.01 mm hr^{-1}) and evapotranspiration (from 0.85 to 1.2). Both parameters can be modified by the user via the online interface. This minimal calibration allowed us to critically assess WEPPcloud-EU-WATAR performance. Model performance was assessed against 8 years of observed streamflow data for pre-fire conditions (2014 – 2021) and 6 months of observed post-fire data (July – December 2022) using the following statistics:

- Nash-Sutcliffe Efficiency (NSE): shows the agreement between observed and predicted values (NSE < 0.2 insufficient, 0.2 – 0.3 sufficient, 0.4 – 0.6 good, 0.6 – 0.8 very good, > 0.8 excellent; Foglia et al., 2009).
- Percent Bias (PBIAS, %): evaluates the tendency of a model to overestimate or underestimate observed values.

Copyright © FirEUrisk Consortium. All rights reserved.

- Coefficient of determination (R^2): represents the proportion of the measured data explained by the model (Table 2.4).

Table 2.5 Streamflow model results before and after the 2022 fire in the SSNP for annual (A), monthly (M) and daily (D) streamflow averages.

	Average runoff (m3)			Simulated runoff (m3)			NSE			PBIAS			R2		
	A	M	D	A	M	D	A	M	D	A	M	D	A	M	D
Pre-fire	95008.2	97172.3	95274.7	96520.8	99652.4	96574.0	-1.52	-0.6	-0.17	1.6	2.4	1.4	0.47	0.4	0.17
Post-fire	NA	76436.2	79073.8	NA	60632.1	45833.1	NA	-2.6	-0.39	NA	-20.7	-42	NA	0.55	0.25

Conclusions

Both for pre- and post-fire conditions, WEPPcloud-EU-WATAR was able to simulate the hydrograph trends, showing better results for monthly average runoff than for daily estimates (Figure 2.29, b). However, the model had difficulty simulating streamflow in this large catchment with minimal calibration as indicated by NSE values between -2.6 and -0.17 for annual and daily simulations, respectively (Table 3). This is likely related with parameterization of baseflow, lateral flow and channel and sediment transport routing (Brooks et al., 2016; Neris et al., 2021; Srivastava et al., 2018). Interactions between the complex geology of the Bohemian and Saxon Switzerland National Parks and potential impacts of management on the hydrologic regime not captured by the model are further challenges in this example (Brooks et al., 2016). In smaller European catchments (from 100 to 5,200 ha), WEPPcloud-EU-WATAR showed good performance, both for pre- and post-fire conditions, with NSE values ranging from 0.4 to 0.63, R^2 from 0.58 to 0.71, and PBIAS from -30.8 to 7 (Basso et al., *in prep*; Sánchez-García, et al., *in prep*).

Copyright © FirEURisk Consortium. All rights reserved.

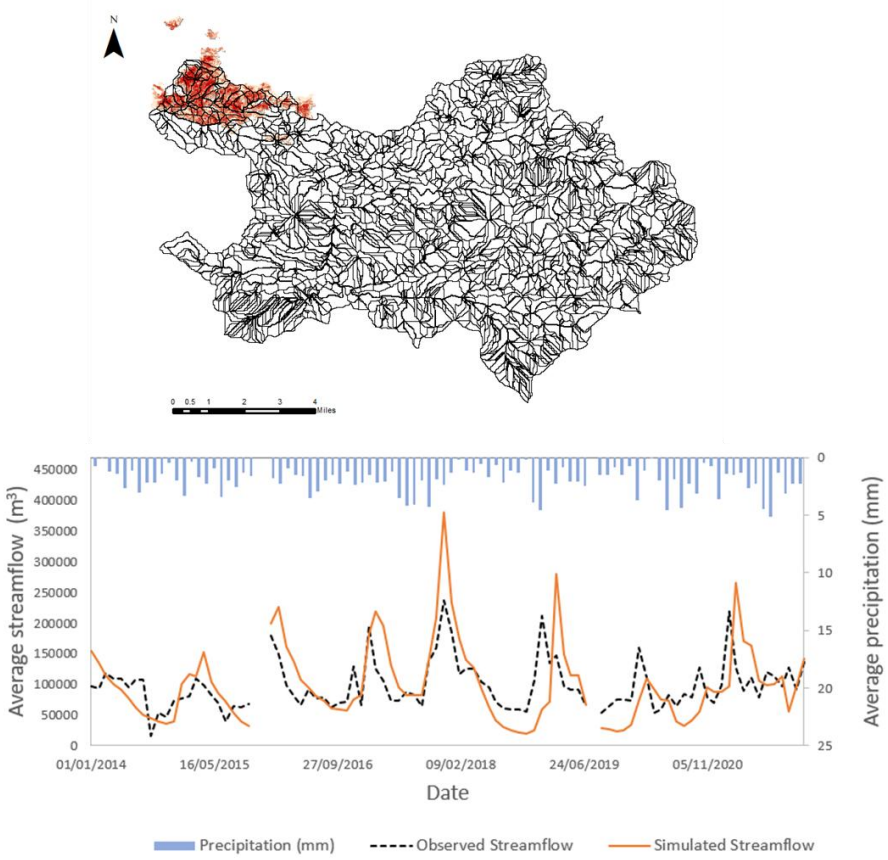


Figure 2.29 (Top, a) Hillslope delineation for the area contributing to the Hřensko gauging station (location represented by the blue pin). The orange area represents the area burnt by the 2022 fire. (Bottom, b) Streamflow comparison between observed (dotted black line) and predicted (orange line) monthly data.

Policy recommendations

WEPPcloud-EU-WATAR's high-resolution simulations can help prioritise areas for on-ground monitoring and the implementation of operational mitigation measures, anticipate the risk of water contamination, and identify areas with high susceptibility of ash and sediment transport. We recommend that when using uncalibrated WEPPcloud-EU-WATAR in large catchments, to use the spatial and return period analyses capabilities to inform on-ground mitigation measures. Sediment yield and ash transport estimates should be treated as indicative only and, where possible, validated with observed data. Enhancing water quality monitoring systems in regions prone to wildfires is, therefore, crucial for generating observed datasets needed for calibration and validation.

Improvements in model calibration for different catchment sizes and conditions will enhance post-fire decision-making. Therefore, it is important that funding supports not only the development but also the refinement of post-fire erosion and water contamination models to meet the needs of land and water managers.

Copyright © FirEUrisk Consortium. All rights reserved.

References

Brooks, E. S., Dobre, M., Elliot, W. J., Wu, J. Q., & Boll, J. (2016). Watershed-scale evaluation of the Water Erosion Prediction Project (WEPP) model in the Lake Tahoe basin. *Journal of Hydrology*, 533, 389–402. https://doi.org/10.1016/j.jhydrol.2015.12.004

Cerdà, A., & Doerr, S. H. (2008). The effect of ash and needle cover on surface runoff and erosion in the immediate post-fire period. *Catena*, 74(3), 256–263. https://doi.org/10.1016/j.catena.2008.03.010

Danielescu, S., MacQuarrie, K.T.B., Popa, A (2018) SEPHYDRO: A Customizable Online Tool for Hydrograph Separation. *Groundwater* 56: 589-593. https://doi.org/10.1111/gwat.12792

Flanagan, D. C., Livingston, S. J., Ascough, J. C., Baffaut, C., Barfield, B., Deer-Ascough, L. A., Kidwell, M. R., Kottwitz, E. R., Laflen, J. M., Lindley, M., Nearing, M. A., Nicks, A. D., Savabi, M. R., Singher, A., Stott, D. E., Weltz, M. A., & Whittemore, D. A. (1995). Editors: Contributors: WEPP QUICK START GUIDE.

Foglia, L., Hill, M.C., Mehl, S.W., Burlando, P., 2009. Sensitivity analysis, calibration, and testing of a distributed hydrological model using error-based weighting and one objective function. *Water Resour*. Res. 45, 1–18.

Gomez-Isaza, D. F., Cramp, R. L., & Franklin, C. E. (2022). Fire and rain: A systematic review of the impacts of wildfire and associated runoff on aquatic fauna. *Global Change Biology*, 28, 2578–2595. https://doi.org/10.1111/gcb.16088

Laflen, J. M., Elliot, W. J., Flanagan, D. C., Meyer, C. R., & Nearing, M. A. (1997). WEPP-Predicting water erosion using a process-based model. *Journal of Soil and Water Conservation*, 52(2), 96–102. https://www.jswconline.org/content/52/2/96

Matthews, F., et al. (2023). EUSEDcollab: a network of data from European catchments to monitor net soil erosion by water. *Sci Data* 10, 515. https://doi.org/10.1038/s41597-023-02393-8

McGehee et al., (2020). WEPPCLIFF: A command-line tool to process climate inputs for soil loss models. *Journal of Open Source Software*, 5(49), 2029. https://doi.org/10.21105/joss.02029

Neris, J., Santin, C., Lew, R., Robichaud, P. R., Elliot, W. J., Lewis, S. A., Sheridan, G., Rohlfs, A. M., Ollivier, Q., Oliveira, L., & Doerr, S. H. (2021). Designing tools to predict and mitigate impacts on water quality following the Australian 2019/2020 wildfires: Insights from Sydney's largest water supply catchment. *Integrated Environmental Assessment and Management*, 17(6), 1151–1161. https://doi.org/10.1002/ieam.4406

Nicks, A. D., Lane, L. J., & Gander, G. A. (1995). Chapter 2. Weather generator. In D. C. Flanagan & M. A. Nearing (Eds.), Water Erosion Prediction Project Hillslope Profile and Watershed Model Documentation.

Lew, R., Dobre, M., Srivastava, A., Brooks, E. S., Elliot, W. J., Robichaud, R., & Flanagan, D. C. (2022). WEPPcloud: An online watershed-scale hydrologic modeling tool. Part I. Model description. *Journal of Hydrology*, 608(February), 127603. https://doi.org/10.1016/j.jhydrol.2022.127603

Renard, K. G., Foster, G. R, Weesies, G. A., McCool, D. K., Yoder, D. C. (1997). Predicting soil erosion by water: A guide to conservation planning with the Revised Universal Soi Loss Equation (RUSLE*). U. S. Department of Agriculture, Agriculture Handbook*, No. 703, 404pp.

Sánchez-García, C., Santín, C., Neris, J., Sigmund, G., Otero, X. L., Manley, J., González-Rodríguez, G., Belcher, C. M., Cerdà, A., Marcotte, A. L., Murphy, S. F., Rhodes, C., Sheridan, G., Strydom, T., Robichaud, P. R., & Doerr, S. H. (2023). Chemical characteristics of wildfire ash across the globe and their environmental and socio-economic implications. *Environment International,* 178, 108065. https://doi.org/https://doi.org/10.1016/j.envint.2023.108065

Copyright © FirEUrisk Consortium. All rights reserved.

Santín, C., Doerr, S. H., Otero, X. L., & Chafer, C. J. (2015). Quantity, composition and water contamination potential of ash produced under different wildfire severities. *Environmental Research*, 142(July), 297–308. https://doi.org/10.1016/j.envres.2015.06.041

Smith, H. G., Sheridan, G. J., Lane, P. N. J., Nyman, P., & Haydon, S. (2011). Wildfire effects on water quality in forest catchments: A review with implications for water supply. *Journal of Hydrology*, 396(1–2), 170–192. https://doi.org/10.1016/j.jhydrol.2010.10.043

Srivastava, A., Wu, J. Q., Elliot, W. J., Brooks, E. S., & Flanagan, D. C. (2018). A simulation study to estimate effects of wildfire and forest management on hydrology and sediment in a forested watershed, Northwestern U.S. *Transactions of the ASABE*, 61(5), 1579–1601. https://doi.org/https://doi.org/10.13031/trans.12326

3 Case study developed in Central Portugal (Pilot Site #3)

3.1 Short-term human health impacts resulting from smoke from an extreme wildfire in Central Portugal

Miranda, A.I., Lopes, D., Menezes, I., University of Aveiro, UAVR

Introduction

The frequency of Extreme Wildfire Events (EWE) is projected to increase under climate change since future projections suggest an increase in the number of droughts, heat waves, and dry spells (Turco et al., 2019). Smoke is one of the most disturbing consequences of these events, with the release of large amounts of gaseous and particulate pollutants into the atmosphere (Fernandes et al., 2022) that strongly impact human health (D'Evelyn et al., 2022; Sebastião et al., 2019).

The World Health Organization (WHO), aware of the health effects of smoke from wildfires, has already provided air quality guidelines for wildfire events to protect the population (WHO, 1999), particularly in the Wildland-Urban Interface (WUI) due to the high risk of human exposure (Ager et al., 2019; Miranda et al., 2008). Exposure to high air pollution levels during wildfire events can lead to a wide range of adverse health outcomes, including increases in respiratory morbidity (Black et al., 2017; Cascio, 2018; Elliott et al., 2013; Haikerwal et al., 2016; Reid et al., 2016) and there is also emerging evidence of adverse cardiovascular outcomes (Haikerwal et al., 2015; Wettstein et al., 2018; Yao et al., 2016). The population most vulnerable to smoke exposure are the common risk groups (e.g., children and older adults) (Rappold et al., 2017) and personnel involved in firefighting operations (Miranda et al., 2012, 2010; Sebastião et al., 2019).

The 2017 EWE in Portugal highlighted the relevance of smoke impacts on human health (Augusto et al., 2020; Barbosa et al., 2022; Fernandes et al., 2022). During the wildfire season, several air quality monitoring stations registered high concentrations of atmospheric pollutants due to wildfire emissions and air pollution transport from burning areas (APA, 2018), and many people needed medical assistance due to smoke intoxication (Viegas et al., 2019, 2017). Due to the severity of these EWE, several studies have been performed by the scientific community regarding smoke emissions (Fernandes et al., 2022), climate drivers (Turco et al., 2019) and air pollution impact on human health and its associated costs (Augusto et al., 2020; Barbosa et al., 2022). The main purpose of this case study is to evaluate the short-term

Copyright © FirEUrisk Consortium. All rights reserved.

impacts on human health resulting from the Portuguese EWE of October 2017. More details can be found in Lopes et al. (2024).

The October 2017 wildfires

The year 2017 will be recorded as one of the deadliest and most intense Portuguese fire seasons (Guerreiro et al., 2018; Turco et al., 2019; Viegas et al., 2019). Seven EWE were registered in the central region of Portugal, on the 15th and 16th of October, causing a high number of human victims (48 fatalities and about 67 injured people), the destruction of 1712 homes and 768 company facilities, and burning more than 241,000 hectares in less than 24 hours (about 2.4% of the national territory), with several environmental damages (Guerreiro et al., 2018; Viegas et al., 2019) that included dragging up fire-generated atmospheric pollutants into northwest Europe and affecting populations very far from the EWE (Augusto et al., 2020). The period of abnormal droughts and heat waves (Change, 2017; Sánchez-Benítez et al., 2018) caused by climate change, an unusual meteorological phenomenon in the Portuguese territory (i.e., Hurricane Ophelia) (Augusto et al., 2020; Turco et al., 2019) and firefighter teams partially demobilised (period out of the official fire season window established by the Portuguese authorities) were identified as the triggers of hundreds of fire ignitions during this EWE (Guerreiro et al., 2018; Viegas et al., 2019). These seven EWE were produced by one or more ignitions in the central region of mainland Portugal, which covers the Pilot Site 3 of the project (Figure 3.1), which propagated continuously between 6 a.m. on October 15th and 8 a.m. on October 16th, 2017.

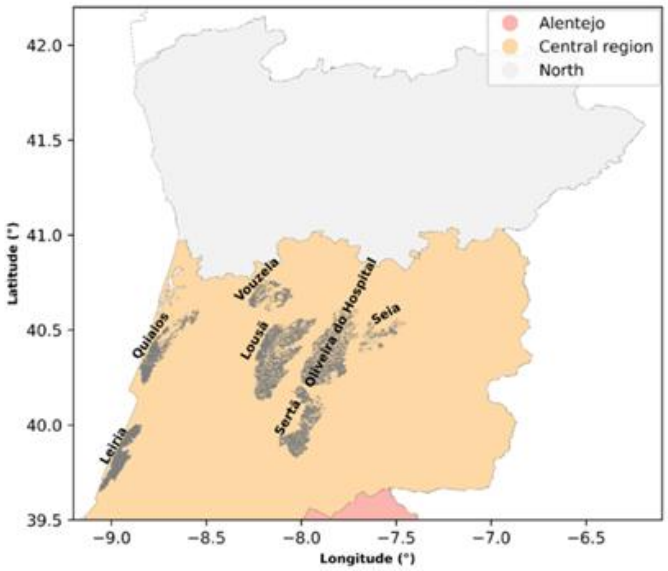


Figure 3.1 Location of the areas affected by the EWE on October 15 and 16, 2017.

The first forest fire alert was registered in Seia (at 6 a.m.), where about 17,000 ha of forest and shrubland burnt, while the second wildfire occurrence was verified three hours later in Lousã (54,400 ha burnt). The EWE in Oliveira do Hospital started at 10:26 a.m. and it was one of the most impactful events, with 25 human fatalities, the destruction of several homes and industrial facilities, as well as an extensive area of burnt forest (51,430 ha). The EWE in Sertã started around

Copyright © FirEUrisk Consortium. All rights reserved.

noon on October 15th and it was considered dominated by protection authorities thirteen hours later after some rain (30,977 ha burnt). In the coastal area of mainland Portugal, the first wildfire warning was issued around 2 p.m. in Leiria and Quiaios, with burnt areas of 20,014 and 23,844 ha, respectively. The last fire alert was verified at 5 p.m. in Vouzela, with the smallest burnt area (15,959 ha) (Viegas et al., 2019).

Methodology

The Weather Research and Forecasting Model (Skamarock et al., 2008) combined with a semi-empirical fire-spread algorithm (WRF-SFIRE) was used to simulate the dispersion of emitted pollutants during the EWE. WRF-SFIRE is also coupled to a prognostic fuel moisture model, which assesses the moisture based on local WRF meteorology. WRF-SFIRE simulates landscape-scale physics in a two-way integration between fire and dynamical thermodynamic meteorology, through the atmospheric boundary layer. The WRF-SFIRE can resolve in a fully coupled way fire progression, plume rise, and smoke dispersion of the air pollutants emitted from the forest fires (Mandel et al., 2011).

The setup for the WRF-SFIRE system was built over a coarse domain (D1) with a horizontal resolution of 20×20 km^2 comprising the Iberian Peninsula. In addition, three nested domains covering mainland Portugal (D2, 4×4 km^2 resolution), the central region of Portugal (D3, 1×1 km^2 resolution) and each of the EWE areas (D4, 200×200 m^2 resolution) were also used to obtain results with high spatial and temporal resolution.

To initialise the WRF-SFIRE model four kinds of data are needed: i) global meteorological fields; ii) fuel load; iii) ignition points; and iv) emission factors. The global meteorological fields were provided by the European Centre for Medium-Range Weather Forecasts (ECMWF) Re-Analysis Interim (ERA-Interim) model data (ECMWF, 2019) with 0.75° spatial resolution and temporal resolution of 6 h for surface and pressure levels. The fuel load was obtained from the 6th Portuguese Forest Inventory (ICNF 2019). The ignition location and time for each EWE were provided by Viegas *et al.* (2019) who performed a detailed study analysis based on fire data collected in the field, namely on interviews with fire-fighting teams and affected people. Emission factors for Southern-European conditions were selected based on a literature review, taking into consideration the land-use types of the central region of Portugal (Miranda 2004; Alves *et al.* 2011; Martins *et al.* 2012, Van Der Werf *et al.* 2017; Vicente *et al.* 2017, 2012). Atmospheric emissions were estimated using a bottom-up methodology based on the well-known (e.g., Wiedinmyer et al. 2006; Carvalho et al. 2011) equations. Further information on emissions estimation can be find in Fernandes et al. (2022).

The physical configuration used in the model was defined according to sensitivity analysis from previous studies for Portugal (Carvalho et al., 2012; Monteiro et al., 2015). The parameterizations included: Morrison double-moment scheme (Morrison et al., 2009); Rapid Radiative Transfer Model short- and long-wave radiation model (RRTMG) (Mlawer et al., 1997); MM5 similarity surface layer scheme (Zhang and Anthes, 1982); Noah Land Surface Model (Chen and Dudhia, 2001) with soil temperature and moisture in four layers, fractional snow cover and frozen soil physics; Mellor-Yamada-Janjic (MYJ) Planetary Boundary Layer scheme (Mellor and Yamada, 1982) and Grell-Freitas Ensemble Scheme for cumulus parameterization (Grell and Freitas, 2014).

The analysis of simulation results was focused on particles with an aerodynamic diameter less than or equal to 2.5 µm (PM2.5), because they include inhalable particles that can easily penetrate the thoracic region of the respiratory system

Copyright © FirEUrisk Consortium. All rights reserved.

and go into the bloodstream, similar to oxygen molecules (Costa et al., 2014), and lead to respiratory and cardiovascular diseases (CVD) (Breysse et al., 2013).

Short-term health effects (Equation 1) of PM2.5 exposure were estimated considering non-linear (Equation 2) concentration-response functions (CRF) and relative risks (RR) provided by the Health Risks of Air Pollution in Europe (HRAPIE) project (WHO, 2013).

$$\text{Health effect}_p = \sum_{i=1}^{n} \text{Inc}_{i,j} \times \text{Pop}_j \times \text{RR}_{i,p} \qquad \textit{Equation 1}$$

Non-linear:

$$RR_{p,i} = exp[\beta_i \times \ln(C_P + 1) - \ln(C_0 + 1)] \qquad \textit{Equation 2}$$

where, Inc is the incidence rate of the health endpoint i for a population group j; Pop is the spatial and temporal distribution for a population group j; RR correlates a pollutant p concentration variation ($C - C_0$) with the probability of experiencing or avoiding a specific health endpoint i; β coefficient denotes the change in the RR for a unit change in concentration C (expressed as the natural logarithm of RR); C is the concentration of the pollutant p ($\mu g.m^{-3}$); C_0 indicates the pollutant p cut-off or counterfactual concentration value ($\mu g.m^{-3}$) above which health impacts are calculated.

The incidence rate for the analysed health endpoints (i.e., hospital admissions for respiratory and CVD) by population group in 2017 was acquired from the National Health Service (NHS, 2022). The spatial distribution of the population (at the neighbourhood level) was obtained from the Portuguese Census dataset (INE, 2011), while the temporal and spatial distribution of the firefighter teams was provided by Viegas et al. (2019). The default values of RR, β and C_0 (Table 3.1) datasets were provided by the AirQ+ software (tool for health risk assessment of air pollution) developed by the WHO (WHO, 2022). The spatial (1×1 km^2) and temporal (hourly) resolution of the air pollution levels (i.e., PM2.5) were provided by the WRF-SFIRE modelling system.

Table 3.1 Input datasets used to assess the short-term health impacts.

Pollutant	Health endpoint	Range of concentration (C_0)	RR (95% CI) per 10 $\mu g.m^{-3}$
PM2.5	Hospital admissions: respiratory disease, 0+ years	> 25 $\mu g.m^{-3}$	1.019 (95% CI: 1 – 1.0402)
	Hospital admissions: CVD (including stroke), 0+ years		1.0091 (95% CI: 1.0017 -1.0166)

Results

In Figure 3.2, we display the spatial distribution (1×1 km^2 resolution) of the average PM2.5 concentrations simulated by the WRF-SFIRE between October 15 and 16, 2017 (24 h). The daily averages measured by the air quality monitoring stations are also represented by small circles (the concentration scale is the same).

Copyright © FirEURisk Consortium. All rights reserved.

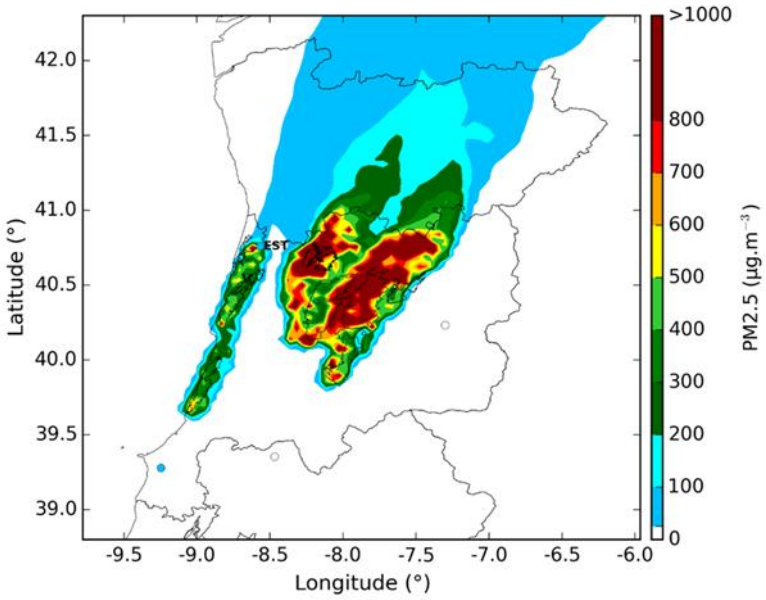


Figure 3.2 Spatial distribution of the PM2.5 concentrations between October 15th and 16th, 2017.

The PM2.5 values estimated by WRF-SFIRE are very high and would have strongly affected the population living in the central part of Portugal. To better understand smoke effects on human health, Table 3.2 shows the estimated number of hospital admissions for respiratory disease and CVD (including stroke), by NUTS, caused by the PM2.5 levels during the Portuguese EWE between 15 and 16 October (this study). The number of hospital admissions, registered by the National Health Service in October 2017, are also presented.

Table 3.1 Hospital admissions estimated in this study (between 15 and 16 October 2017) and reported by the NHS (October 2017).

NUTSII	Hospital admissions (95% CI)			
	Respiratory disease		CVD (including stroke)	
	This study	NHS	This study	NHS
North	681 (95% CI: 0–1465)	2613	387 (95% CI: 72–709)	2970
Central region	766 (95% CI: 0–1691)	1558	429 (95% CI: 79–795)	1895
Alentejo	0 (95% CI: 0–0)	290	0 (95% CI: 0–0)	432
Total	1447 (95% CI: 0–3156)	4461	732 (95% CI: 151–1504)	5297

During the Portuguese EWE (24h period), a total of 1447 (95% CI: 0–3156) hospital admissions by respiratory diseases and 816 (95% CI: 151–1504) hospital admissions by CVD (including stroke) were estimated. The quantified hospital admissions for firefighters for both health endpoints (i.e., respiratory and cardiovascular diseases) were less than 3. The obtained values (24-hour period) were lower (> 3000 hospital admissions) than those reported by the National

Copyright © FirEURisk Consortium. All rights reserved.

Health Service in October 2017 (one month) with a total of 4461 and 5297 hospital admissions for respiratory and cardiovascular diseases, respectively.

In Figure 3.3, we show the spatial distribution of hospital admissions related to the October 2017 EWE. The highest number of hospital admissions was estimated for the Leiria, Quiaios and Lousã EWE, where the largest number of inhabitants was registered too.

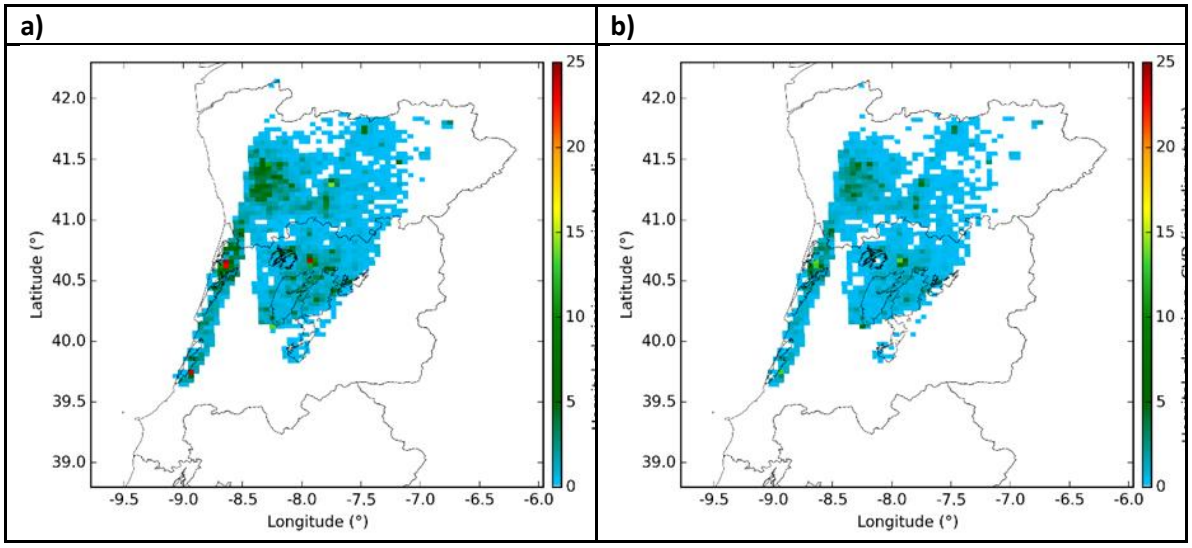


Figure 3.3 Spatial distribution of the hospital admissions, in Portugal, for respiratory (a) and cardiovascular (b) diseases due to PM2.5 levels caused by the 2017 October EWE.

Conclusions

This modelling case study highlights the relevance of smoke for human health considering air pollutants concentration values in the air and health indicators such as respiratory and cardiovascular diseases. It also shows the spatial variability of these effects. Being able to forecast and provide this type of health information to stakeholders from the health sector could be a relevant advance towards better preparedness. Moreover, supporting communication with health outcomes easily understood by the population would also facilitate social awareness about smoke and its impacts and prevent human exposure to smoke.

Policy recommendations

Smoke from wildfires can affect the health of exposed populations and of exposed firefighters. To mitigate these effects, the following policy recommendations are proposed:

Public Health Alert Systems

- To develop and implement a standardized, nationwide public health alert system for wildfire smoke to provide timely information on air quality conditions and recommended actions. Alerts should include guidelines for at risk populations and the public on protective measures such as limiting outdoor activities, using masks, and

Copyright © FirEUrisk Consortium. All rights reserved.

improving indoor air quality. Moreover, local health departments should work closely with environmental/air quality agencies to ensure seamless communication about risks and protective actions.

- Emergency Response and Healthcare Support
- Hospitals and clinics should be equipped to handle spikes in respiratory and cardiovascular cases during wildfire smoke events. Provide mental health services for individuals and communities affected by wildfire smoke, especially in regions with prolonged or frequent exposure. This includes support for managing anxiety, stress, and trauma associated with wildfire events.
- Enhance Occupational Health Protection
- To ensure that workers exposed to wildfire smoke are covered by occupational health regulations, including air quality thresholds that mandate stopping work or transitioning to indoor environments when air quality reaches hazardous levels. Also, provide additional healthcare resources and mental health support for wildland firefighters, who face prolonged smoke exposure and elevated health risks.
- To promote Indoor Air Quality Protection
- To promote "clean air shelters" in affected areas, such as community centres and libraries, equipped with filtration systems to provide safe spaces for individuals.

Public Awareness and Education Campaigns

- To launch public health campaigns focused on the risks associated with wildfire smoke exposure and strategies to reduce individual risk, such as staying indoors, using air purifiers, and creating "clean air spaces." Campaigns should target schools, workplaces, and community centres. Communications strategies should address sensitive populations, including individuals with asthma, heart disease, pregnant women, and outdoor workers. Outreach should include easy-to-understand materials in multiple languages and formats, such as social media, television, and community outreach programs. Schools in fire-prone regions should have wildfire smoke response plans, including ensuring clean indoor air, shifting outdoor activities indoors, and providing information to parents and staff about how to reduce exposure during smoke events.

International Collaboration

- Wildfires often affect regions across borders, necessitating international collaboration. Countries should work together to share data, resources, and strategies for mitigating the transboundary effects of wildfire smoke on health. Establish global research networks focused on the health impacts of wildfire smoke, enabling scientists and policymakers to share findings and best practices across regions experiencing similar challenges.
- By implementing these policy recommendations, governments and communities can reduce the health risks associated with wildfire smoke, protect vulnerable populations, and build resilience against the increasing threat of wildfires exacerbated by climate change.

Copyright © FirEUrisk Consortium. All rights reserved.

References

Ager, A.A., Palaiologou, P., Evers, C.R., Day, M.A., Ringo, C., Short, K., 2019. Wildfire exposure to the wildland urban interface in the western US. Appl. Geogr. 111, 102059. https://doi.org/10.1016/j.apgeog.2019.102059

Alves, C., Vicente, A., Nunes, T., Gonçalves, C., Fernandes, A.P., Mirante, F., Tarelho, L., Sánchez de la Campa, A.M., Querol, X., Caseiro, A., Monteiro, C., Evtyugina, M., Pio, C., 2011. Summer 2009 wildfires in Portugal: Emission of trace gases and aerosol composition. Atmos. Environ. 45, 641–649. https://doi.org/10.1016/j.atmosenv.2010.10.031

APA, (Agência Portuguesa do Ambiente), 2018. Identificação e avaliação da ocorrência de eventos naturais em Portugal em 2017.

Augusto, S., Ratola, N., Tarín-Carrasco, P., Jiménez-Guerrero, P., Turco, M., Schuhmacher, M., Costa, S., Teixeira, J.P., Costa, C., 2020. Population exposure to particulate-matter and related mortality due to the Portuguese wildfires in October 2017 driven by storm Ophelia. Environ. Int. 144, 106056. https://doi.org/10.1016/j.envint.2020.106056

Barbosa, J. V., Nunes, R.A.O., Alvim-Ferraz, M.C.M., Martins, F.G., Sousa, S.I.V., 2022. Health and Economic Burden of the 2017 Portuguese Extreme Wildland Fires on Children. Int. J. Environ. Res. Public Health 19. https://doi.org/10.3390/ijerph19010593

Black, C., Tesfaigzi, Y., Bassein, J.A., Miller, L.A., 2017. Wildfire smoke exposure and human health: Significant gaps in research for a growing public health issue. Environ. Toxicol. Pharmacol. 55, 186–195. https://doi.org/10.1016/j.etap.2017.08.022

Breysse, P.N., Delfino, R.J., Dominici, F., Elder, A.C.P., Frampton, M.W., Froines, J.R., Geyh, A.S., Godleski, J.J., Gold, D.R., Hopke, P.K., Koutrakis, P., Li, N., Oberdörster, G., Pinkerton, K.E., Samet, J.M., Utell, M.J., Wexler, A.S., 2013. US EPA particulate matter research centers: Summary of research results for 2005-2011. Air Qual. Atmos. Heal. 6, 333–355. https://doi.org/10.1007/s11869-012-0181-8

Carvalho, A., Monteiro, A., Flannigan, M., Solman, S., Miranda, A.I., Borrego, C., 2011. Forest fires in a changing climate and their impacts on air quality. Atmos. Environ. 45, 5545–5553. https://doi.org/10.1016/j.atmosenv.2011.05.010

Carvalho, D., Rocha, A., Gómez-Gesteira, M., Santos, C., 2012. A sensitivity study of the WRF model in wind simulation for an area of high wind energy. Environ. Model. Softw. 33, 23–34. https://doi.org/10.1016/j.envsoft.2012.01.019

Cascio, W.E., 2018. Wildland fire smoke and human health. Sci. Total Environ. 624, 586–595. https://doi.org/10.1016/j.scitotenv.2017.12.086

Change, N.C., 2017. Spreading like wildfire. Nat. Clim. Chang. 7, 755. https://doi.org/10.1038/nclimate3432

Chen, F., Dudhia, J., 2001. Coupling an Advanced Land Surface–Hydrology Model with the Penn State–NCAR MM5 Modeling System. Part I: Model Implementation and Sensitivity. Mon. Weather Rev. 129, 587–604. https://doi.org/10.1175/1520-0493(2001)129<0587:CAALSH>2.0.CO;2

Costa, S., Ferreira, J., Silveira, C., Costa, C., Lopes, D., Relvas, H., Borrego, C., Roebeling, P., Miranda, A.I., Paulo Teixeira, J., 2014. Integrating health on air quality assessment - Review report on health risks of two major european

Copyright © FirEUrisk Consortium. All rights reserved.

outdoor air pollutants: PM and NO2. J. Toxicol. Environ. Heal. - Part B Crit. Rev. https://doi.org/10.1080/10937404.2014.946164

D'Evelyn, S.M., Jung, J., Alvarado, E., Baumgartner, J., Caligiuri, P., Hagmann, R.K., Henderson, S.B., Hessburg, P.F., Hopkins, S., Kasner, E.J., Krawchuk, M.A., Krenz, J.E., Lydersen, J.M., Marlier, M.E., Masuda, Y.J., Metlen, K., Mittelstaedt, G., Prichard, S.J., Schollaert, C.L., Smith, E.B., Stevens, J.T., Tessum, C.W., Reeb-Whitaker, C., Wilkins, J.L., Wolff, N.H., Wood, L.M., Haugo, R.D., Spector, J.T., 2022. Wildfire, Smoke Exposure, Human Health, and Environmental Justice Need to be Integrated into Forest Restoration and Management. Curr. Environ. Heal. Reports 9, 366–385. https://doi.org/10.1007/s40572-022-00355-7

ECMWF, (European Centre for Medium-Range Weather Forecasts), 2019. European Centre for Medium-Range Weather Forecasts Re-Analysis Interim model data [WWW Document]. URL https://www.ecmwf.int/en/forecasts/datasets/reanalysis-datasets/era-interim.

Elliott, C.T., Henderson, S.B., Wan, V., 2013. Time series analysis of fine particulate matter and asthma reliever dispensations in populations affected by forest fires. Environ. Heal. A Glob. Access Sci. Source 12, 1–9. https://doi.org/10.1186/1476-069X-12-11

Fernandes, A.P., Lopes, D., Sorte, S., Monteiro, A., Gama, C., Reis, J., Menezes, I., Osswald, T., Borrego, C., Almeida, M., Ribeiro, L.M., Viegas, D.X., Miranda, A.I., 2022. Smoke emissions from the extreme wildfire events in central Portugal in October 2017. Int. J. Wildl. Fire 1–13. https://doi.org/10.1071/WF21097

Grell, G.A., Freitas, S.R., 2014. A scale and aerosol aware stochastic convective parameterization for weather and air quality modeling. Atmos. Chem. Phys. 14, 5233–5250. https://doi.org/10.5194/acp-14-5233-2014

Guerreiro, J., Fonseca, C., Salgueiro, A., Fernandes, P., Lopez, I.E., de Neufville, D., Mateus, F., Castellnou, R.M., Sande, S.J., Moura, J.M., Castro, R.F., Caldeira, D.N., 2018. Avaliação dos incêndios ocorridos entre 14 e 16 de outubro de 2017 em Portugal Continental.

Haikerwal, A., Akram, M., Monaco, A. Del, Smith, K., Sim, M.R., Meyer, M., Tonkin, A.M., Abramson, M.J., Dennekamp, M., 2015. Impact of fine particulate matter (PM2.5) exposure during wildfires on cardiovascular health outcomes. J. Am. Heart Assoc. 4, 1–10. https://doi.org/10.1161/JAHA.114.001653

Haikerwal, A., Akram, M., Sim, M.R., Meyer, M., Abramson, M.J., Dennekamp, M., 2016. Fine particulate matter (PM2.5) exposure during a prolonged wildfire period and emergency department visits for asthma. Respirology 21, 88–94. https://doi.org/10.1111/resp.12613

ICNF, (Instituto da Conservação da Natureza e das Florestas), 2019. IFN6 - Inventário Florestal Nacional 6 [WWW Document]. URL https://www.icnf.pt/florestas/flestudosdocumentosestatisticasindicadores.

INE, (Instituto Nacional de Estatística), 2011. Statistics Portugal, 2011. CENSUS, 2011- statistical data for Portugal [WWW Document]. URL http://censos.ine.pt (accessed 12.10.20).

Lopes, D., Menezes, I., Reis, J., Coelho, S., Almeida, M., Viegas, D.X., Borrego, C., Miranda, A.I., 2024. Short-term Impacts of the 2017 Portuguese Wildfires on Human Health and Visibility: A Case Study. Fire. In press.

Mandel, J., Beezley, J.D., Kochanski, A.K., 2011. Coupled atmosphere-wildland fire modeling with WRF 3.3 and SFIRE 2011. Geosci. Model Dev. 4, 591–610. https://doi.org/10.5194/gmd-4-591-2011

Copyright © FirEUrisk Consortium. All rights reserved.

Martins, V., Miranda, A.I., Carvalho, A., Schaap, M., Borrego, C., Sá, E., 2012. Impact of forest fires on particulate matter and ozone levels during the 2003, 2004 and 2005 fire seasons in Portugal. Sci. Total Environ. 414, 53–62. https://doi.org/10.1016/j.scitotenv.2011.10.007

Mellor, G.L., Yamada, T., 1982. Development of a turbulence closure model for geophysical fluid problems. Rev. Geophys. 20, 851–875. https://doi.org/10.1029/RG020i004p00851

Miranda, A.I., 2004. An integrated numerical system to estimate air quality effects of forest fires. Int. J. Wildl. Fire 13, 217–226. https://doi.org/10.1071/WF02047

Miranda, A.I., Amorim, J.H., Martins, V., Pimentel, C., Rodrigues, R., Tavares, R., Borrego, C., 2008. Numerical modelling of the impact of wildland-urban interface fires on Coimbra air quality. WIT Trans. Ecol. Environ. 119, 333–342. https://doi.org/10.2495/FIVA080331

Miranda, A.I., Martins, V., Cascão, P., Amorim, J.H., Valente, J., Tavares, R., Borrego, C., Tchepel, O., Ferreira, A.J., Cordeiro, C.R., Viegas, D.X., Ribeiro, L.M., Pita, L.P., 2010. Monitoring of firefighters exposure to smoke during fire experiments in Portugal. Environ. Int. 36, 736–745. https://doi.org/10.1016/j.envint.2010.05.009

Miranda, A.I., Martins, V., Casco, P., Amorim, J.H., Valente, J., Borrego, C., Ferreira, A.J., Cordeiro, C.R., Viegas, D.X., Ottmar, R., 2012. Wildland smoke exposure values and exhaled breath indicators in firefighters. J. Toxicol. Environ. Heal. - Part A Curr. Issues 75, 831–843. https://doi.org/10.1080/15287394.2012.690686

Mlawer, E.J., Taubman, S.J., Brown, P.D., Iacono, M.J., Clough, S. a., 1997. Radiative transfer for inhomogeneous atmospheres: RRTM, a validated correlated-k model for the longwave. J. Geophys. Res. 102, 16663. https://doi.org/10.1029/97JD00237

Monteiro, A., Ferreira, J., Ribeiro, I., Fernandes, A.P., Martins, H., Gama, C., Miranda, A.I., 2015. Air quality over Portugal in 2020. Atmos. Pollut. Res. 6, 788–796. https://doi.org/10.5094/apr.2015.087

Morrison, H., Thompson, G., Tatarskii, V., 2009. Impact of cloud microphysics on the development of trailing stratiform precipitation in a simulated squall line: Comparison of one- and two-moment schemes. Mon. Weather Rev. 137, 991–1007. https://doi.org/10.1175/2008MWR2556.1

NHS, (National Health Service), 2022. Morbilidade e Mortalidade Hospitalar por Instituição [WWW Document]. URL https://transparencia.sns.gov.pt/explore/dataset/morbilidade-e-mortalidade-hospitalar/table/?sort=periodo (accessed 10.18.22).

Rappold, A.G., Reyes, J., Pouliot, G., Cascio, W.E., Diaz-Sanchez, D., 2017. Community Vulnerability to Health Impacts of Wildland Fire Smoke Exposure. Environ. Sci. Technol. 51, 6674–6682. https://doi.org/10.1021/acs.est.6b06200

Reid, C.E., Brauer, M., Johnston, F.H., Jerrett, M., Balmes, J.R., Elliott, C.T., 2016. Critical review of health impacts of wildfire smoke exposure. Environ. Health Perspect. 124, 1334–1343. https://doi.org/10.1289/ehp.1409277

Sánchez-Benítez, A., García-Herrera, R., Barriopedro, D., Sousa, P.M., Trigo, R.M., 2018. June 2017: The Earliest European Summer Mega-heatwave of Reanalysis Period. Geophys. Res. Lett. 45, 1955–1962. https://doi.org/10.1002/2018GL077253

Sebastião, R., Sorte, S., Valente, J., Miranda, A.I., Fernandes, J.M., 2019. Detecting changes in the heart rate of firefighters to prevent smoke inhalation and health effects. Evol. Syst. 10, 295–304. https://doi.org/10.1007/s12530-018-9241-0

Copyright © FirEUrisk Consortium. All rights reserved.

Skamarock, W.C., Klemp, J.B., Dudhi, J., Gill, D.O., Barker, D.M., Duda, M.G., Huang, X.-Y., Wang, W., Powers, J.G., 2008. A Description of the Advanced Research WRF Version 3, Technical Report. https://doi.org/10.5065/D6DZ069T

Turco, M., Jerez, S., Augusto, S., Tarín-Carrasco, P., Ratola, N., Jiménez-Guerrero, P., Trigo, R.M., 2019. Climate drivers of the 2017 devastating fires in Portugal. Sci. Rep. 9, 1–8. https://doi.org/10.1038/s41598-019-50281-2

van der Werf, G.R., Randerson, J.T., Giglio, L., Van Leeuwen, T.T., Chen, Y., Rogers, B.M., Mu, M., Van Marle, M.J.E., Morton, D.C., Collatz, G.J., Yokelson, R.J., Kasibhatla, P.S., 2017. Global fire emissions estimates during 1997-2016. Earth Syst. Sci. Data 9, 697–720. https://doi.org/10.5194/essd-9-697-2017

Vicente, A., Alves, C., Monteiro, C., Nunes, T., Mirante, F., Cerqueira, M., Calvo, A., Pio, C., 2012. Organic speciation of aerosols from wildfires in central Portugal during summer 2009. Atmos. Environ. 57, 186–196. https://doi.org/10.1016/j.atmosenv.2012.04.030

Vicente, A., Calvo, A., Fernandes, A.P., Nunes, T., Monteiro, C., Pio, C., Alves, C., 2017. Hydrocarbons in particulate samples from wildfire events in central Portugal in summer 2010. J. Environ. Sci. (China) 53, 122–131. https://doi.org/10.1016/j.jes.2016.02.022

Viegas, D.X., Almeida, M.A., Ribeiro, L.M., Raposo, J., Viegas, M.T., Oliveira, R., Alves, D., Pinto, C., Rodrigues, A., Ribeiro, C., Lopes, S., Jorge, H., Viegas, C.X., 2019. Análise dos Incêndios florestais ocorridos a 15 de Outubro de 2017.

Viegas, X., Almeida, M.F., Ribeiro, L.M., Raposo, J., Viegas, M.T., Oliveira, R., Alves, D., Pinto, C., Humberto, J., Rodrigues, A., Lucas, D., Lopes, S., Silva, L.F., 2017. O Complexo De Incêndios De Pedrógão Grande E Concelhos Limítrofes, Iniciado a 17 De Junho De 2017.

Wettstein, Z.S., Hoshiko, S., Fahimi, J., Harrison, R.J., Cascio, W.E., Rappold, A.G., 2018. Cardiovascular and cerebrovascular emergency department visits associated with wildfire smoke exposure in California in 2015. J. Am. Heart Assoc. 7. https://doi.org/10.1161/JAHA.117.007492

WHO, (World Health Organization), 2022. AirQ+: software tool for health risk assessment of air pollution [WWW Document]. URL https://www.who.int/europe/tools-and-toolkits/airq---software-tool-for-health-risk-assessment-of-air-pollution (accessed 10.18.22).

WHO, (World Health Organization), 2013. Health risks of air pollution in Europe – HRAPIE project. https://doi.org/10.1021/acs.est.5b05833

WHO, (World Health Organization), 1999. Health guidelines for vegetation fire events. Geneva, Switzerland.

Wiedinmyer, C., Quayle, B., Geron, C., Belote, A., McKenzie, D., Zhang, X., O'Neill, S., Wynne, K.K., 2006. Estimating emissions from fires in North America for air quality modeling. Atmos. Environ. 40, 3419–3432. https://doi.org/10.1016/j.atmosenv.2006.02.010

Yao, J., Eyamie, J., Henderson, S.B., 2016. Evaluation of a spatially resolved forest fire smoke model for population-based epidemiologic exposure assessment. J. Expo. Sci. Environ. Epidemiol. 26, 233–240. https://doi.org/10.1038/jes.2014.67

Zhang, D., Anthes, R.A., 1982. A high-resolution model of the planetary boundary layer - sensitivity tests and comparisons with SESAME-79 data. J. Appl. Meteorol. 21, 1594–1609. https://doi.org/10.1175/1520-0450(1982)021<1594:AHRMOT>2.0.CO;2

Copyright © FirEUrisk Consortium. All rights reserved.

4 Case studies in Demonstration areas

4.1 Effects of air pollution through the emissions of nuclear smoke in the Chornobyl Exclusion Zone during wildfires

Zibtsev S., Kashparov V., Myroniuk V., Holiaka D., Bogomolov V., Regional Eastern Europe Fire Monitoring Center, REEFMC

(This section has been partially published as Kashparov, V., Kirieiev, S., Yoschenko, V., Levchuk, S., Holiaka, D., Zhurba, M., Bogdan, L., Vyshnevskyi, D., & Oughton, D. H. (2024). Assessment of exposures to firefighters from wildfires in heavily contaminated areas of the Chornobyl Exclusion Zone. Journal of Environmental Radioactivity, 274. https://doi.org/10.1016/j.jenvrad.2024.107410).

Introduction

This paper presents the main estimation parameters of wildfires for predicting radionuclides (RN) emission into atmospheric air as well as estimated data of their resuspension in dynamics and summarised for the entire period during April 2020 in radioactivity-contaminated territories because of the Chornobyl accident in 1986. The study area includes the Chornobyl Exclusion Zone (ChEZ) and adjacent territories where these fires were often started by the traditional burning of dry grass near settlements before the start of the growing season.

The time of the start of a series of large fires on radioactively contaminated land can be considered the morning (8-00 AM) on April 3, 2020, near the Narodychi urban-type village in the Zhytomyr region in the wetlands on the right bank of the River Uzh. The fire reached the ChEZ the very next day. On April 28, 2020, when the region experienced heavy precipitation (rain), it can be considered the actual end of the period of active fire development. In total, it was possible to distinguish at least 4 isolated centres (sources) of fires within the ChEZ. The area of the burn was about 60,000 hectares in the exclusion zone and another 40,000 hectares outside it but on the tracks of the Chornobyl RN fallout. This has never been seen before in this region.

Data Methods

We used to estimation of radionuclides emission in atmospheric air next sources (as in the previous Report): maps of main Chornobyl RNs (these are the following isotopes: Sr-90, Cs-137, plutonium isotopes (Pu-238-240) and Am-241) density contamination of soil (top layer to up a depth of 20 cm) as of 2020; own field data on a fuel load of forest stands, for open landscapes - information from the handbook (technical report – Standard Fire Behavior Fuel Models: A Comprehensive Set for Use with Rothermel's Surface Fire Spread Model) (Scott & Burgan, 2005), radionuclides content and transfer factors from the soil into biomass components are output results of researches performed during 2000-2020, landscape classification implemented based on satellites remote sensing (IAEA, 2010; Kashparov et al., 2018; Kashparov et al., 2020; Holiaka et al., 2020a,b).

Copyright © FirEUrisk Consortium. All rights reserved.

Study region

The study region encompasses the entire Ukrainian part of the ChEZ and adjacent territories, which are characterised by the highest levels of radionuclide contamination and were affected by landscape fires in April 2020. Although there were two additional large-scale wildfires in close proximity, one to the west and the other to the east of the ChEZ, these wildfires are not considered in this study (see Figure 4.1). The reason is that they exhibit at least 100 times lower levels of Cs-137 densities per unit area compared to the average contamination observed in the 10-kilometre zone around the Chornobyl NPP. Moreover, this difference is even more significant for other radioisotopes (more than 1000 times).

RNs content in soil and biomass

Most of the post-fire area in 2020 consists of undisturbed soils after the Chornobyl accident, excluding temporary localisations of radioactive waste (RWTLS) such as the "Red Forest," “Yaniv station”, "Chystogalivka," and "Kopachy" as well as a few industrial objects of the Chornobyl NPP. In total, these territories with disturbed soils comprise approximately 500 hectares of the total burnt area. So, for estimation of RNs activity in the soil and biomass components use typically radioecological methods that are based on RNs spatial distribution in soil and aggregated transfer factors for biological mobile RNs (Sr-90 and Cs-137) from soil to individual vegetation parts (which are a source of combustible materials: foliage, bark and so on). For the Red Forest RWTLS, the determination of RNs and biomass inventory have been used empirical data from two forest sites in 2015 and 2019. For herbaceous landscapes, we took radioecological parameters from scientific publications where the material collections were obtained within ChEZ. The main input data parameters for the calculation of RN activity are present in Table 4.1.

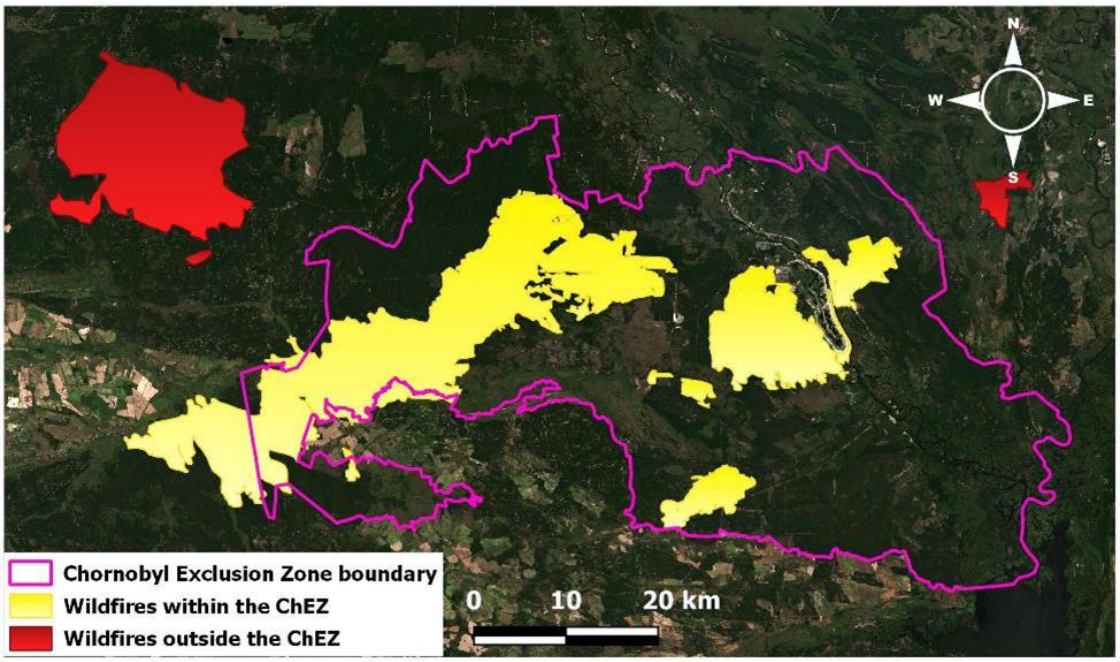


Figure 4.1 Spatial distribution of areas affected by “big” wildfires (>100 ha) during April 2020: fires that were mostly localised in the ChEZ are marked in yellow; fires outside the ChEZ are marked in red

Copyright © FirEUrisk Consortium. All rights reserved.

Table 4.1 Combustible biomass and radioecological parameters for 2020 Fire (Beresford et al., 2018; IAEA, 2010; Kashparov et al., 2020; Holiaka et al., 2020a,b)

Landscape	Combustible biomass, kg/m^2 (Paskevich, 2005; Borsuk, 2019)	Aggregated transfer factor **($Tf_{ag}(i)$)**, (Bq/kg)/(kBq/m^2) (outside "Red Forest" RWTSP)		Activity concentration in combustible biomass, kBq/kg (within"Red Forest" RWTSP)	
		Sr-90	Cs-137	Sr-90	Cs-137
Sparse grass	0.01	14	2.3	22±18**	0.6±0.6
Pine forest	1.43 (+2.2)*	100±74	23.8	855±450	43±24
Swamp	0.74	7.4±4.9	1.7±0.9	22±18	0.6±0.6
Meadow	0.27	14	2.3	22±18	0.6±0.6
Birch / Deciduous forest	0.35 (+1.7)*	100±74	16	1950±960	95±66
Dead forest	3.6	100±74	23.8	855±450	43±24

*Note: * is if crown fire needs to add this weight; ** is standard deviation*

Biomass of combustible materials was determined by using data from technical reports, Paskevich`s and Borsuk`s dissertation thesis (Paskenich, 2005; Borsuk, 2020). They studied these aspects within Chornobyl Exclusion Zone for herbaceous and forest ecosystems respectively. RNs (i) activity concentration of fire material ($A(i)_{fm}$, Bq kg^{-1}) was calculated as:

$$A(i)_{fm}=Tf_{ag}(i)\cdot A_{soil}(i) \qquad \textit{(Equation 3)}$$

where $A_{soil}(i)$ is soil density of contamination with i-radionucledes, kBq m^{-2}; $Tf_{ag}(i)$ is aggregated transfer factor that is the ratio of the dry mass activity concentration ($A(i)_{fm}$, Bq kg^{-1}) in fire material to the unit soil density of contamination ($A_{soil}(i)$, kBq m^{-2}). Transuranic elements (TUE: plutonium isotopes and Am-241) are not actively accumulated in plants. Therefore, the emission of these RNs into the atmospheric air during fires is calculated based on the density of their soil contamination and the estimated amounts of combustible materials. Based on the results of experimental studies (Yoschenko et al., 2006a,b) and measurements obtained from an Automatic System for Monitoring the Radiation Situation (ASMRS) around the Chornobyl NPP before, during, and after a fire occurred in 2016 (the Red Forest wildfire), the share of Pu-238-240 emissions into the air exhibits significant variability, spanning two orders of magnitude. The minimum values of this parameter are approximately 8E-07 for grass wildfires and 24E-07 for forest fires, based on soil contamination density. Therefore, to determine the most probable value (the median) for this indicator, the minimum share of plutonium isotopes resuspension needs to be multiplied by 10, and to calculate the maximum value, it needs to be multiplied by 100. Am-241 activity concentration has a relatively stable ratio with plutonium radionuclides (Pu-238-240) in the atmospheric air, usually being 5 times greater. The emissions of Sr-90 and Cs-137 into the air account for about 1% and 2% of their activity in vegetation-combustible materials, respectively.

Copyright © FirEURisk Consortium. All rights reserved.

Recalculation of radioactive contamination of soil as of fire time

Determination of RNs contamination density of soils (unit in kBq m^{-2}) on the specific time has been done classical method: Radioactive Decay Law. So, reduction of RNs activity was calculated based on the RNs half-life:

$$N = N_0 \cdot 2^{-\frac{\Delta t}{T_{1/2}}}, \qquad \textit{(Equation 4)}$$

where N is final contamination (activity/density/dose rate), N_0 is initial contamination (activity/density/dose rate); Δt is time period is a difference between the final and the initial measurement of time, $T_{1/2}$ is the half-life of the radionuclide. RNs half-lives ($T_{1/2}$) have obtained from IAEA web-application "Livechart - Table of Nuclides - Nuclear structure and decay data" (https://www-nds.iaea.org/relnsd/vcharthtml/VChartHTML.html#dcy1). Decay and half-life of the main radionuclides (^{90}Sr, ^{137}Cs, ^{238}Pu, ^{239}Pu, ^{240}Pu, ^{241}Pu and ^{241}Am) presented in the equation list below:

$$^{90}_{38}Sr \xrightarrow{28.79\ years} {}^{90}_{39}Y + {}^{-}\beta; \quad \text{and then} \quad {}^{90}_{39}Y \xrightarrow{64\ hours} {}^{90}_{40}Zr + {}^{-}\beta, \qquad \textit{(Equation 5)}$$

$$^{137}_{55}Cs \xrightarrow{30.08\ years} {}^{137m}_{56}Ba + {}^{-}\beta; \quad \text{and then} \quad {}^{137m}_{56}Ba \xrightarrow{2.552\ min} {}^{137}_{56}Ba + \gamma, \qquad \textit{(Equation 6)}$$

$$^{238}_{94}Pu \xrightarrow{87.7\ years} {}^{234}_{92}U + {}^{4}_{2}\alpha; \quad \text{and then} \quad {}^{234}_{92}U \xrightarrow{2.455\cdot10^{5}\ years} {}^{230}_{90}Th + {}^{4}_{2}\alpha, \qquad \textit{(Equation 7)}$$

$$^{239}_{94}Pu \xrightarrow{24110\ years} {}^{235}_{92}U + {}^{4}_{2}\alpha; \text{ and then} \quad {}^{235}_{92}U \xrightarrow{7\cdot10^{8}\ years} {}^{231}_{90}Th + {}^{4}_{2}\alpha, \qquad \textit{(Equation 8)}$$

$$^{240}_{94}Pu \xrightarrow{6561\ years} {}^{236}_{92}U + {}^{4}_{2}\alpha; \quad \text{and then} \quad {}^{236}_{92}U \xrightarrow{23\cdot10^{6}\ years} {}^{232}_{90}Th + {}^{4}_{2}\alpha, \qquad \textit{(Equation 9)}$$

$$^{241}_{94}Pu \xrightarrow{14.33\ years} {}^{241}_{95}Am + {}^{-}\beta; \quad \text{further} \quad {}^{241}_{95}Am \xrightarrow{432.6\ years} {}^{237}_{93}Np + {}^{4}_{2}\alpha. \qquad \textit{(Equation 10)}$$

^{241}Pu is an especially important radionuclide, although it is a low-energy beta-radiation emitter, and its daughter isotope (^{241}Am) is characterized by alfa-decay (Eq. 10). Previous studies of transuranic elements indicate that the ratios between the activities of the plutonium isotopes and ^{241}Am remain constant for the full study region because the isotopes have essentially the same chemical properties and their distribution in different parts of the reactor is nearly similar (Preprint IAE-5268/3: Reactor Fuel of Unit 4 of the Chernobyl NPP Begichev et al, 1990).

Copyright © FirEUrisk Consortium. All rights reserved.

Landscape classification and definition of fire boundaries

Establishing the possibilities of determining the landscape types, combustible biomass, and burnout degree of the above-ground components on the forest plots and partly of the burnt areas boundaries was carried out based on the Sentinel-1 and Sentinel-2 satellite data in 2019 and 2020. As the 2020 wildfires occurred in early spring (in April), satellite data from the year 2019 were used to evaluate the investigated parameters in the ChEZ. Classification algorithms realised in XGBoost library and Scikit-learn API. The total accuracy of landscape classification was about 77%, and for forests (coniferous +deciduous) was more than 90%.

The initial processing of the received satellite data was performed using the SNAP software platform with built-in Sentinel Toolboxes applications developed and supported by the ESA (The European Space Agency). The partially processed results of the Sentinel-1 satellite sensor images as products: S1B_IW_GRDH_1SDV_20190521... (2019) and S1A_IW_GRDH_1SDV_20200521... (2020), as well as Sentinel-2 satellite sensors: S2A_MSIL1C_20190824... (2019) and S2B_MSIL1C9020201... (2020) were used to form a collection of spectral and radar data. Calibration, correction, and filtering of rasters were performed according to the algorithms presented in the official documentation on the Sentinel Online web page (ESA, 2022). Raster data placed in different grid tiles were combined into a mosaic and cut off at the level of a 5-kilometre external buffer from the border of the Ukrainian part of the ChEZ and 2020 wildfires. Further, based on the review of previous publications, several satellite bands were left for next use and 4 synthetic layers were calculated, which have the highest "predictive" ability in the landscape's classification (first of all for the identification of forest ecosystems) and the assessment of species compositions of stands, according to the research of other authors. This data collection includes the bands of sensors from Sentinel-2 satellite constellations: B2 - blue (wavelength center of electromagnetic radiation on satellite A: 492 nm), B3 - green (560 nm), B4 - red (665 nm), B8 - near-infrared (NIR: 833 nm), B11 – far infrared-1 (SWIR-1: 1614 nm), B12 – far infrared-2 (SWIR-2: 2202 nm), and calculated vegetation indices: NDVI (Carlson & Ripley, 1997), NDWI (Mc Feeters, 1996), NBR (Escuin et al., 2008) and the difference between NBR 2019 and 2020 (attached to the 2020 data list); as well as added Sentinel-1 radar bands with polarization: VH, VV and the simple ratio between VV and VH (VV / VH). The spatial resolution of all rasters is 10 m, with the same fixed extent.

A training set for landscape classification was carried out using a sample of points that were evenly located within the ChEZ with a step of 800 m in vertical and horizontal directions in the E32636 – WGS 84 / UTM zone 36N projected coordinate system. The following types of landscapes were identified: water bodies, surfaces without vegetation, meadows and fallows (herbaceous vegetation on dry and moderately moistened soils), swamps (herbaceous vegetation on moist and over-moistened soils), single and/or groups of bushes and/or trees (areas of woody vegetation, on which closed stands may form in the near future where dominated by Scots pine (up 70%) and Silver birch (up 25%)), coniferous forests (Scots pine covers more than 99% of areas), deciduous forest, dead stands as a result of fire damage, dead stands due to the action of other factors. SPOT-6 2018-2019 satellite images gained during the Japanese-Ukrainian SATREPS project for ChEZ and their comparison with the RGB image of the earth's surface obtained using a band combination from the processed collection of Sentinel space data for 2019-2020 were utilized to improve the quality of these landscape identification. The points that got on the dividing lines between different landscapes removed from the training sample: when they were located at a distance of less than 15 m to the dividing line(s). In total, only 2,211 of all 3,185 created points were included in the training sample for the task of landscape classification.

Copyright © FirEUrisk Consortium. All rights reserved.

Assessment and validation of models

The vast majority of obtained research results in this work were obtained using the XGBoost (eXtreme Gradient Boosting) algorithm and a library with the same name that is written in C++ programming language (Chen & Guestrin, 2016; XGBoost developers, 2022). Classification task for the available data obtained at the regional (ChEZ satellite survey) level was performed on based of JupyterLab interface in an interactive web environment using Python 3.9 programming language. With a series of additional libraries installed and imported for processing data exploiting scientific (NumPy, Numba, Scikit-learn, SciPy, SHAP) and geographic (rasterio, GDAL) approaches, their graphical visualisation (matplotlib, SHAP, Seaborn, Graphviz) and so on.

The implementation of the XGBoost algorithm is carried out in several stages: preprocessing of training data and characterisation of their homogeneity, search for algorithm optimal hyperparameters, evaluation of the initial trained model, ranking of the importance of the model input features and saving the model. All categorical data presented in the test format were converted into a numerical format (whole number), so the woody species names and/or landscape types were coded in this way. The homogeneity of the training sample (in this case, the presence/absence of individual observations that significantly impact model predictive properties when algorithm training on other observations from a sample) was checked by simply her dividing into 3-4 parts of training data without repetitions and their k-fold cross-validation (XGBoost developers, 2022). The optimal hyperparameter tuning of the XGBoost model was performed by generating random integers or float numbers in empirically determined ranges (Random Search) of at least 3000 iterations with a minimum of three repetitions on training samples with randomly selected observations. These searches were performed for the following hyperparameters: "colsample_bytree" was in the pursuit range (0,05; 0,9). Next, the numerical search interval for other hyperparameters will also be indicated in parentheses: "gamma" was (0,0; 0,5), "learning_rate" was (0,01; 0,3), "max_depth" was (2; 5), "n_estimators" was (50, 200), "subsample" was (0.3, 0.7) (XGBoost developers, 2022).

All prepared data were transformed into DMatrix data structure or object to effectively use the computer's CPU, which accelerated the training of the XGBoost model by 3-5 times than when using Pandas data frames (XGBoost developers, 2022). Validation of models was carried out by calculating comparative statistics between empirical and simulated values of test samples of observations, which comprised 20–30% of all available observations. The metrics for validation of predicted features were the statistics that are offered by the library developers by default: for multi-class classification – multi-class logarithmic loss function (mlogloss) (Demirkaya et al., 2020). The final quality assessment of the most successful XGBoost models, that were proposed for use, was performed based on the following approaches/metrics: confusion matrix, F-score (or F-measure), classification accuracy.

RNs activity concentration in the air

The authors of the report used data collection from points of the ASMRS around the Chornobyl nuclear power plant in the 2016 wildfire in Red Forest to estimate the radionuclide's resuspension into the atmosphere during wildfires and their transfer by air masses. ASMRSs pump large volumes of air through special filters to detect even extremely low concentrations of RNs. In rows of the output table contains data on the name of the ASMRSs, their coordinates, the date of finishing air sampling, volume air pumped, and RNs activity concentrations (Sr-90, Cs-137, Pu-238, Pu-239-240

Copyright © FirEURisk Consortium. All rights reserved.

and Am-241) in the air: units are Bq m^{-3} (presented in the previous report: D2.5 – Online modelling tool for extreme fire behaviour and smoke emission and dispersion).

Prediction of Chornobyl wildfire dynamics in April, 2020

The growth of the wildfires was simulated using semi-empirical approaches. Since the landscape wildfires lasted for more than 20 days (from 2020-04-03T08:00:00 UTC to 2020-04-26T02:00:00 UTC) in different parts of the ChEZ, the available software for modelling fire growth was not suitable for this task. We collected data from various satellite systems to identify burnt areas and the active fire edges with energy release. These data were utilised to refine the boundaries of the burnt areas and provide a temporal approximation of the spatial dynamics of fire propagation. The following sources were used to obtain input data: vector layers from the FIRMS site; near- and far-infrared raster bands of MODIS, Sentinel-2, and Landsat satellites; as well as space-based RGB images from the Planets satellites. The burning places were converted into a vector layer containing information about geocoordinates and date/time, following the Coordinated Universal Time (UTC) standard.

The Kriging library in the SAGA environment was utilised to approximate the development of the 2020 wildfires, specifically to identify the probable occurrence of wildfires in certain locations. Then, the morphological libraries in the SAGA API enabled the calculation of intermediate parameters of fire dynamics, employing classical morphological indicators of the relief: slope (α) and aspect (A). In this context, the slope represents the ratio between time (t) and distance (s) (Figure 4.2).

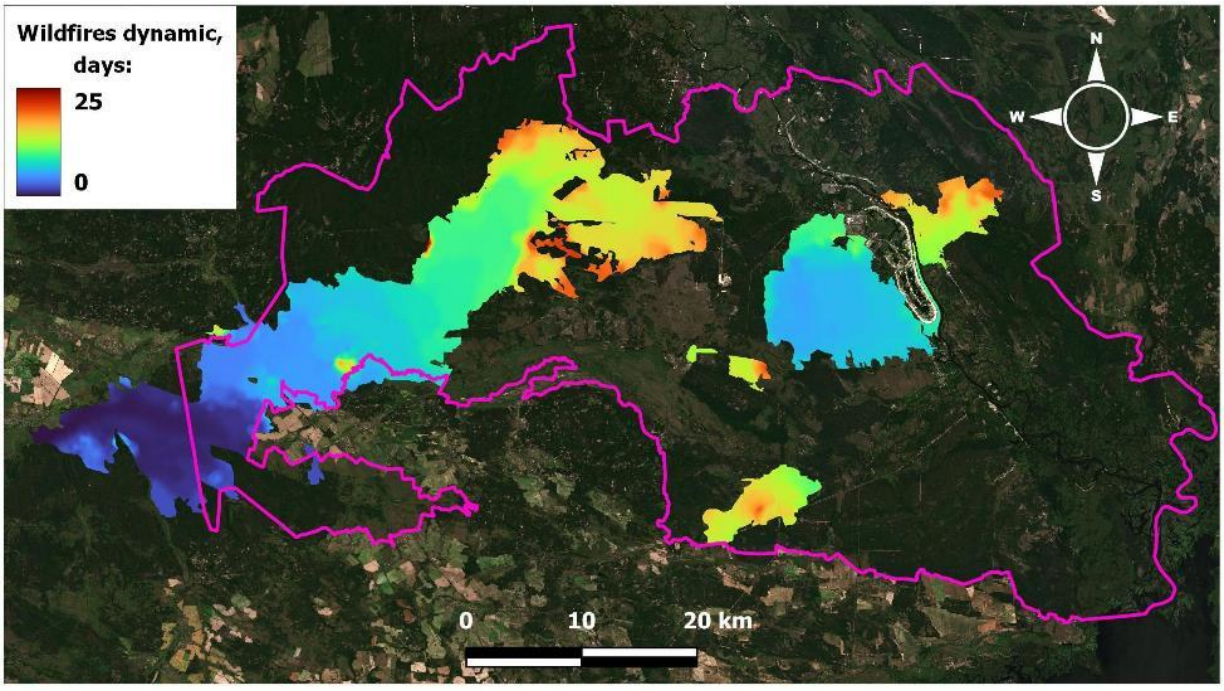


Figure 4.2 Simulated wildfire dynamic: start time – 2020-04-03 T 08:00:00

Copyright © FirEUrisk Consortium. All rights reserved.

These features were employed for mathematical transformations, facilitating the estimation of the speed of fire spread (v=s/t):

then if: $tan\, a = \frac{t}{s}$, *a in degrees* *(Equation 11)*

then in m day^{-1} $v = \frac{1}{\tan a} = \frac{1}{\tan(\frac{180 \cdot \alpha}{\pi})}$, or in m s^{-1} $\Rightarrow v = \frac{1}{\tan(\frac{180 \cdot \alpha}{\pi}) \cdot 86400}$. (Equation 12)

This allowed us to apply established approaches for evaluating fire indicators, similar to proven software applications such as FlamMap v.6.2, which incorporates the FARSITE fire behaviour modelling approach (Finney 1998, 2004; Ager et al., 2019; Myroniuk et al., 2021). However, it should be noted that all units were presented in SI units. We used a set of raster layers of 10-m (landscape classification: Figure 4.3) and 30-m (radionuclide contamination) spatial resolution. The simulation was performed within the delineated final fire outline (Figure 4.4). Given the information about the location of the wildfires at a specific moment in time and its total duration, we generated perimeters using a 6-h time lag.

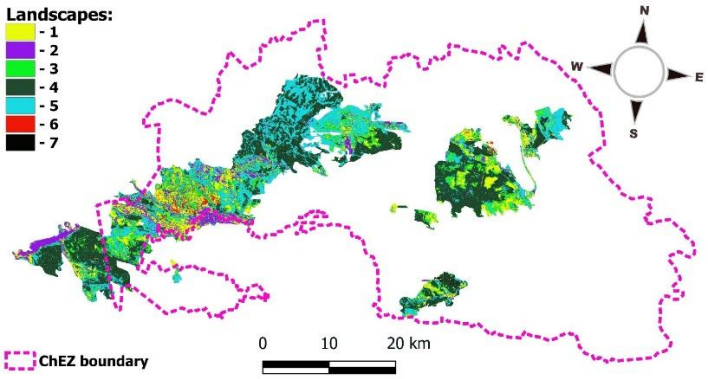


Figure 4.3 Landscape spatial distribution before wildfires in 2020 based on Sentinel-1 and 2 images as of 2019: 1 – meadow or fallow, 2 – swamp, 3 – single or groups of bushes and trees, 4 – coniferous forest, 5 – deciduous forest; 5 – dead stand after fire damage, 7 – dead stand without the influence of the pyrogenic factor.

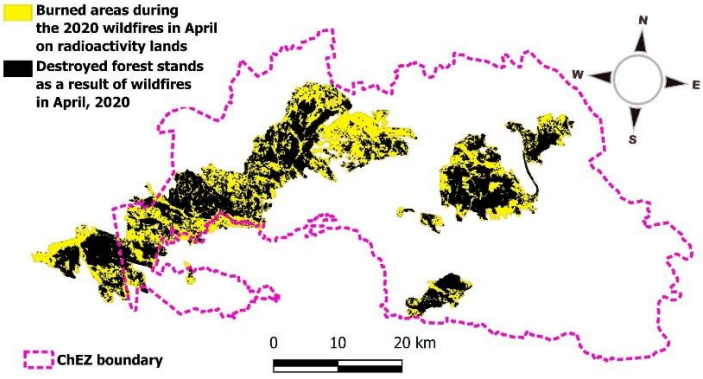


Figure 4.4 Fire outline. Areas affected by fire located in radioactivity land and destroyed forest stands

The mathematical basis for calculating the surface fire characteristics includes Byram's (1959) fireline intensity and flame length models and the linkages among them. These models address only the flaming front of the surface fire, which is influenced primarily by fine fuels. The surface fire model describes fire spreading through fuels that include litter, grass, brush, and other dead and live vegetation within about 5 m of the ground. Heat per unit area is available from intermediate calculations in the spread model. Byram's fireline intensity is calculated from the rate of spread and heat per unit area, forming the basis for the fire characteristics (Byram, 1959):

Copyright © FirEUrisk Consortium. All rights reserved.

$$I_B = H_A\, v \qquad \textit{(Equation 13)}$$

where I_B is Byram's fireline intensity (J m^{-1} s^{-1}), H_A is heat per unit area (J m^{-2}), v is rate of spread or fire speed (m s^{-1}). Flame length is calculated from fireline intensity, according to Byram's (1959) equation in its original form:

$$F_B = 0.45\, I_B^{0.46} \qquad \textit{(Equation 14)}$$

where F_B is Byram's flame length (ft), I_B is Byram's fireline intensity (Btu ft^{-1} s^{-1}).
Byram (1959) presented his model for fireline intensity in an identical form which was used in this research only based on SI units as:

$$I_B = H\, m\, v \qquad \textit{(Equation 15)}$$

where I_B is Byram's fireline intensity (J m^{-1} s^{-1}), H is heat yield (J kg^{-1} of fuel) based on data by Scott & Burgan (2005), m is the weight of the available fuel (kg m^{-2}), and v is a rate of spread (m s^{-1}).
Heat per unit area (H_A) is used to estimate $H\,m$, leading to equation (1). Heat per unit area is the heat energy released per unit area within the flaming front. "Available fuel", therefore, included only the fuel that burns in the flaming front and not the total fuel consumed.

Results

List of data to be transferred

We determined a series of parameters related to the spatiotemporal development of fires during April 2020 (from the 3rd to the 28th) using the methodological approaches described in Section 2. The classification results based on Sentinel-1 and 2 satellite images were used to estimate the biomass of combustible materials and heat energy release. Combining these initial data with the soil contamination densities of the main radionuclides (Sr-90, Cs-137, Pu-238-240 and Am-241) in the areas allowed us to calculate the emission of the studied isotopes into the atmospheric.

Using the primary input indicators such as the speed and direction of fire spread (Appendix, Figure A 6.1 and Figure A 6.2), the characteristics of combustible materials including biomass and heat of combustion (Table 1 and data provided by), and the results of the 2019 landscape classification with an overall accuracy of approximately 77%, we established the spatial distribution during the wildfire event the following parameters:

- Heat of combustion for combustible materials per unit area (Appendix, Figure A 6.3).
- Fireline intensity (Appendix, Figure A 6.4).
- Byram's flame length (Appendix, Figure A 6.5).

These combustion parameters at the time of wildfires can be valuable for simulating the transfers of "emitted" RNs in the air over significant distances.

Copyright © FirEUrisk Consortium. All rights reserved.

The density values of spatial soil contamination with the main RNs (Appendix, Figure A 6.6, Figure A 6.7, Figure A 6.8, Figure A 6.9), the transfer factors of these RNs into vegetation biomass (Table 4.1), probable coefficients of their resuspension into the air during wildfires based on previous experimental studies by other authors, and the ratio of these radioisotopes observed during the 2016 wildfire in the Red Forest (in the previous report: D2.5) were utilised to calculate the emission of RNs into the air from the wildfire-affected areas in April 2020 for different parts of the study region (Appendix, Figure A 6.10, Figure A 6.11,Figure A 6.12, Figure A 6.13).
The obtained output data were converted and saved in .dat format (typical data structure for working in the FORTRAN programming language environment) as a grid with a spatial extension of 100 m with an attribute table with columns:

- X_UTM_N36 is x coordinates in UTM zone n36 (CRS),
- Y_UTM_N36 is y coordinates in UTM zone n36 (CRS),
- Fire_time (days) is the time since the fire started, days
- Am_emi (Bq_sq_m) is americium-241 activity emission in the air from 1 sq. mmetre (Bq m-2),
- Cs_emi (KBq_sq_m) is cesium-137 activity emission in the air from 1 sq. metre (KBq m-2),
- Pu_emi (Bq_sq_m) is plutonium-238-240 isotopes activity emission in the air from 1 sq. metre (Bq m-2),
- Sr_emi (KBq_sq_m) is strontium-90 activity emission in the air from 1 sq. metre (KBq m-2),
- v (m_s) is a rate of spread (m s-1),
- Flame_length (m) is Byram's flame length (m),
- Combustion energy (MJ_sq_m) is fuel heat per unit area (MJ m-2),
- Fireline_intensity (kJ_m_s) is Byram's fireline intensity (kJ m-1 s-1).

There is also a grid with a spatial extension of 10 m, but it has a size of about 1.0 GB of memory.

Summary research results on RNs emissions during the wildfires in April 2020

The landscape wildfires within the most radioactively contaminated territories of Ukraine (ChEZ and adjacent areas) covered an area of over 70,000 hectares within a relatively short period in April 2020 (25 days), which had never been observed before in the studied region. Approximately 900 Kt of organic matter was burnt, resulting in the release of around 350 Gg of Carbon. Moreover, the wildfires translocated approximately 216 GBq of Cs-137, 80 GBq of Sr-90, 106 MBq of Pu isotopes, and 530 MBq of Am-241 into the atmospheric air. The dynamics of wildfire developments (Figure 4.5) and radionuclide emissions (Figure 4.6) over time indicate that they are non-monotonic, influenced by both weather conditions and the spatial heterogeneity of landscape distribution and radionuclide contamination within the burn areas.

Copyright © FirEUrisk Consortium. All rights reserved.

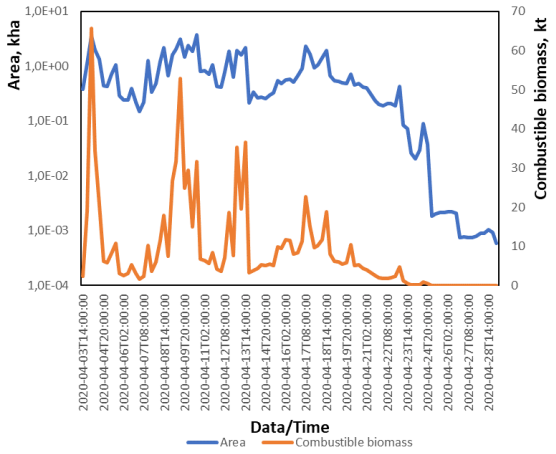


Figure 4.5 Dynamics of burnt areas and combusted materials during the 2020 wildfires in April using a 6-h time lags.

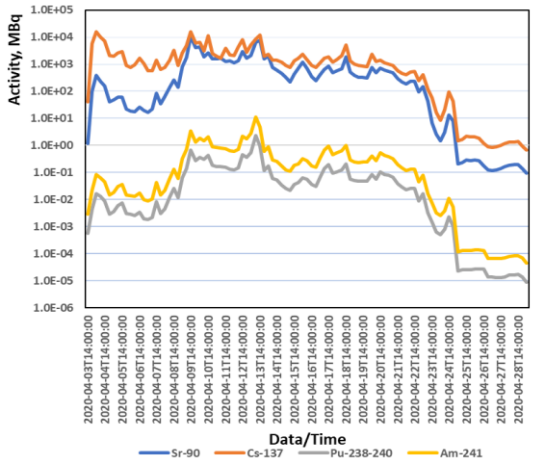


Figure 4.6 Time series of RNs emissions during the Chornobyl wildfires in April 2020.

Note: the minimum predictive values are presented for TUE (Pu-238-240, Am-241), multiply the TUE RNs activity in the table by 10 to obtain the most "probable" values.

In general, the wildfire spread in waves because this territory had a large number of obstacles to the movement of the fire: roads, railways, water basins and mineralised strips. The slight wind at separate time intervals did not allow the fire to "jump over" these obstacles to get to other territories. And on the night of April 28th (2020), the rain extinguished all active sources of fire.

A comparison of the assessment results of radioisotope activity emissions during the 2016 wildfire in the Red Forest and the "large" wildfires in April 2020 indicates that the immediate zone around the Chornobyl NPP is the primary source of TUE and Sr-90 resuspension into the atmospheric air when wildfires spread in the ChEZ (Figure 4.2). In our cases, despite a more than 200-fold difference in burnt areas between these compared events, the volumes of transuranium element resuspension differ only by about 2 times, and Sr-90 by approximately 3.1 times. It is these radioisotopes that can contribute significantly to the internal dose load of firefighting participants during the extinguishing of wildfires in the nearest 10-kilometre zone around the Chornobyl NPP.

Table 4.2 Areas and RNs emissions during the Chornobyl wildfires in Red Forest (2016) and in the ChEZ and adjacent territories (April, 2020).

Wildfires:	Area, ha	The total emission of RN activity into the atmospheric air taking into account the radioactive decay as of April 15, 2020, GBq			
		Sr-90	Cs-137	Pu-238-240	Am-241
in Red Forest (2016)	366	25.3	27.0	0.0050*	0.025*
in the ChEZ and adjacent territories (2020)	71800	80.2	216	0.0106*	0.053*

Note: * the minimum predictive values are presented for TUE, multiply the TUE RNs activity in the table by 10 to obtain the most "probable" values.

Conclusions

In light of the aforementioned, the primary focus for implementing activities to prevent the occurrence and development of wildfires should be on territories with a high density of soil contamination with Sr-90, Pu-238-240, and

This project has received funding from the European Union's Horizon 2020 research and innovation programme under grant agreement No 101003890.

Am-241 isotopes. This is particularly crucial in areas where plantation pine forests grow under moderate soil moisture conditions, as these plant communities have the potential to generate significant biomass of combustible materials.

Policy recommendations

Landscape fires in radionuclide-contaminated areas of the ChEZ are a major source of radionuclide resuspension into the atmosphere, creating non-standard health risks for firefighters working on the fireline. The following two groups of policy recommendations (radiation safety and organisational activities) must be considered by responsible fire management agencies:

1) Radiation safety:
   - To develop zoning of contaminated territories based on the level of inhalation doses for firefighters and the probability of ignition/burn.
   - To improve protocols for safety rules and establish strategies and tactics for fire suppression that minimize inhalation doses for firefighters and risks to nuclear infrastructure.

2) Organisational activities to improve the speed and effectiveness of wildfire detection and suppression, which also help to reduce firefighters' exposure to ionizing radiation and health risks by minimizing the time spent on tasks in contaminated areas:
   - To develop software with an updated map of roads and fire ponds for fire engines, including modelling the expected time of arrival of fire crews at potential fire locations and the time needed for water delivery, integrated with fire behaviour models.
   - To enhance prevention measures to keep fires contained within fire blocks using fire breaks, roads, and responsive actions.
   - To develop a fire detection map for reliable prediction of fire coordinates, optimising the placement of detection cameras based on topography and fire hazard.
   - To establish a system for aggressive initial attacks by interagency crews during extreme fire weather conditions.

References

Ager, A. A., Lasko, R., Myroniuk, V., Zibtsev, S., Day, M. A., Usenia, U., Bogomolov, V., Kovalets, I. & Evers, C. R., (2019). The wildfire problem in areas contaminated by the Chernobyl disaster. Science of the Total Environment, 696, 133954. https://doi.org/10.1016/j.scitotenv.2019.133954

Begichev, S. N., Borovoy, A. A., Burlakov, E. V., Havrilov, S. L., Dovbenko, A. A., Levina, L. A., Markushev, D. M., Marchenko, A. E., Stroganov, A. A. & Tataurov A. K. (1990). Preprint IAE-5268/3: Reactor Fuel of Unit 4 of the Chernobyl NPP (a brief handbook), Moscow, Publisher Kurchatov Institute of Atomic Energy, 21 pp. (in Russian)

Beresford N.A., Barnett C.L., Gashchak S., Maksimenko A., Guliaichenko E., Wood M.D. & Izquierdo M. (2021). Radionuclide transfer to wildlife at a 'Reference site' in the Chernobyl. Journal of Environmental Radioactivity https://doi.org/10.1016/j.jenvrad.2018.02.007

Copyright © FirEUrisk Consortium. All rights reserved.

Byram, G.M. (1959). Combustion of forest fuels. In K.P. Davis (ed.). Forest fire: control and use. pp. 61–89, 554–555. McGraw Hill, NewYork, NY

Borsuk, O. (2020). Comprehensive assessment of the fire hazard of forests in the exclusion zone [Text] : Diss. cand. agr sciences : 06.03.03 / Oleksandr Anatoliyovych Borsuk; National University of Life and Environmental Sciences of Ukraine. - Kiev, - 188 p.

Chen, T. & Guestrin, C. (2016). XGBoost: A scalable tree boosting system. Proc. ACM SIGKDD Int. Conf. Knowl. Discov. Data Min. 13-17-August-2016, 785–794. https://doi.org/10.1145/2939672.2939785

Crookston, N. L. & Dixon, G. E. (2005). The forest vegetation simulator: A review of its structure, content, and applications. Computers and Electronics in Agriculture, 49(1), 60–80. https://doi.org/10.1016/j.compag.2005.02.003

Demirkaya, A., Chen, J. & Oymak, S. (2020). Exploring the Role of Loss Functions in Multiclass Classification. 2020 54th Annu. Conf. Inf. Sci. Syst. CISS 2020. https://doi.org/10.1109/CISS48834.2020.1570627167

Finney, M. A. (1998). FARSITE: Fire Area Simulator–model development and evaluation. Research Paper RMRS-RP-4 Revised. Ogden, UT: U.S. Department of Agriculture, Forest Service, Rocky Mountain Research Station. (1,667 KB; 47 pages)

Finney, M. A. (2004). FARSITE: Fire Area Simulator–model development and evaluation. Research Paper RMRS-RP-4 Revised. Ogden, UT: U.S. Department of Agriculture, Forest Service, Rocky Mountain Research Station. (1,667 KB; 47 pages)

European Space Agency. (2022). Sentinel Technical Guide. https://sentinels.copernicus.eu/web/sentinel/sentinel-technical-guides (accessed 28 April 2023)

Holiaka, D. M., Levchuk, S. E., Kashparov, V. A., Holiaka, M. A., Yoschenko, L. V., Otreshko, L. N., Kosarchuk, O. V. & Lazarev, N. M. (2020a). Vertical distribution of ^{90}Sr in soil profiles and its uptake by scots pine (Pinus sylvestris l.) wood growing within the chernobyl exclusion zone. Nuclear Physics and Atomic Energy, 21(2), 157–165. https://doi.org/10.15407/jnpae2020.02.157

Holiaka, D. M., Levchuk, S. E., Yoschenko, V. I., Kashparov, V. A., Yoschenko, L. V., Holiaka, M. A., Pavliuchenko, V. V., Diachuk, P. P., Zadorozhniuk, R. M. & Morozova, V. S. (2020b). ^{90}Sr and ^{137}Cs inventories in the depots and biogenic fluxes of the typical forest stands in the chernobyl exclusion zone. In Nuclear Physics and Atomic Energy (Vol. 21, Issue 3, pp. 256–264). https://doi.org/10.15407/JNPAE2020.03.256

IAEA. (2010). Handbook of parameter values for the prediction of radionuclide transfer in terrestrial and fresh-water environments. Vienna: IAEA-TRS-472, 194p. http://www-pub.iaea.org/MTCD/publications/PDF/trs472_web.pdf

Kashparov, V., Levchuk, S., Zhurba, M., Protsak, V., Beresford, N.A. & Chaplow, J.S. (2020). Spatial radionuclide deposition data from the 60 km radial area around the Chernobyl Nuclear Power Plant: Results from a sampling survey in 1987. Earth Syst. Sci. Data 12, 1861–1875. https://doi.org/10.5194/essd-12-1861-2020

Kashparov, V., Levchuk, S., Zhurba, M., Protsak, V., Khomutinin, Y., Beresford, N.A. & Chaplow, J.S. (2018). Spatial datasets of radionuclide contamination in the Ukrainian Chernobyl Exclusion Zone. Earth Syst. Sci. Data 10, 339–353. https://doi.org/10.5194/essd-10-339-2018

Copyright © FirEUrisk Consortium. All rights reserved.

Myroniuk, V., Zibtsev, S., Bogomolov, V., Soshenskyi, O., Gumeniuk, V. & Vasylyshyn, R. (2021). A web-based platform LANDSCAPE FIRES: Regional-level fire management information system for Northern Ukraine. Geoinformatics, 1–6. https://doi.org/10.3997/2214-4609.20215521113

Paskevich S. (2005). Radiation weight of phytocenoses of meadows and fallows of the Chornobyl exclusion zone at the stage of the late phase of the accident [Text] : Diss. cand. biological sciences: 03.00.01 / Serhii Anatoliyovych Paskevich; National Academy of Sciences of Ukraine, Institute of Prob. NPP safety. - Chernobyl, - 188 p.

Scott, J. H. & Burgan, R. E. (2005). Standard fire behavior fuel models: A comprehensive set for use with Rothermel's surface fire spread model (RMRS-GTR-153). U.S. Department of Agriculture, Forest Service, Rocky Mountain Research Station. https://doi.org/10.2737/RMRS-GTR-153

XGBoost developers. (2022). XGBoost Documentation. https://xgboost.readthedocs.io/en/stable/index.html (accessed 28 Dec 2022)

Yoschenko, V.I., Kashparov, V.A., Levchuk, S.E., Glukhovskiy, A.S., Khomutinin, Y. V., Protsak, V.P., Lundin, S.M. & Tschiersch, J. (2006a). Resuspension and redistribution of radionuclides during grassland and forest fires in the Chernobyl exclusion zone: Part II. Modeling the transport process. J. Environ. Radioact. 87, 260–278. https://doi.org/10.1016/j.jenvrad.2005.12.003

Yoschenko, V.I., Kashparov, V.A., Protsak, V.P., Lundin, S.M., Levchuk, S.E., Kadygrib, A.M., Zvarich, S.I., Khomutinin, Y. V., Maloshtan, I.M., Lanshin, V.P., Kovtun, M. V. & Tschiersch, J., (2006b). Resuspension and redistribution of radionuclides during grassland and forest fires in the Chernobyl exclusion zone: Part I. Fire experiments. J. Environ. Radioact. 86, 143–163. https://doi.org/10.1016/j.jenvrad.2005.08.003

4.2 Post-fire landslides: Landslide susceptibility and related cascading effects after a fire event

Laneve, G., Universita Degli Studi di Roma La Sapienza, SIA

Introduction

In the literature, the most commonly used definition of the landslide is the following: *movement of a mass of rock, soil or debris along a slope" (Cruden, 1996) as a prevailing effect of the force of gravity and can be subject to extremely different speeds depending on the predisposing factors*. Landslides are complicated events to study, precisely because of the multiplicity of factors that intervene in triggering a landslide movement.

These factors can be determining factors, which give rise to the landslide movement such as rainfall, earthquakes, etc. or predisposing factors which facilitate the formation of landslides such as the slope of the land, the structure of the soil, etc. A landslide can have triggered by natural causes such as rain or earthquakes, or by artificial causes such as deforestation which depletes the soil of roots, or any constructions on slopes. The occurrence of landslides is therefore the result of the combination of different factors which must be, as far as possible, monitored also in relation to the obvious damage that landslides can cause. Predisposing factors can be classified into:

Factors that do not vary over time and therefore are characteristic of a mountainside and we can mention:

Copyright © FirEUrisk Consortium. All rights reserved.

- Morphological factors: the slope is typical, as the steeper the slope the greater the instability (landslide movements are a function of the gravitational force) since the shear stresses applied to the slope increase, furthermore the more the surface is steep the more the speed of landslide movements is high.
- Geotechnical factors: they give a measure of the resistance that the masses or soils have with respect to shear stresses, they can be measured in the laboratory with specific investigations.
- Geological factors: type of land and rock masses considered.
- Hydrogeological factors: linked to geological ones and to the porosity and permeability of rocks. Of significant importance is precisely the permeability of the rocks which influences underground and surface water circulation.
- Structural factors: such as the presence of stratification surfaces, faults or fractures, therefore everything that causes weak surfaces of the deposit.

Factors that vary over time and must be monitored for their variability such as:

- Vegetation and climatic factors: clearly extensive forest vegetation opposes atmospheric agents, reducing the possibility of triggering landslides, therefore greatly influencing the presence or absence of landslides. As regards the climate, it also has a fundamental role, especially if we consider seasonal events such as periods of drought or abundant rainfall which can lead to the triggering of landslides. For example, a high rainfall rate can lead to variations in the flow rate of the drainage network with a significant increase in erosive events.
- Anthropic factors: i.e. human intervention, which in a very short time creates sudden changes in natural situations that have stabilized over a very long time, altering the natural balance. Among these interventions we include deforestation, excavations and consequent slopes instability. They can be considered both as triggering and predisposing causes.

The main trigger factor for landslides is rainfall, in fact rapid and superficial phenomena such as debris flow and soil slip (which affect the superficial layer of soil cover) occur after intense rainfall.

Landslide Classification

One of the classifications most used by scholars, precisely because of its simplicity of use and applicability at work, is that of Varnes 1978 which takes into consideration two aspects regarding landslide phenomena:

- Type of material involved: we can highlight different mechanical behaviour depending on the type of material.
- Type of mass movement: it defines the dynamics with which landslide movements occur.

As regards the type of material involved, we find:

- Rock: by rock we mean "a natural aggregate of granules or minerals bound by high cohesion, which is not lost even after drying or prolonged immersion" in water (for example limestone, granite, sandstone, travertine, etc.).
- Soil: is defined as "a natural aggregate of granules or cohesive minerals with a granule size of less than 2 mm" (n), which may be either not bonded to each other or may disintegrate after prolonged contact with water (causing the material to become plastic) or with modest stresses (for example clays, lake silts, etc.).

Copyright © FirEUrisk Consortium. All rights reserved.

- Debris: means a "natural or artificial aggregate constituting the roof, with low to no cohesion"; The detrital elements tend to disintegrate easily with modest stresses or by agitation of water. Generally, it is material larger than 2 mm (e.g. groundwater debris, regolith, weathered sand, landfill materials, pozzolans and volcanic pumice, etc.). In this definition we can also include the soil, meaning only the most superficial part of the cover.

Instead, as regards the types of mass movements, with respect to the above-mentioned classification we distinguish the various movements into:

- Collapses (Rock falls, Debris falls, Earth falls): collapses mean the landslide movement characterized by "free fall of blocks of rock, debris or earth, detached from the slope along predominantly vertical discontinuities". Generally, it is a rapid and characteristic phenomenon on very steep slopes. The predisposing causes include the presence of lithological and structural discontinuities (in fact they occur above all along pre-existing newly formed discontinuities), cracks, tectonic fracturing. Certainly, the determining causes can be found in intense meteorological events, seismic stress or evident changes in the geometry of the slope.
- Reversals (Rock topple, Debris topple, Earth topple): they are represented by rigid rotations of masses or by inflections around a fulcrum placed under the centre of gravity of the mass itself. The causes that predispose this type of landslide are of a structural nature such as the presence of a family of discontinuities. The triggering causes can vary from major meteorological events to seismic stress and artificial vibrations. The speeds at which they can happen are very variable.
- Rotational slides (Rotational slides, Rock slump, Debris slump, Earth slump): they are represented by rotational movements around a point or an axis that is external to the slope and above the centre of gravity of the displaced mass. the failure surface is curved, and the resulting concavity is upwards. The moving mass can break down into several blocks rotated in different directions, but if clayey and marly lithotypes are largely present it leads the movement to become a slow flow. The determining causes can be multiple such as sudden increases in shear stress, heavy rainfall events, breakages of water networks or anthropogenic changes to the geometry of the affected areas.
- Translational slides (Translational slide, Rock block slide, Earth block slide): these movements involve translational movements of variable speed, along predominantly planar discontinuity surfaces in the direction of maximum slope. This occurs when the discontinuity surfaces are placed in the same direction as the slope with an inclination equal to or less than that of the slope. The determining causes generally lie in a sudden increase in shear stresses due to weighting of the slopes or seismic events, or in a decrease in shear resistance which can be caused by an increase in the water content in the soil due for example to meteoric events intense or water infiltrations.
- Slow flows: These are slow mass deformations characterised by an accentuated plastic deformation. The movement can involve the entire landslide body, in fact it can involve an extremely variable thickness of soil. The speed of these flows is generally slow but still depends on the slope of the ground, the water content and also on the space since it can undergo variations between the centre (where it is often faster) and the edges, and it is precisely this characteristic that determines the shape. This type of landslide mainly affects land and

Copyright © FirEUrisk Consortium. All rights reserved.

the predisposing factor is often the presence of clayey soils or soils that have low cohesion and weak consolidation.

- Rapid flows (Debris flow, Mud flow, Stony debris flow, Dry sand flow, Debris avalanche, Debris slide): they occur when we are in the presence of an extremely loose set of materials and water, and all this flows down the slopes or along impluvium lines. Even entire slopes can affect very large areas.
- Lateral spreading: To understand this type of landslide we can give as an example rigid rock bodies (massive sandstones, limestones or volcanic deposits) resting on soils with plastic behaviour. These landslide phenomena occur when a change in pressure on the rock mass creates a deformation of the underlying soil. Once the deformation has been created, the block is divided along pre-existing or newly formed fractures and lowers in a different way, moving laterally towards the valley. These movements, in addition to being very slow, so much so that they are not appreciated on the human time scale, can also occur at great depths. When the rigid plate fractures, it splits into blocks and lowers, moving laterally downstream. The clay-type materials rise between the fractures, creating lateral bulges on the rigid plate. Other landslide movements of lateral expansion involving stone materials and terrigenous deposits may be associated. The most common are translational, collapse, overturning, collapse and rotational sliding.
- Complex movements: This type of landslide is called complex because it derives from the combination in space and time of two or more types of landslides among the previous ones. An example is the DGPV (Deep Slope Gravitational Deformations) which are categorized as complex movements. Their main characteristic is the progressive and slow (in the order of millimetres per year) deformation of large masses. A continuous cutting surface is not always found.

In Italy, the IFFI (Inventory of landslide Phenomena in Italy) project (Trigila et al.), coordinated by ISPRA (Higher Institute for Environmental Protection and Research) aims at providing in detail all the data on the distribution of landslide phenomena at national level. With almost 470,000 landslides recorded over an area of approximately 20,000 km^2, equal to 6.6% of the national territory, this inventory represented a very important database at a national, European and international level. The Italian municipalities affected by landslides are 5,596, equal to 69% of the total. The data from the IFFI Project have been integrated into the Regional Geographic Information Systems, have been used by the regional, provincial and municipal Administrations for the definition of landslide hazard in the Hydrogeological Management Plans (PAI, Piani di Assetto Idrogeologico), for the drafting of the Territorial Provincial Coordination Plans (PTCP), General Regulatory Plans (PRG) and Civil Protection Plans.

The census of each landslide phenomenon is carried out by compiling a "Landslide form" composed of three levels:

Basic information (location, type of movement, activity status).
In-depth knowledge (previous activation dates, geology, land use, morphology, lithology).
Detailed information on hydrogeology, damage and restoration interventions.
In the cartographic database, however, each landslide phenomenon is mapped using three elements:
PIFF (Landslide Phenomenon Identification Point).
Polygon: when the landslide surface can be mapped at the survey scale adopted (e.g. 1 hectare for 1:25,000 scale).
Line: when the width of the landslide cannot be mapped.

Copyright © FirEUrisk Consortium. All rights reserved.

If we look at the total number of landslides, in Italy, the percentages of landslide types we find are:

- Rotational/translational slides: 32.83% of the total number of landslides.
- Slow landslides: 5.5% of the total number of landslides.
- Rapid landslides: 14.86% of the total number of landslides.
- Complex movements: 11.6% of the total number of landslides.
- Areas subject to widespread collapses/overturns: 11.51% of the total number of landslides.
- Areas subject to widespread shallow landslides: 5.31% of the total number of landslides.
- Areas subject to widespread landslides: 0.02% of the total number of landslides.
- Collapse/overturn: 3.44% of the total number of landslides.
- DGPV: 0.32% of the total number of landslides.
- Sinking: 0.8% of the total number of landslides.
- Expansions: 0.05% of the total number of landslides.
- Areas subject to widespread landslides: 0.02% of the total number of landslides.
- Not Available: 4.47% of the total number of landslides.

Data and Methods

Correlation between fires and debris flows

Having explained the individual phenomena that we intend to study, it is now necessary to correlate them and focus attention on how, after the presence of fires, the same areas can be affected by debris flows, mudflows and erosion processes. Erosion processes that generate debris flow on areas affected by fire are very frequent in the literature, for example in the United States 210 basins were studied, 76% of which produced debris flows after the fire (Gartner et al. 2011, DeGraff et al., 2015; Cannon and DeGraff, 2009, DeGraff 2014, Di Napoli et al. 2021). Clearly, in the presence of an extensive fire, we immediately recognise a threat, but even the landscape, which has been altered by the fire, can cause serious damage due to flooding and debris flows triggered by rain events. These problems can even occur from a few days up to 2 - 3 years after the fire (Cannon and DeGraff 2009, Staley, 2013, McGuire, 2021). This is very relevant because in the presence of fire and intense rainfall, the probability of these erosion events occurring in an area affected by fires is high up to approximately 3 years after the fire event. Many scholars and researchers have studied the correlation, the triggering factors, the behaviour, and the connection of the two phenomena through prediction models based on probabilistic regression models, in most cases, to define the probability of occurrence of flows debris. Fires cause numerous changes to the vegetative characteristics and physical and chemical properties of the soil. Reducing plant cover on slopes increases soil exposure to rainfall, which can lead to increased erosion from rainfall and runoff. Fires increase the rate of runoff production as they increase the hydrophobicity of the soil, introducing with burning, chemical changes in the soil itself such as depletion of organic substances necessary to aggregate soil particles and maintain permeability, without which it is reduced the infiltration capacity of water contributing to greater erosion and surface runoff. In fact, it is the plant material that when burnt contributes to the formation of a hydrophobic layer. The resistance of the soil to erosive processes is increased by the presence of roots especially near the surface which strengthen its compactness. Some researchers have quantified the static action of the roots and consequently modified the expression of the safety factor in the case of an indefinite slope (Di Napoli et al. 2020). It is precisely these changes

Copyright © FirEUrisk Consortium. All rights reserved.

that contribute to greater runoffs that allow the triggering of floods and debris flows, even with less rainfall than if the ground had not been affected by fires. The combined action of physical and chemical changes in the soil (due to fires), with steep slopes and with a large amount of sediment, greatly increases the probability of post-fire debris flows.

Landslide susceptibility

The inputs and therefore the information layers used to assess the landslide susceptibility are all predisposing factors that influence differently the presence of these events. In the following table, (Table 4.3), the inputs used, the sources of the data, the format of these information layers and finally the information used in this work are shown.

Table 4.3 List of information layers used to identify the landslide susceptibility.

Input layers	*Source*	*Format*	*information*
DEM (*Digital Elevation Model*)	Copernicus	Raster	Hight, Slope, Aspect ratio
Phytoclimate	Ministry of Environment	Shape file	Phytoclimatic zones
Lithology	Copernicus	Shape file	Territory lithology
Corine Land Cover	Copernicus	Shape file	Land cover/land use map
Inventory of the landslides, IFFI	ISPRA	Shape file	Areas interested by landslide
Burnt areas	SIA	Shape file	Areas burnt

The purpose of the methodology implemented is the estimate of an index of susceptibility to landslides after the occurrence of fires. Susceptivity is the basis of the subsequent calculation of danger and risk and allows us to improve the monitoring, control and protection of the territories that have experienced these natural disasters. The land affected by fires, have a greater probability of being subject to landslides in the two or three years after the occurrence of the fire. The types of landslides considered by this study are debris flows and erosion. In fact, not all types of landslides are involved in this phenomenon, since the fire influences soil instability processes in particular on this type of landslide movements taken into consideration. Precipitation in burnt areas, which as mentioned act as a trigger of the types of landslides involved, can produce a flow of debris of about 1000 times higher than the pre-fire, with a consequent high transport of solid material. For these reasons, the study is focused on the susceptibility of landslide after fires in relation to the debris flows and erosion mentioned above. The method, developed in the GIS environment, is described in the high -level block diagram illustrated below.

As done in the case of the identification of the areas deserving a management of the vegetation fuel to reduce the probability of wildfire (Laneve et al., 2020), the first step to assess the spatial distribution of landslide susceptibility consists in dividing in classes each one of the layers listed in Table 4.3 with the aim of creating a map of homogeneous classes called HTC (Homogeneous Territorial Classes) where each class is made up of pixels that have the same characteristics.

Copyright © FirEUrisk Consortium. All rights reserved.

The estimate of landslide susceptibility is subject to the use of landslide perimeters dataset. Our interest is focused on the susceptibility of landslide in relation to the burnt areas, for this reason we present a couple of examples concerning the two Italian islands of Stromboli and Ischia.
Since we are mainly interested in assessing the impact of wildfires, in combination with other phenomenon (heavy rain) in enhancing the probability of landslide phenomenon, from the IFFI dataset only the types of landslides potentially related to the presence of fires were considered. In this way we took into consideration only the landslides of interest, reducing possible errors in the methodology. From the new perimeter, a pre-fire landslide mask (IFFI Project) was created, which was applied to the HTC map, with the aim of obtaining:

- Areas that had undergone landslides (always in reference to the pre-fire).
- HTC homogeneous classes corresponding to these areas.

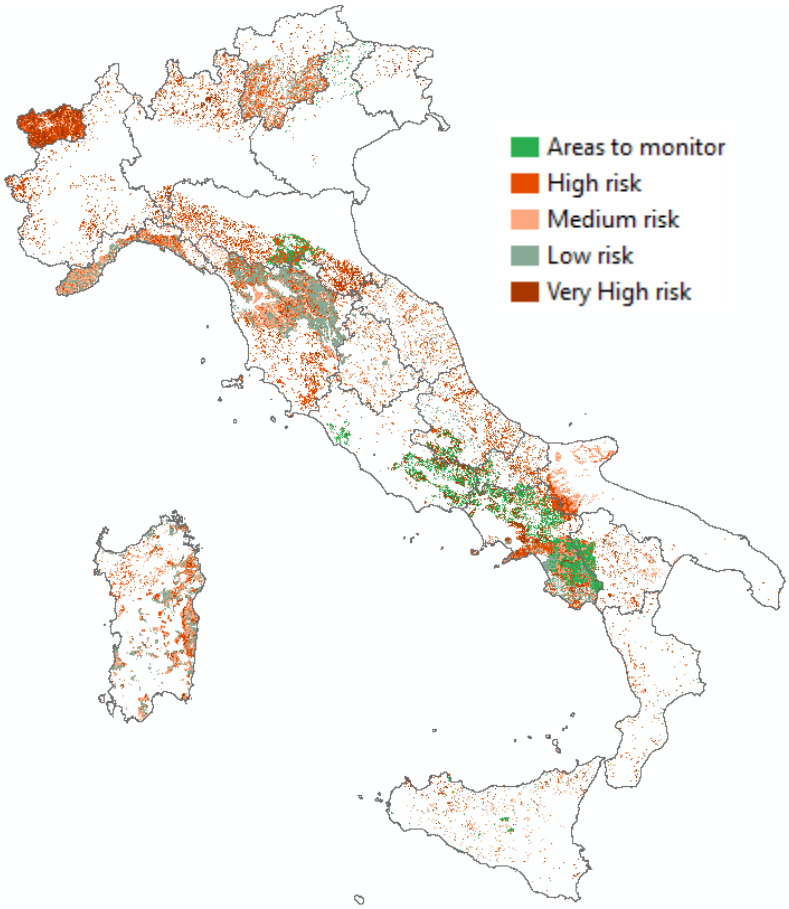
The estimate of landslide susceptibility of each homogeneous class is now introduced, which has been calculated as follows:

$$S = \frac{N_f}{N_{htc} \cdot Y}$$

where:
N_f represents the number of pixels landslides for the i-th class, since it is taken from the intersection between landslides of the IFFI and HTC project.
N_{htc} represents the total number of pixels of the I-th class (therefore defines the area of the i-th class). This figure was taken from the map of homogeneous classes (HTC) initially created, which allowed to know the number of pixels belonging to each i-th class. *Y* represents the interval of years considered in the perimeter file of the landslide areas.

Copyright © FirEURisk Consortium. All rights reserved.

We must consider the parameter Y as it has allowed us to compare the susceptibility before and after fires. It would be an error not to take this into account since the IFFI project considers at least 50 years of landslides, unlike the post-fire landslide areas that we consider the following 3 years. Initially, to estimate the pre-fire landslides susceptibility using the IFFI project data, we considered Y = 52. This choice derives from the fact that until the 1950s the estimated landslides were few due to poor technology. It is precisely in the 1950s that the first aerial photos began and made it possible to detect a considerable number of landslides. The susceptibility of landslides is calculated for each homogeneous class. Subsequently, the data is further refined through the creation of five susceptibility classes:



Very low (0% - 20%)
Bassa (21% - 40%)
Moderate (41% - 60%)
High (61% - 80%)
Very high (81% - 100%)

Figure 4.7 Distribution of areas subjected to landslide in Italy (source: ISPRA).

Results

Two examples are showcased in this section, one on Stromboli Island and another in Formia (Lazio region).

Stromboli volcanic island

This Italian Island was affected by a large fire on the 25th of May 2022. Figure 4.8 shows the burnt area as detected by applying dNBR index to Sentinel-2 images. The catastrophic fire burnt a large part of the natural oasis on the slopes of the volcano. During the first violent storm in mid-August, a few hours of torrential rain were enough and Stromboli town, located at the north-east of the island, found itself in the middle of the mud. The damage the next day was enormous. Houses evacuated, hotels suffocated by mud, tourists on the run (Figure 4.8).

Copyright © FirEURisk Consortium. All rights reserved.

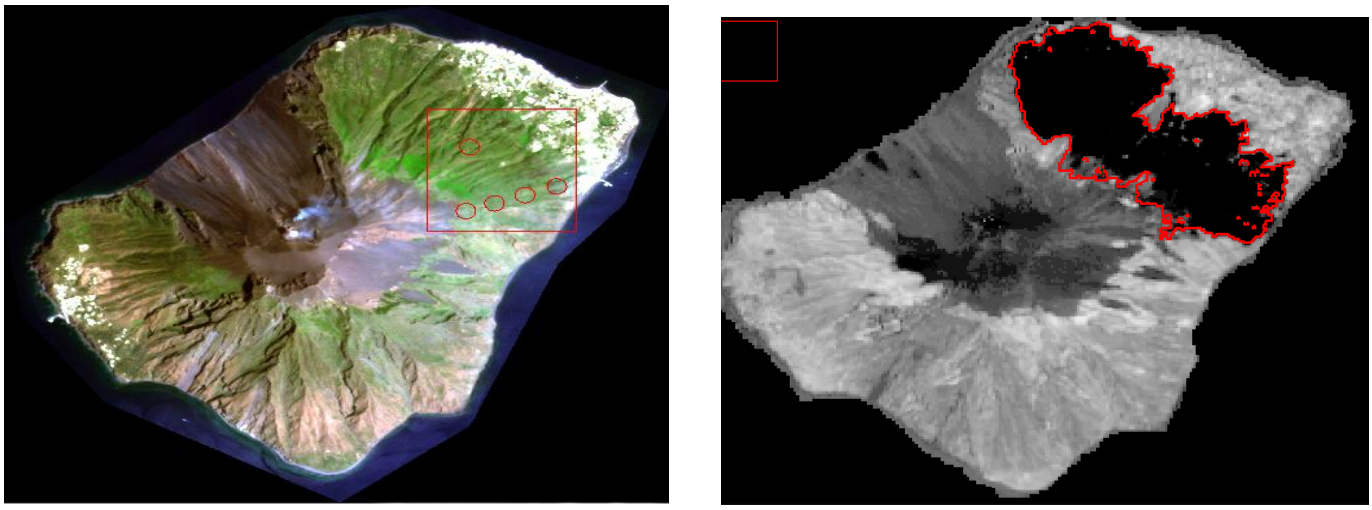


Figure 4.8 (left) Planescope RGB image acquired on 01/06/2022. Red circles represent the hot spots observed at 13:15 (MODIS and VIIRS) of the 25 May. (right) Normalized Burn Ratio (NBR) map computed by using a Sentinel 2 image of 01/06/2022, whit superimposed the shapefile of the burnt area.



Figure 4.9 Image of the impact of the mud avalanche due to the heavy rain occurred some months after a disastrous wildfire in Stromboli (from La Repubblica newspaper).

It is interesting to note as the area affected by the mud flow (the Stromboli town at north-east) in 2022 was not considered at risk in the ISPRA landslide database (Figure 4.9).

Copyright © FirEUrisk Consortium. All rights reserved.

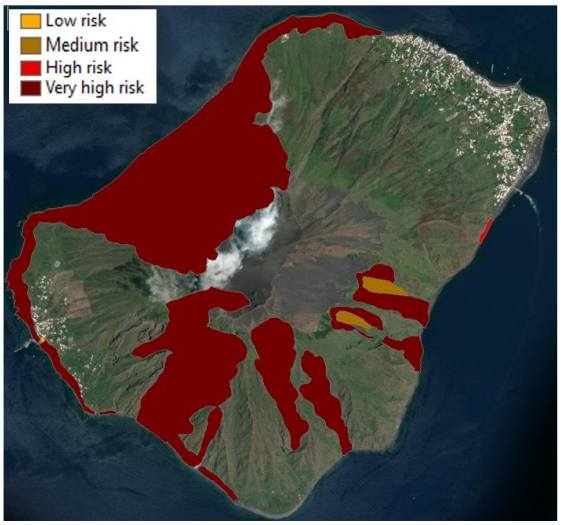


Figure 4.10 Distribution of the landslide risk for the Stromboli Island, from the ISPRA dataset, before 2022 fire event. The legend includes all the levels of risk available in the dataset.

Formia (Lazio region)

A mud flow affected the city of Formia in Italy on September 29th, 2022. The area was affected by a big fire between July 30th and August 3rd, 2022. In Figure 4.10, we show the map of landslide risk in the area in accordance with IFFI data. The same figure shows, in blue, the polygon corresponding to the burn area and in pink the area where the mud avalanche started. It is interesting to observe as the area affected in the event was not considered, up to 2021, at risk in the landslide risk map. The event took place after a violent storm. In

Figure 4.11, it is also shown the DEM of the area interested by the debris flow.

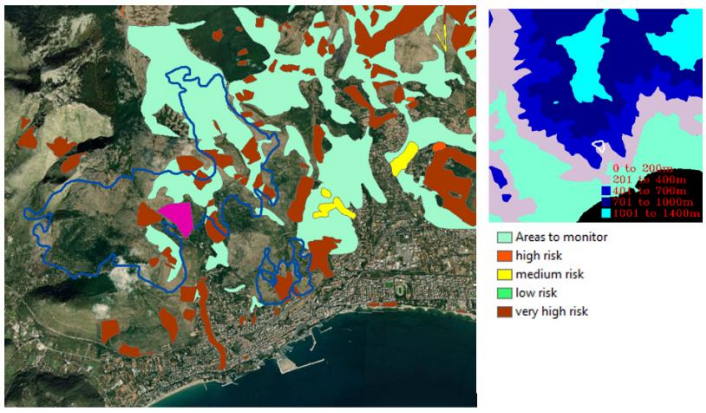


Figure 4.11 Formia town area. Distribution of landslide risk, from ISPRA dataset, before 2022 fire event. The blue polygon shows the area burnt by a fire between July 30th and August 3rd, 2022. In pink the area from where the debris flow originated. The inset on upper left shows the DEM in the area with superimposed, in white, the polygon of the origin of the debris flow.

Conclusions

The negative effects of landslides can be amplified because of specific environmental factors. Especially, topography, vegetation, and anthropic factors together with the occurrence of natural hazards such as wildfire and floods greatly impact on the potential cascading effects related to landslides. The potential impacts of the concurrence of several

Copyright © FirEUrisk Consortium. All rights reserved.

hazards are not easy to be foreseen. For example, it is interesting to note as the area affected by the mud flow (the Stromboli town at north-east) in 2022 was not considered at risk in the ISPRA landslide database. Therefore, this analysis will contribute to increase awareness and improve the preparedness phase of future events, which will potentially help to reduce the negative impacts.

Policy recommendations

Debris flows are a dangerous fast-moving landslide. Therefore, specific policy measures should be implemented to reduce the impacts. In this study, we have highlighted a clear impact on the stability of slopes due to the removal of vegetation from wildfires. For example, when fires affect a vegetative community on steep slopes, the likelihood of a debris flow event increases (several examples in Italy were given), which
requires an assessment of the potential impacts on nearby populations, properties, and infrastructures as well as the implementation of measures that reduce the risk of these dangerous events. In this context, the following policy recommendations must be considered by responsible post-fire management agencies:

- To estimate accurately the impact of wildfires on the vegetation, especially in steep slopes.
- To update the risk map.
- To implement post-fire evaluation tools to effectively identify, within a burned area, those zones having a greater likelihood of generating debris flows in order to undertake timely and effective mitigation measures.

References

Cannon, S., DeGraff, J. (2009). The Increasing Wildfire and Post-Fire Debris-Flow Threat in Western USA, and Implications for Consequences of Climate Change. In: Sassa, K., Canuti, P. (eds) Landslides – Disaster Risk Reduction. Springer, Berlin, Heidelberg. https://doi.org/10.1007/978-3-540-69970-5_9

Cruden D.M., Varnes D.J. (1996) - Landslide Types and Processes, Special Report, Transportation Research Board.

DeGraff, J.V.; Cannon, S.H.; Gartner, J.E. (2015). The timing of susceptibility to post-fire debris flows in the Western United States Post-Fire debris flow timing. Environ. Eng. Geosci. 21, 277–292.

De Graff V.J. (2014) - Improvement in quantifying debris flow risk for post-wildfire emergency response.

Di Napoli M., Marsiglia P., Di Martire D., Ramondini M, Ullo S.L. and Calcaterra D., (2020). Landslide Susceptibility Assessment of Wildfire Burnt Areas through Earth-Observation Techniques and a Machine Learning-Based Approach, Remote Sensing, 12, 2505; doi:10.3390/rs12152505.

Gartner J.E., Cannon S.H. and Santi P.M. (2011) - Implementation of post-fire debris flow hazard assessments along drainage networks, southern California, U.S.A.

G. Laneve, L. Fusilli, G. Bernini, J. Beltran, (2020). Preventing Forest Fires Through Remote Sensing: Achievements of the Prevention and Recovery of Forest Fires Emergency in the Mediterranean Area project, IEEE Geoscience and Remote Sensing Magazine, DOI: 10.1109/MGRS.2019.2906948

McGuire, L. A., Rengers, F. K., Oakley, N., Kean, J. W., Staley, D. M., Tang, H., de Orla-Barile, M., and Youberg, A. M. (2021). Time Since Burning and Rainfall Characteristics Impact Post-Fire Debris-Flow Initiation and Magnitude, Environmental & Engineering Geoscience, 705 27, 43–56.

Copyright © FirEUrisk Consortium. All rights reserved.

Miller M.E., Elliot W.J., Endsley K.A., Robichaud P.R., Billmire M. (2015) – Rapid response tools and datasets for post-fire erosion modeling: linking remote sensing and process-based hydrological models to support post-fire remediation.

Neary, Daniel G., Ryan, Kevin C., De Bano. Leonard F. (2008) - Wildland fire in ecosystems effects of fire on soils and water.

Staley D.M. (2013). Emergency Assessment of Post-Fire Debris-Flow Hazards for the 2013 Rim Fire, Stanislaus National Forest and Yosemite National Park, California.

Trigila A., Iadanza C. - Statistiche nazionali ed elaborazioni dati del Progetto IFFI. https://www.isprambiente.gov.it/files/pubblicazioni/rapporti/rapporto-frane/capitolo-3-statistiche.pdf

Trigila A., Iadanza C., Rischia I. - Metodologia di lavoro e struttura della banda dati - Progetto IFFI. https://www.isprambiente.gov.it/files/pubblicazioni/rapporti/rapporto-frane-2007/Capitolo_2_Metodologia.pdf

4.3 Post-fire floods: impacts of two storms in Greece

Eftychidis, G. and Gitas. I, Aristotelio Panepistimio Thessalonikis, AUTH

Introduction

Wildfires have a profound impact on storm severity and hydrological responses in burnt areas. They significantly alter peak flows and channel morphology, often leading to larger errors in peak flow estimates (Brogan et al., 2017). The magnitude of post-fire floods and geomorphic changes are affected by the timing, magnitude, duration, and sequence of rainstorms (Pelletier & Orem, 2014).

The aftermath of wildfires has a marked impact on water quality. The severity of storms following wildfires can lead to elevated suspended solids, including initial pulses of ash, impacting water treatment and threatening drinking water standards for turbidity, thus increasing filtration and coagulation costs (Paul et al., 2022). The spatial pattern of post-wildfire erosion largely depends on the pattern of individual storms and the pattern of burn severity, affecting soil hydrophobicity and the degree of runoff erosion on hillslopes (DiBiase & Lamb, 2019). Long-term effects of wildfires on storm consequences include persistent increases in total suspended sediment concentrations, total nitrogen concentrations, and total phosphorus, along with a notable increase in occurrences of heavy precipitation rates and significant severe hail in the western US (Yu et al., 2019; Zhang et al., 2022).

Hydrological analysis of regions affected by forest fire events indicates a change in flood risk, with wildfires having a higher effect on peak flows, potentially increasing the risk of flash floods in post-wildfire conditions (Havel et al., 2017). Several studies have examined the impact of wildfires on flood generation and hydrological response in Mediterranean basins, highlighting the increased risk of flash floods and debris flows following wildfires (Lasanta et al., 2018; Gallart et al., 2011; Fernandez et al., 2013). Changes in flood frequency and intensity have been observed in the European Alps (Stoffel et al., 2014).

Copyright © FirEUrisk Consortium. All rights reserved.

The comprehensive reviews by (Guzzetti et al., 2012) and (Brodsky et al., 2013) provide insights into post-fire debris flows and the impacts of wildfires on hydrological processes in Europe. They discuss the importance of vegetation recovery, soil erosion, and sediment transport in shaping the hydrological response to heavy storms in post-wildfire landscapes. Additionally, (Kundzewicz et al., 2018) and (Alfieri et al., 2015) have reviewed recent developments in flood hazard and risk changes in Europe, highlighting the influence of climate change and land use on these processes.

This report provides inputs on the cascading effects of wildfires in Greece, particularly on the destructive storms Daniel and Ilias, which occurred in 2023. It further examines the ripple effects of these events across other European Union countries, underscoring the interlinked nature of natural hazards. This analysis highlights the urgent need for integrated and comprehensive risk management strategies at both national and EU levels to address and mitigate these interconnected threats effectively.

Cascading Effects in Greece: Storms Daniel and Ilias

In 2023, Greece was struck by two severe storms, Storm Daniel and Storm Ilias, which had significant environmental, infrastructural, and agricultural impacts, particularly in the Region of Thessaly in Central Greece. The weather patterns in Thessaly underscore the broader implications of climate change, underscoring the urgency for countries and stakeholders to proactively address and mitigate the impacts of natural disasters on individuals, communities, and ecosystems. Climate change projections indicate that larger wildfires with higher intensities are to be expected in the future in Greece (Kalabokidis et al., 2015), potentially exacerbating the frequency and severity of subsequent natural disasters such as storms and floods.

The impact of Storm Daniel was extensive, affecting over 100 municipalities, displacing thousands, and causing economic damages estimated to exceed €1 billion, with two fatalities directly attributed to the storm. This phenomenon highlights the interconnected nature of wildfires and extreme weather events, emphasising the need for integrated environmental and disaster management strategies.
Wildfires contribute to a reduction in vegetation, an increase in erosion, and altered soil moisture retention capacities. Consequently, the affected soil struggles to absorb moisture during subsequent severe storms, heightening the risk of flash floods and landslides (Evelpidou et al., 2021). Furthermore, wildfires deteriorate air quality, potentially aggravating respiratory conditions (Masoom et al., 2023). These events revealed the extreme effects of climate change in Greece, as evidenced by the case of Sesklo village, situated in central Greece near the port city of Volos. This area has emerged as a climate change hotspot, witnessing increasingly frequent fierce storms and floods, compounded by hotter and drier summers conducive to wildfires. In July 2023, a devastating wildfire scorched the Sesklo area, ravaging about 70% of the village's almond and olive oil production. Storm Daniel followed this in early September 2023, which struck Thessaly after Greece's most prolonged heatwave in over three decades, claiming 16 lives and inundating the region, leading to massive agricultural losses (https://tinyurl.com/294j3qkn). Ash deposits from the fire increase surface runoff and decrease the soil's capacity to absorb water, exacerbating flood conditions (Rovithakis et al., 2021). Shortly after that, Storm Elias, though less intense, caused unexpected flooding, damaging property and local infrastructure in Sesklo (https://tinyurl.com/22am87cb). These events in Thessaly epitomise the cascading effects of wildfires followed by severe storms. The subsequent floods compounded the devastation by destroying crops for the remainder of the year, inflicting long-term severe damage.

Copyright © FirEUrisk Consortium. All rights reserved.

Storm DANIEL (4–8 Sep 2023)

In September 2023, the Mediterranean region experienced a significant meteorological event with the onset of Storm Daniel. The Hellenic National Meteorological Service officially named the storm on September 4, anticipating its potential to bring heavy rainfall and strong winds, mainly to Greece's Thessaly region. Subsequently, the city of Volos witnessed severe flooding. Remarkably, the village of Zagora recorded an unprecedented 754 mm of rain within 24 hours on September 5, culminating in a total rainfall of 1,096 mm during the storm's passage.

The consequent period from September 5-7 was marked by extreme rainfall in Thessaly, leading to widespread and severe flooding. This natural disaster resulted in substantial loss of life, livestock, crops, and property. As of September 10, fatalities were confirmed across multiple countries: 16 in Greece, seven in Turkey, and four in Bulgaria.

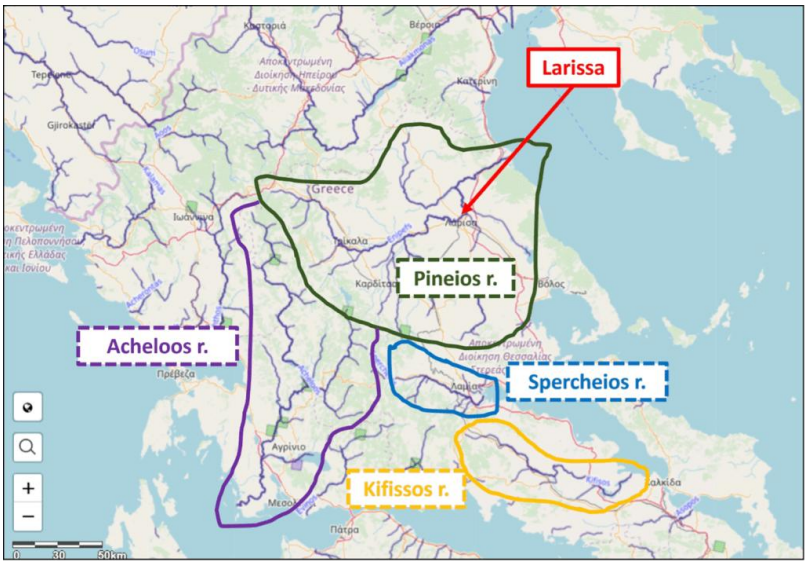


Figure 4.12 Main basins potentially affected by the flood peaks.

The floodwaters inundated an area of approximately 720 square kilometres, affecting several regions, including Thessaly's Plain, Palamas, Karditsa, and the city of Larisa. Rescue efforts led to the evacuation of hundreds of civilians. Notably, in the Halkidiki region, several coastal villages, including Ierissos, sustained damage from the storm's strong winds. A case in point is the seaside village of Toroni in Halkidiki, where the winds swept away a woman canoeing but later found.

Storm Daniel was attributed to a cut-off low-pressure system, which underwent a subtropical transition on September 9, developing a warm core. An ASCAT pass identified sustained winds of 45 knots before its landfall near Benghazi, Libya. In Libya, the storm's effects were catastrophic, leading to flooding in Marj and the collapse of two dams in Derna and the Jabal al Akhdar district, as well as Benghazi, Susa, and Misrata. The resultant flooding and heavy rainfall led to the tragic loss of at least 11,300 lives, making it the deadliest Mediterranean tropical-like cyclone on record and prompting Libyan authorities to declare a state of emergency.

Copyright © FirEUrisk Consortium. All rights reserved.

In Greece, in the immediate aftermath, satellite imagery was employed to monitor and delineate the affected areas. Initial reports on September 6 at 04:40 UTC indicated that 18,393 hectares had been impacted by flooding. This figure escalated to 72,951 hectares by September 7 at 16:25 UTC, less than 60 hours from the onset of the rains. The regions of Palamas and Larissa were particularly affected, with nearly 17,000 ha and over 15,000 ha inundated, respectively, impacting an estimated 22,500 residents. Subsequent assessments showed a gradual recession of floodwaters, yet significant areas remained inundated for an extended period, especially in Stefanovikeio near Lake Karla, which lacks a natural drainage outlet.

In response, local authorities implemented emergency measures, distributing drinking water and supplies and providing fodder to livestock farmers. Additionally, the Ministry for Climate Crisis and Civil Protection initiated the release of compensations to the affected farmers as part of the broader effort to mitigate the storm's impacts.

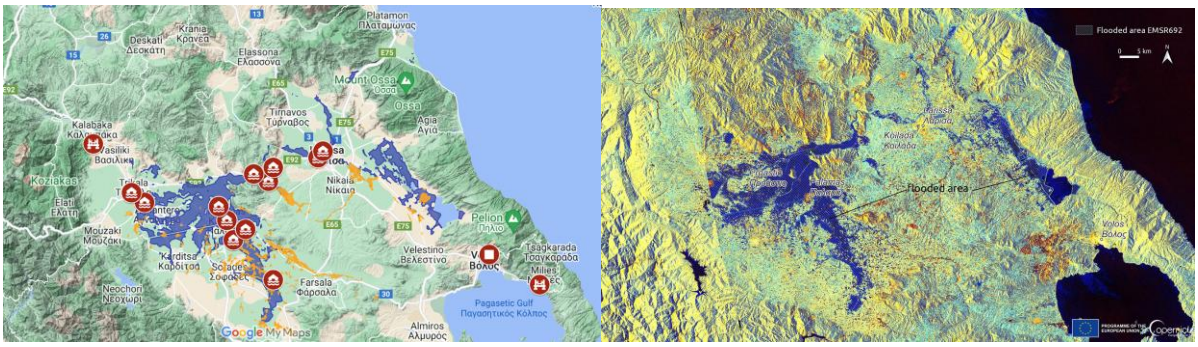


Figure 4.13 Visual Analysis of Thessaly Flood Impact (Source: NoA left and Copernicus right)

The Figure above provides a detailed geographical representation of the impacted areas during the flooding events in the Thessaly region following Storm Daniel in September 2023. The left panel illustrates a map with overlaid indicators denoting specific damage locations, rescue operations, and flood extents within populated areas and key infrastructure. The right panel, acquired from Copernicus Sentinel data (2023), displays satellite imagery with spectral analysis to visually depict the extent of the flooded regions, highlighting the contrasts between inundated areas and the surrounding terrain. Such remote sensing analyses were crucial in evaluating the scope of the floods and directing rescue and relief efforts.

The next Figure illustrates the total precipitation over Greece during the Storm Daniel, as per the ECMWF HRES model. Notably, the regions of Zagora and Potamia experienced record-breaking rainfall with the village of Zagora receiving 754 mm in 24hrs. The image below, sourced from the National Observatory of Athens/Meteo.gr, provides a regional breakdown of rainfall measurements. The colour gradient on the map represents the intensity of precipitation, confirming the significant variance in rainfall across different areas (Weatherzone, 2023).

Copyright © FirEURisk Consortium. All rights reserved.

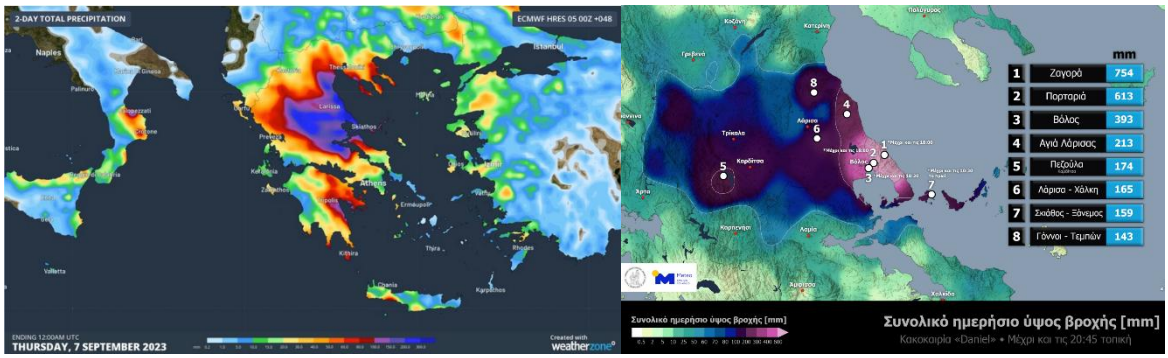


Figure 4.14 Comprehensive rainfall distribution map during Storm Daniel in Greece, detailing record-breaking precipitation across various regions, with an emphasis on Thessaly's most affected areas. (Source: Weatherzone left and NoA right).

Storm ELIAS (25-28 Sep 2023)

In September 2023, three weeks after the severe impacts of Storm Daniel, Storm Elias hit Central Greece, bringing intense rainfall, strong winds, and hail to the region and compounding the devastation in the midst of the 2022–23 European windstorm season.

The storm's impact was particularly severe in areas already affected by wildfires, which fortunately didn't have a large extent. The impact of the storm led to extensive destruction, including floods and landslides that resulted in damages exceeding €2 billion and the tragic loss of seven lives (Wikipedia, 2023). This event underscores the critical importance of examining the relationship between storms and wildfires, especially in the Mediterranean region, where extreme weather occurrences are becoming more frequent. It is essential to conduct comprehensive temporal and spatial analyses to gain a deeper understanding of how these phenomena interact and the cumulative impacts they have on the environment, infrastructure, and communities (Copernicus, 2023).

Comparison of the two Storms

The analysis of the rainfall data from the National Observatory of Athens highlights significant variations between Storm Daniel and Storm Elias, underscoring the importance of tailored environmental management and disaster response strategies. The data indicates Thessaly experienced higher rainfall during Storm Daniel, while Evia was more affected during Storm Elias, except for the Oreus and Steni stations. Interestingly, Volos saw a rapid increase in rainfall during Storm Elias. Such insights stress the necessity for enhanced forecasting and infrastructure planning to manage the risks of climate variability effectively. Further investigation into these patterns is essential for advancing our comprehensive risk management approaches in the era of climate change.

Copyright © FirEURisk Consortium. All rights reserved.

Figure 4.15 Rainfall data from the National Observatory of Athens.

Station	Storm Daniel	Rain (mm)	Storm Elias	Rain (mm)
Pertouli	04-Aug-2023 to 08-Sep-2023	643	25-Sep-2023 to 28-Sep-2023	205
Pezoula Karditsas	Not Available	NA	25-Sep-2023 to 28-Sep-2023	241
Trikala	04-Aug-2023 to 08-Sep-2023	477	25-Sep-2023 to 28-Sep-2023	143
Karditsa - city	04-Aug-2023 to 08-Sep-2023	656	25-Sep-2023 to 28-Sep-2023	130
Larisa - Chalkis	04-Aug-2023 to 08-Sep-2023	305	25-Sep-2023 to 28-Sep-2023	65
Zagora	04-Aug-2023 to 08-Sep-2023	1096	25-Sep-2023 to 28-Sep-2023	96
Volos	04-Aug-2023 to 08-Sep-2023	617	25-Sep-2023 to 28-Sep-2023	316
Istiaia	04-Aug-2023 to 08-Sep-2023	355	25-Sep-2023 to 28-Sep-2023	494
Orei Evias	04-Aug-2023 to 08-Sep-2023	447	25-Sep-2023 to 28-Sep-2023	387
Vatera Evias	04-Aug-2023 to 08-Sep-2023	149	25-Sep-2023 to 28-Sep-2023	274
Makrykapa Evias	04-Aug-2023 to 08-Sep-2023	153	25-Sep-2023 to 28-Sep-2023	254
Steni Evias	04-Aug-2023 to 08-Sep-2023	192	25-Sep-2023 to 28-Sep-2023	126

At least two rain gauges in Central Greece received more than half a meter of rain in less than 24 hours on Tuesday 5/9/2023.

Cascading Effects in Other EU Countries

In 2023, Southern Europe, particularly Greece, Spain, Italy, and Portugal, experienced severe wildfires exacerbated by heatwaves and droughts. These conditions rendered the landscapes vulnerable to fires, significantly impacting the region. The arrival of extreme weather events further complicated the situation, notably Storm Daniel and Storm Elias. The persistence of the severe weather that hit Greece was due to the steady high-pressure system in Central Europe. This configuration, called “Omega” because of its shape resembling the Greek letter. This same system has also caused

Copyright © FirEUrisk Consortium. All rights reserved.

flooding in central Spain and a heatwave in northern Europe, breaking temperature records in France, United Kingdom, and the Netherlands. This highlights the connection between extreme floods and exceptional temperatures.
In Greece, the wildfires created conditions that made the land more susceptible to flooding. When Storm Daniel arrived, it brought significant rainfall and strong winds to regions such as Thessaly, Attica, and Euboea. Thessaly, already weakened by wildfires, experienced devastating flooding with record-breaking rainfall, resulting in long-term soil infertility and extensive damage to infrastructure. Over 800 people were rescued, and at least 17 fatalities were reported. Storm Elias further compounded the damage, hindering recovery efforts (Wikipedia, 2023; Reuters, 2023; Al Jazeera, 2023; Copernicus EMS, 2023).

In Spain, the aftermath of the wildfires left regions like Galicia, Asturias, and the Balearic Islands vulnerable to Storm Elias, which brought heavy rainfall and winds in 2023. This resulted in substantial damage to infrastructure and agriculture and raised the risk of further environmental issues. Similarly, Italy witnessed the impacts of Storm Elias in Tuscany, Umbria, and Lazio. The storm aggravated the conditions in areas already affected by wildfires, causing notable damage to infrastructure and agricultural areas. Portugal, too, faced the brunt of Storm Elias following severe heatwaves and droughts. Particularly in the Alentejo and Ribatejo regions, the storm led to flash flooding and landslides, exacerbating the effects of earlier wildfires. Moreover, the smoke plumes from these widespread wildfires have been detected across various EU countries, including Cyprus and Turkey, contributing to air pollution and respiratory health issues (Wikipedia, 2023; Reuters, 2023; Al Jazeera, 2023; Copernicus EMS, 2023).
These incidents have highlighted the increasing frequency of extreme weather events and the interconnectedness of wildfires, storms, and floods, underscoring the urgent need for robust disaster preparedness and response mechanisms. The Greek government has announced financial relief measures and sought additional funds from the European Union to address the aftermath of these storms.

Conclusions and Policy Recommendations

The cascading effects of wildfires and extreme storms have highlighted the urgent need for a comprehensive and integrated disaster risk reduction approach in Southern Europe. Such an approach would require addressing root causes of wildfires and managing the exacerbating factors of extreme storms. To build a more resilient Southern Europe, the following key broad actions are listed:

- Strengthening early warning systems that integrate weather forecasting models, ground-based sensors, and satellite imagery to provide accurate and timely alerts about potential wildfire outbreaks and extreme storms.
- Expanding emergency response capabilities, including the establishment of additional fire stations, shelters, and communication networks to enable prompt and efficient responses to wildfires and storms.
- Enhancing firefighting resources by increasing the number of firefighters, water bombers, and helicopters.
- Implementing proactive wildfire mitigation strategies, such as prescribed burning under controlled conditions, vegetation management, and sustainable land-use planning to reduce fuel loads and enhance forest resilience.
- Increaseasing public awareness through effective educational and awareness-raising campaigns. Communities should be informed about the risks of wildfires and storms and how to protect themselves and their property, including developing evacuation plans and clearing flammable vegetation around homes.

Copyright © FirEUrisk Consortium. All rights reserved.

- Upgrading building codes and standards to ensure structures are fire-resistant and can withstand extreme storms. Reinforced structures and emergency escape routes should be made mandatory.
- Fostering research and development focused on wildfire and storm risk reduction, including the development of more reliable early warning systems, exploration of new methods for vegetation management and fire suppression, and examination of forests' role in mitigating hydrological impacts.

As aforementioned, "wildfires contribute to a reduction in vegetation, an increase in erosion, and altered soil moisture retention capacities. Consequently, the affected soil struggles to absorb moisture during subsequent severe storms, heightening the risk of flash floods and landslides". In addition, wildfires impact water quality, noting "elevated suspended solids, including initial pulses of ash, impacting water treatment and threatening drinking water standards for turbidity." To address these cascading effects, we recommend specific guidelines for enhancing post-wildfire hydrological modelling and flood risk assessment; and adapting water resource management in fire-prone areas:

1) Enhancing post-wildfire hydrological modelling and flood risk assessment.
   Towards the implementation of this objective, specific actions should be addressed to:

   - Update flood risk maps to account for increased runoff and erosion in recently burned areas
   - Develop scenario-based flood forecasts that consider recent wildfire activity, particularly in regions like Thessaly that experienced severe wildfires followed by storms
   - Implement immediate post-fire land management measures: The study highlights the increased vulnerability of burned areas to flooding, as seen in Sesklo village where "ash deposits from the fire increase surface runoff and decrease the soil's capacity to absorb water, exacerbating flood conditions." To mitigate this:
   - Prioritise rapid implementation of erosion control measures in burned areas
   - Focus on quick vegetation restoration strategies to stabilise soils and reduce flood risk

2) Adapting water resource management in fire-prone areas:

   Towards the implementation of this objective, specific actions should be addressed to:

   - Develop contingency plans for water supply management in areas at risk of post-fire flooding
   - Implement sediment management strategies for water bodies likely to be affected by post-fire erosion and runoff
   - Integrate wildfire and flood early warning systems: The study emphasizes the need for improved early warning systems, particularly in light of the rapid succession of wildfires and floods observed in Greece. To better predict and respond to post-fire flood risks we need to:
   - Develop coupled fire-weather-hydrology models for more accurate predictions of post-fire flood potential
   - Establish trigger points for evacuations based on both recent fire history and incoming storm potential.

Copyright © FirEUrisk Consortium. All rights reserved.

References

Alfieri, A., Viglione, A., & De Filippis, R. (2015). Flood hazard and risk changes in Europe: A systematic review of the literature. Journal of Hydrology, 531, 275-289.

Brodsky, E. E., Guzzetti, F., & Cardinali, M. (2013). The hydrological impacts of wildfires on European catchments. Forest Ecosystems, 1(1), 1.

Brogan, J. M., Kalamaras, A. S., & Kalliakis, N. M. (2017). The impact of forest fires on the vulnerability of peri-urban catchments to flood events: The case of the Eastern Attica Region, Greece. Journal of Hydrology, 553, 1384-1396.

DiBiase, R. A., & Lamb, M. P. (2019). Impact of wildfire on hydrology, erosion, and sediment transport in the California headwaters of the Colorado River. Journal of Hydrology, 578, 109-119.

Evelpidou, N., Tzouxanioti, M., Gavalas, T., Spyrou, E., Saitis, G., Petropoulos, A., & Karkani, A. (2021). Assessment of Fire Effects on Surface Runoff Erosion Susceptibility: The Case of the Summer 2021 Forest Fires in Greece. Land. https://doi.org/10.3390/land11010021.

Fernandez, I., De Rigo, D., & Poyato, J. F. (2013). The impact of wildfire on flood generation and hydrological response in Mediterranean basins. Journal of Hydrology, 498, 152-164.

Gallart, F., Llorens, P., Martí, V., & Martín, J. A. (2011). The impact of forest fires on the hydrological regime of Mediterranean catchments: A review and synthesis. Hydrological Processes, 25(2), 417-434.

Guzzetti, F., Rossi, M., & Cardinali, M. (2012). A review of post-fire debris flows and their relationship to forest management and climate change. Earth-Science Reviews, 113(1-2), 3-44.

Havel, J., Koutny, M., & Herold, N. (2017). Assessing the influence of forest fires on the hydrological response of Mediterranean catchments. Journal of Hydrology, 556, 538-554.

Kalabokidis, K., Palaiologou, P., Gerasopoulos, E., Giannakopoulos, C., Kostopoulou, E., & Zerefos, C. (2015). Effect of Climate Change Projections on Forest Fire Behavior and Values-at-Risk in Southwestern Greece. Forests, 6, 2214-2240. https://doi.org/10.3390/F6062214.

Kundzewicz, Z. W., Arnell, N. W., Döll, P., Kabat, P., Lettenmaier, D. P., Matczak, J., ... & Zhang, W. (2018). Flood risk and climate change: Global and regional perspectives. Hydrology and Earth System Sciences, 22(9), 4607-4626.

Lasanta, A., Martínez-Mena, M., & San-Miguel, F. (2018). The impact of wildfires on flood generation and hydrological response in Mediterranean basins. Global Change Biology, 24(1), 224-236.

Masoom, A., Fountoulakis, I., Kazadzis, S., Raptis, I., Kampouri, A., Psiloglou, B., Kouklaki, D., Papachristopoulou, K., Marinou, E., Solomos, S., Gialitaki, A., Founda, D., Salamalikis, V., Kaskaoutis, D., Kouremeti, N., Mihalopoulos, N., Amiridis, V., Kazantzidis, A., Papayannis, A., Zerefos, C., & Eleftheratos, K. (2023). Investigation of the effects of the Greek extreme wildfires of August 2021 on air quality and spectral solar irradiance. Atmospheric Chemistry and Physics. https://doi.org/10.5194/acp-23-8487-2023.

Pelletier, R., & Orem, W. (2014). Climate and hydrology of the western United States and implications for potential water availability. US Geological Survey Fact Sheet 2014-3023.

Paul, A. M., & Arain, M. A. (2005). Water quality and treatment challenges following large wildfires in California: A case study. Water Research, 39(10), 2219-2228.

Copyright © FirEUrisk Consortium. All rights reserved.

Rovithakis, A., Grillakis, M., Seiradakis, K., Giannakopoulos, C., Karali, A., Field, R., Lazaridis, M., & Voulgarakis, A. (2021). Future climate change impact on wildfire danger over the Mediterranean: the case of Greece. Environmental Research Letters, 17. https://doi.org/10.1088/1748-9326/ac5f94.

Stoffel, M., Stoffel, A., & Stoffel, S. (2014). Hydrological and geomorphological impacts of mountain wildfires in the European Alps. Earth Surface Processes and Landforms, 39(8), 1227-1242.

Yu, H., Chen, Z., Wang, G., Sun, W., & Zhang, L. (2019). Changes in storm characteristics and their relationships with wildfire occurrence in the western United States. International Journal of Climatology, 39(10), 3675-3692.

Zhang, Y., Guo, Y., Xu, H., & Zhang, L. (2022). The influence of climate change and land use on flood hazard and risk changes in Europe. Journal of Environmental Management, 328, 112750.

Webography

NOAA Climate.gov. (2018, November 16). Heavy Rains Help Dampen Wildfires, But Droughts Can Resurrect Flames. [Web article]. Retrieved from https://www.ncei.noaa.gov/

ScienceDaily. (2019, July 16). Storms Can Precede Wildfires, Study Finds. [Web article]. Retrieved from https://www.sciencedaily.com/news/earth_climate/wildfires/

National Interagency Fire Center. (2018, October 3). Aftermath of Storms Can Create Wildfire Risk. [Web article]. Retrieved from https://www.nifc.gov/fire-information

Climate Action Tracker. (2023, October 4). Greece's Storms Daniel and Ilias Highlight Need for Climate Change Adaptation. [Web article]. Retrieved from https://climateactiontracker.org/

Heinrich Böll Stiftung. (2023, October 4). Greece's Experiences from Storms Daniel and Ilias: A Call for Enhanced Resilience. [Web article]. Retrieved from https://gr.boell.org/en

Reuters. (2023, October 4). Greece Invests in Flood Forecasting and Disaster Response. [Web article]. Retrieved from https://www.reuters.com/world/europe/greek-floods-fires-expose-europes-frail-climate-defences-2023-11-21/

Euronews. (2024, January 4). Greece Aims to Improve Land Use Planning to Reduce Disaster Risk. [Web article]. Retrieved from https://www.youtube.com/watch?v=fkA6wvaluwg

Environment and Climate Change Canada. (2022, May 17). Understanding the Interplay of Floods and Wildfires. [Web article]. Retrieved from https://thenarwhal.ca/opinion-wildfires-climate-change-relationship/

United Nations Office for Disaster Risk Reduction (UNDRR). (2022, June 1). Developing Comprehensive Risk Management Strategies for Climate Change. [Web article]. Retrieved from https://www.undrr.org/climate-action-and-disaster-risk-reduction/comprehensive-disaster-and-climate-risk-management

Hellenic National Meteorological Service (HNMS). Storm Daniel: Heavy rains, floods, and landslides in Greece. September 2023. http://emy.gr/emy/en

Kathimerini newspaper. Economic damage from Storm Daniel reaches €1 billion. September 2023. https://www.ekathimerini.com/news/1219660/storm-daniel-death-toll-rises-to-14/

Copyright © FirEUrisk Consortium. All rights reserved.

5 Main Conclusions

In this section, we summarise the main conclusions derived from the results of our analysis highlighted per topic of interest.

5.1 Wildfires

We have proposed a novel and integrated methodological framework to create a predictive model of spruce bark beetle attack for Central Europe in 2021. The timeframe was selected to understand the environmental conditions prior to the fire that occurred in the Bohemian and Saxon Switzerland National Parks in 2022. The area was, and still is, highly affected by bark beetle. Bark beetle dynamics increase the amount of deadwood, which directly influences how wildfires behave and their impact on ecological processes. The combination of open geospatial datasets with machine learning techniques have revealed that these tools are relevant to predict a bark beetle outbreak and prioritise management options. It is important to note that the dead spruce stands were left in situ for the sake of biodiversity enhancement within the parks, however, the trees were removed for economic reasons resulting in a habitat change outside of the parks.

The study of the characteristics of the terrain and the fire occurred in 2022 in the Bohemian and Saxon Switzerland National Parks showed that the intensity of the deadwood areas burning ensured that adjacent forest parcels were affected. The height at which the standing deadwood burnt most likely contributed to spot fires and the spread of the fire. Most of the small diameter woody debris in the dead stands affected by the fire were consumed, meaning that only emergent vegetation and large diameter logs remain. The post-fire mortality or the remains of unburnt dead branches that fell after the fire contribute to increase the accumulation of deadwood. Especially, large swathes of dead spruce stands remain in the Parks that were not affected by the fire, they remain in a highly combustible state and thus the danger remains. This danger level is expected to be reduced gradually as the small woody debris decomposes. Outside of the national parks, the clear-felling of spruce as a result of actual or expected bark beetle infestation has changed the landscape and fuel types, which have an impact on the possibility of fires spreading to established forests.

The integration of ecological disturbances, particularly bark beetle damage, into wildfire risk assessments will improve the analysis of wildfire propagation potential analyses in Pilot Site 2. Updated forest disturbance conditions and fuel models can improve the prediction of fire behaviour and propagation. However, since we could not define Scott and Burgan categories associated with biotic damages based on in-situ data, further analyses will be necessary to derive conclusions.

The pre- and post-fire conditions of the fire that occurred in the Bohemian and Saxon Switzerland National Parks including the hydrograph trends were simulated the hydrograph trends using WEPPcloud-EU-WATAR. The best results were obtained for monthly average runoff rather than daily estimates. However, the model had difficulty simulating streamflow in this large catchment with minimal calibration. Interactions between the complex geology of the Bohemian and Saxon Switzerland National Parks and potential impacts of management on the hydrologic regime not captured by the model are further challenges in this example. In smaller European catchments (from 100 to 5,200 ha), WEPPcloud-EU-WATAR showed good performance. We, therefore, recommend that when using uncalibrated

Copyright © FirEUrisk Consortium. All rights reserved.

WEPPcloud-EU-WATAR in large catchments, to use the spatial and return period analyses capabilities to inform on-ground monitoring and operational mitigation measures. Sediment yield and ash transport estimates should be treated as indicative only and where possible validated with observed data.

5.2 Air pollution

In Central Portugal, our modelling showcases the importance of air pollution and the impact of smoke on human health producing respiratory and cardiovascular diseases. We showed the spatial variability of these effects being able to forecast and provide stakeholders with health information easily to understand. This will contribute to a better preparedness phase, increase social awareness of the air pollution related risks and prevent human exposure. Policy recommendations should consider the strengthening of public health alert systems, enhancing public awareness, and establishing education campaigns, and international collaboration.

Moreover, in areas affected by radioactive soil contamination, it is especially important avoid wildfires and smoke dispersion with air pollutants including radionuclides. In the surroundings of the Chornobyl Exclusion Zone implementing activities to prevent the occurrence and development of wildfires is particularly important, especially, in areas where artificial pine forests grow under moderate soil moisture conditions, as these plant communities have the potential to generate significant biomass of combustible materials. The policy recommendations in radionuclide-contaminated areas include radiation safety and organisational activities to improve the effectiveness of wildfire detection and suppression.

5.3 Post-fire landslides

In our analysis, we identified specific environmental factors such as topography, vegetation, and anthropic factors that can amplify the negative effects of wildfires and floods causing damaging landslides events. The main lesson learnt is that the potential impacts of the concurrence of several hazards are not easy to be foreseen and this type of analysis help to raise awareness of specific factors and improve the preparedness phase to reduce and mitigate the impacts of future landslide events. Specific policy measures should be considered such as estimating accurately the impact of wildfires on the vegetation, especially in steep slopes, updating risk maps, implementing post-fire evaluation tools to effectively identify, within a burned area, those zones having a greater likelihood of generating debris flows in order to undertake timely and effective mitigation measures.

5.4 Post-fire floods

The effects derived from the occurrence of floods and wildfires in the same location require guidelines to address and mitigate the impacts. For example:

- To strengthen early warning systems that integrate weather forecasting models, ground-based sensors, and satellite imagery to provide accurate and timely alerts about potential wildfire outbreaks and extreme storms.

Copyright © FirEUrisk Consortium. All rights reserved.

- To expand emergency response capabilities, including the establishment of additional fire stations, shelters, and communication networks to enable prompt and efficient responses to wildfires and storms.
- To enhance firefighting resources by increasing the number of firefighters, water bombers, and helicopters.
- To implement proactive wildfire mitigation strategies, such as prescribed burning under controlled conditions, vegetation management, and sustainable land-use planning to reduce fuel loads and enhance forest resilience.
- To increase public awareness through effective educational and awareness-raising campaigns. Communities should be informed about the risks of wildfires and storms and how to protect themselves and their property, including developing evacuation plans and clearing flammable vegetation around homes.
- To upgrade building codes and standards to ensure structures are fire-resistant and can withstand extreme storms. Reinforced structures and emergency escape routes should be made mandatory.
- To foster research and development focused on wildfire and storm risk reduction, including the development of more reliable early warning systems, exploration of new methods for vegetation management and fire suppression, and examination of forests' role in mitigating hydrological impacts.

Specific recommendations towards an integrated approach should enhance post-wildfire hydrological modelling and flood risk assessment as well as adapt water resource management in fire-prone areas.

Copyright © FirEUrisk Consortium. All rights reserved.

6 Appendix A: Section 4.1

Input and output data for estimating combustion parameters and emission volumes of radionuclide activities into atmospheric air during wildfires in the Chornobyl Exclusion Zone in April 2020.

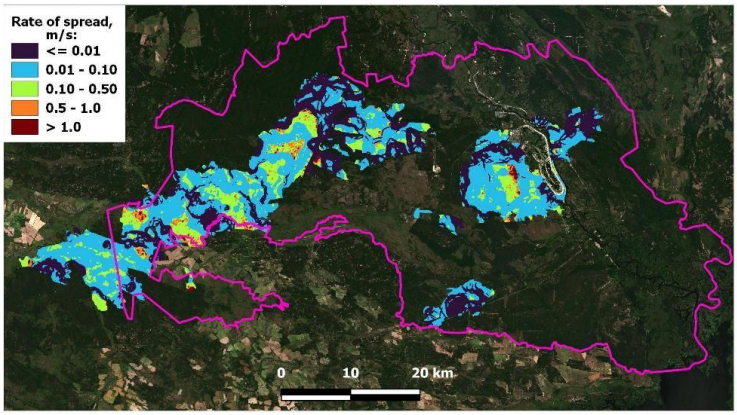


Figure A 6.1 The speed of fire spread at the time of wildfires in the areas.

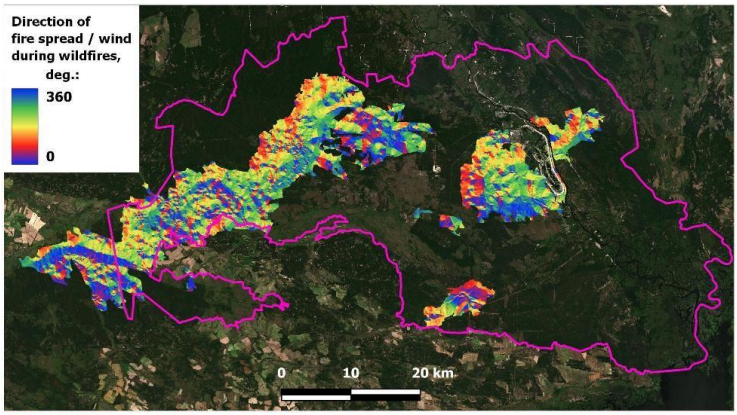


Figure A 6.2 The direction of fire spread at the time of the wildfires in the area.

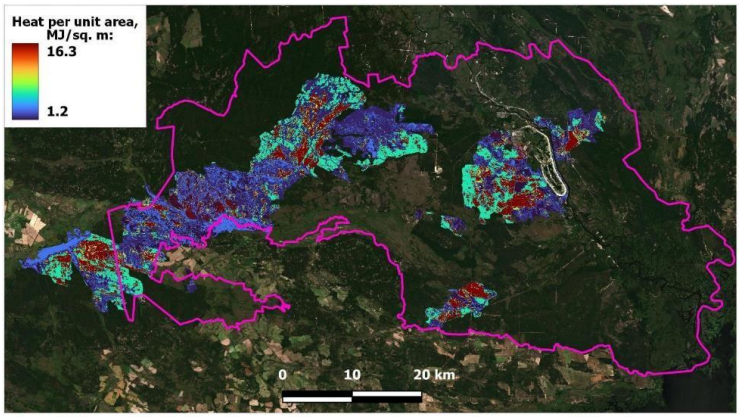


Figure A 6.3 Spatial distribution of heat of combustion for combustible materials per unit surface area during wildfires in April 2020.

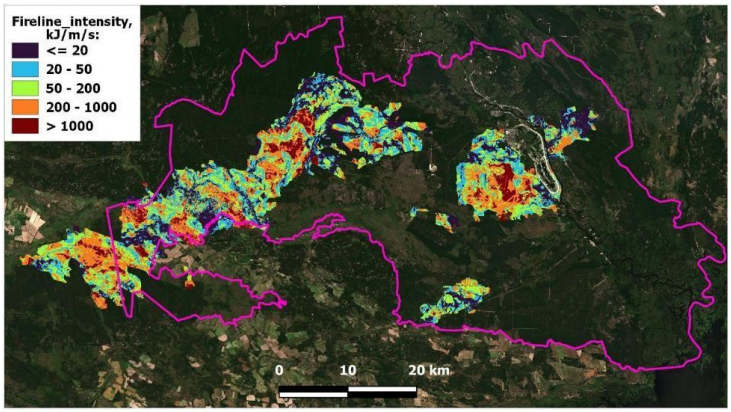


Figure A 6.4 – Spatial distribution of fireline intensity during wildfires in April 2020.

Copyright © FirEUrisk Consortium. All rights reserved.

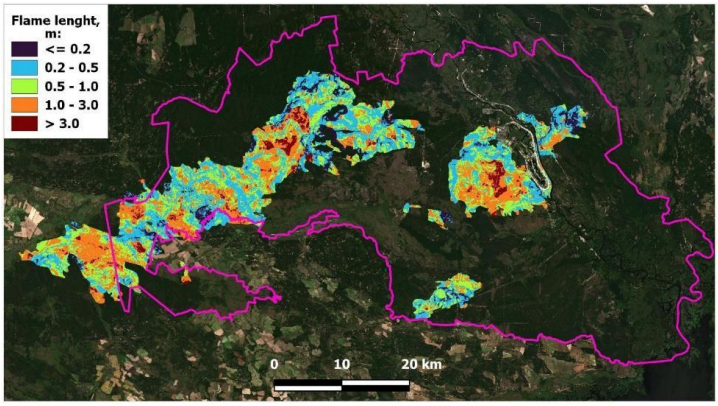


Figure A 6.5 Spatial distribution of Byram's flame length during wildfires in April 2020.

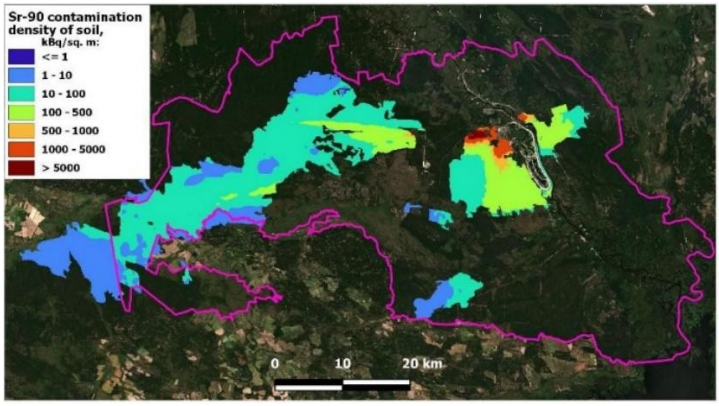


Figure A 6.6 The contamination density of soil with Sr-90 in fire-affected areas in April 2020 in the Chornobyl Exclusion Zone and adjacent territories as of April 15, 2020.

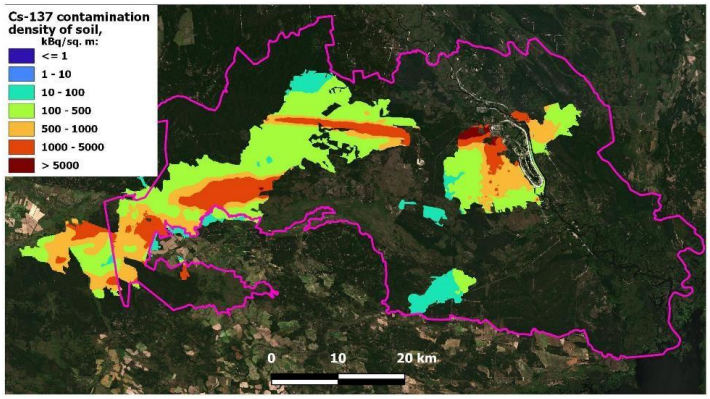


Figure A 6.7 The contamination density of soil with Cs-137 in fire-affected areas in April 2020 in the Chornobyl Exclusion Zone and adjacent territories as of April 15, 2020.

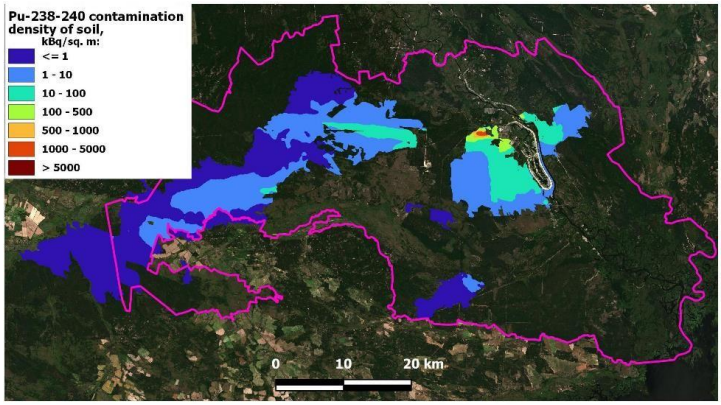


Figure A 6.8 The contamination density of soil with Pu-238-240 in fire-affected areas in April 2020 in the Chornobyl Exclusion Zone and adjacent territories as of April 15, 2020.

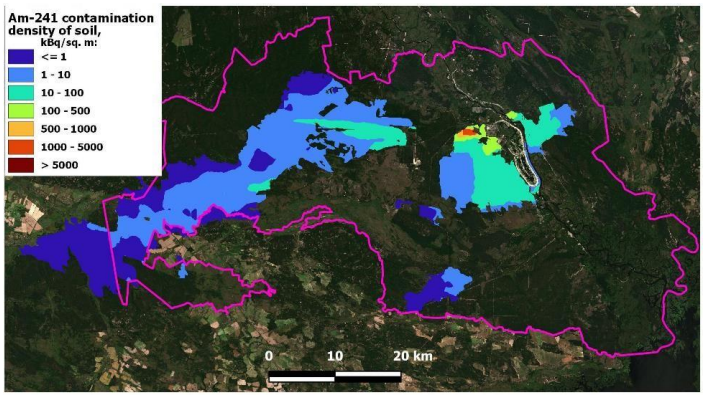


Figure A 6.9 The contamination density of soil with Am-241 in fire-affected areas in April 2020 in the Chornobyl Exclusion Zone and adjacent territories as of April 15, 2020.

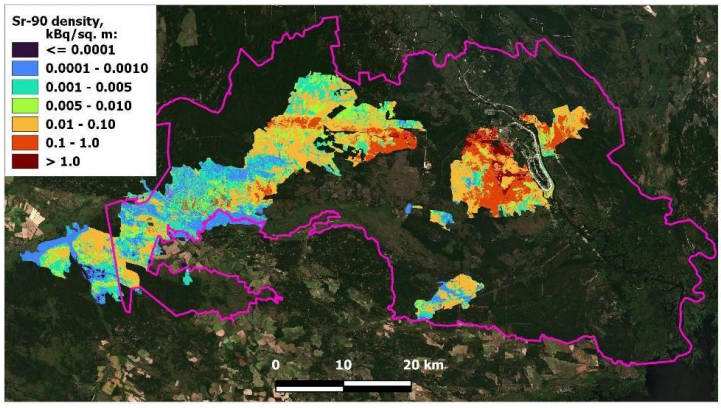


Figure A 6.10 The density of Sr-90 activity emission into atmosphere air from a unit of the surface area during the Chornobyl wildfire in April 2020.

This project has received funding from the European Union's Horizon 2020 research and innovation programme under grant agreement No 101003890.

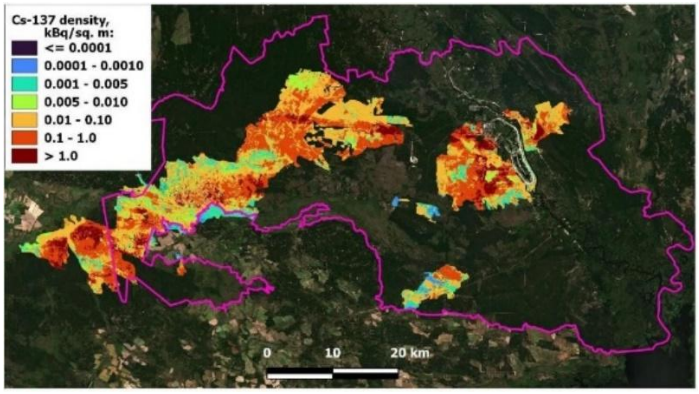


Figure A 6.11 The density of Cs-137 activity emission into atmosphere air from a unit of the surface area during the Chornobyl wildfire in April 2020.

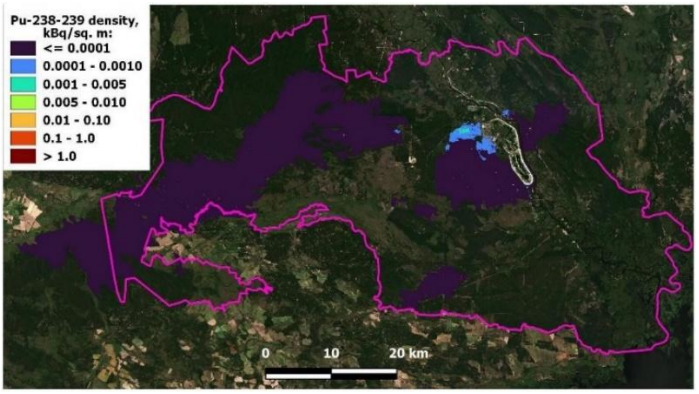


Figure A 6.12 The density of Pu-238-240 activity emission into atmosphere air from a unit of the surface area during the Chornobyl wildfire in April 2020.

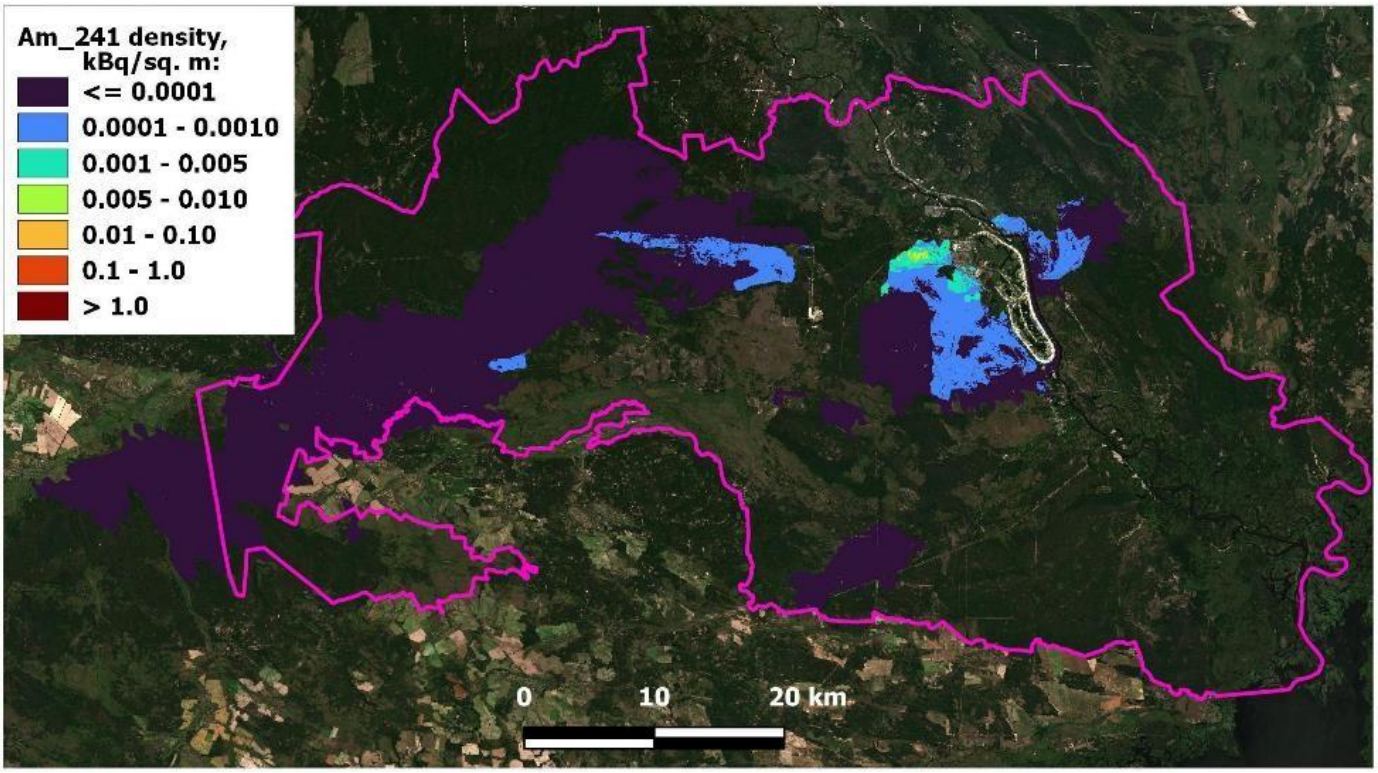


Figure A 6.13 The density of Am-241 activity emission into atmosphere air from a unit of the surface area during the Chornobyl wildfire in April 2020.

This project has received funding from the European Union's Horizon 2020 research and innovation programme under grant agreement No 101003890.

7 Appendix B: Section 2.4

Water quality and wildfires: managing risk to Europe's aquatic resource at catchment management and policy level

Rossana Caroni[1], Gary Free[2], Monica Pinardi[1], Daniela Stroppiana[1], Claudia Giardino[1], Mariano Bresciani[1], Stefan H. Doerr[3], Carmen Sánchez-García[3], Jonay Neris[3,4]

[1]*Consiglio Nazionale delle Ricerche – Istituto per il Rilevamento Elettromagnetico dell'Ambiente (CNR-IREA), 20133 Milano, Via Alfonso Corti 12, Italy*

[2]*European Commission, Joint Research Centre, Directorate for Sustainable Resources, Ispra (VA), Italy*

[3]*Centre for Wildfire Research, Department of Geography, Swansea University, Swansea, SA28PP, UK*

[4]*Universidad de La Laguna, Tenerife, Spain*

Background on the impact of wildfires on water quality

The climate crisis significantly threatens the water environment in several ways, from changing rainfall patterns to rising sea levels, and more frequent and severe droughts. Although most of Europe currently has adequate water resources, climate change is leading to increased water scarcity and droughts. Water scarcity comprises both quantitative and qualitative components, although the latter has often received less attention. Fostering resilience in Europe's water resources must ensure a sufficient quantity of good-quality water to meet both environmental and drinking water needs. The two interrelated EU policy components of water protection – human health covered by the Drinking Water Directive (2020) and environmental objectives covered by the Water Framework Directive (WFD 2000) - help structure the focus on the pressures and solutions for managing the impact of wildfires in aquatic systems in Europe. Fire is an increasingly recognised major threat to water supply globally and (Southern) Europe is a hotspot for greater expected impacts of climate change (Robinne et al. 2021).

Wildfires can degrade the quality of drinking water, particularly when sourced from reservoirs or natural lakes, by increasing erosion and related nutrient inputs, suspended solids (increasing turbidity) and organic carbon – discussed further below. In addition, the transport of wildfire ash, the particulate reside resulting from the burning of vegetation, to water bodies can also introduce potential pollutants of varying toxicity, carcinogenicity and persistence such as PAHs (Polycyclic Aromatic Hydrocarbons), PCBs (Polychlorinated Biphenyls), dioxins and furans as well as heavy metals (Canning & Ryan 2020; Gorshkov et al. 2021; Sanchez-Garcia et al. 2023).

The impacts on aquatic ecosystems such as natural lakes and reservoirs occur both via atmospheric deposition of aerosols from fire emissions and via terrestrial runoff within a burned catchment. Ash and soil transport, and the resulting increased sediment load will depend on burn severity and intensity of post-fire rainfall and associated flow events. The removal of vegetation and litter from the soil surface, and heat-induced changes to the soil may reduce its infiltration capacity, increasing the likelihood of runoff generation, soil erosion, landslides and flash flooding (Cannon et al. 2008; Nunes et al. 2018). These effects can be observed over the short-time (days and weeks after the fire) as well as the long-time (months or even years after the fire) depending on several factors such as pre-fire vegetation characteristics, topography, burn severity (the level of vegetation destruction), post-fire vegetation regeneration, and the timing and intensity of rainstorms. Mitigation plans should be in place and designed considering the different time

Copyright © FirEUrisk Consortium. All rights reserved.

scale of the effects of wildfires on the water systems. Increased runoff to lakes can trigger increases in water turbidity and a temporary decrease in water transparency. In addition, wildfires have the potential to release nutrients, organic matter and potential pollutants stored in soils and vegetation, allowing them to be transferred to aquatic ecosystems in the form of ash (Lewis 2014). Following a fire, concentrations of nitrogen and phosphorus, two key nutrients for primary producers in lakes, often increase in aquatic systems (Carignan et al. 2000), favouring the occurrence of algal blooms. These in turn can lead to oxygen depletion and toxic byproducts. Recent studies on lake water quality at global scale, utilizing satellite derived products, revealed that lake morphology and ecological context are important for the responses in lake chlorophyll-a and turbidity to wildfires (Caroni et al. 2024).

Managing the risk

Effective mitigation opportunities exist before, during and after a wildfire. At all stages there are options for mitigation measures and knowledge gaps to be filled to prevent or reduce environmental, societal and economic impacts. Risk reduction strategies can be implemented proactively as well as in response to fire during (A) the pre-fire stage, (B) during the actual fire and (C) the post-fire period, as summarised in the figure below.

Planning and pre-fire risk

The EU's WFD requires member states to produce a river basin management plan (RBMP) every six years documenting pressures on aquatic systems and producing and implementing a programme of measures to achieve good surface water status. Any barriers to achieving this should be anticipated (Council of the European Communities 2000). Wildfire risk and fire-related risk mitigation plans should be part of RBMP for catchments where fires are identified as a threat to water systems.

In fire-prone catchments, it is recommended to include measures to allow environmental objectives to be achieved despite wildfire occurrence. Approaches to achieving targets and managing aquatic systems in Europe in the context of climate change have been outlined in the recently revised guidance document No. 24 "River basin management in a changing climate" (European Commission: Directorate-General for Environment 2024). As explicitly outlined in this document, adaptation of the integrated water, land and ecosystem management is necessary in view of climate change projections that can highlight pressures and impacts that threaten water quality and availability. Wildfires are among these factors and risk management and mitigation measures could be outlined.

Effective mitigation plans also rely on sufficient knowledge of the lake and catchment characteristics that could determine the impact of fires on the water system as well as the characterisation of fire regimes and expected trends. Knowledge of the catchment and lake should be integrated with the identification of potential chemicals and physical contaminants that could be mobilized by fires as well as major pathways and the probability of rainfall events that could trigger post-fire erosion and water contamination. Where buildings or other structure burns, toxic byproducts from human made materials need to be considered too (Robinne et al. 2021). Fuel management such as fuel reduction or fire breaks, especially on steep hillslopes with high fuel loads, are effective to reduce risk. In addition, the ability to rapidly assess water contamination risk after a fire, as well as having the resources ready to implement mitigation measures are critical.

Copyright © FirEUrisk Consortium. All rights reserved.

Monitoring and mitigating post-fire risk

Mitigating post-fire water contamination risk requires understanding of the ecosystem, the contaminants, their mobility and pathways to the aquatic system (Holdgate 1979; Nunes et al. 2018). Soil and ash are the key sources for sediment, nutrient and pollutant transport following a fire. Applying available knowledge of the ash chemical characteristics (Bodi et al. 2011; Sanchez-Garcia et al. 2023) and where necessary, further analysis, is essential here. For example, nitrogen and phosphorus can contribute to eutrophication and algal blooms, especially where water nutrient levels are already far above target values in EU rivers and lakes (Nikolaidis et al. 2022). Remote sensing approaches (Pešić et al. 2020; Caroni et al. 2024) and dedicated modelling tools such as WEPPcloud-WATAR (Neris et al. 2021) enable the estimation of post-fire soil, ash and pollutant transport to rivers, lakes and reservoirs. While fire and vegetation characteristics determine availability of contaminants after a wildfire, catchment characteristics (soil type, land use, topography, connectivity) and hydrological processes (precipitation regimes, infiltration, runoff, erosion) determine their mobilization and transport to aquatic ecosystems.

To mitigate transport of soil and ash, hillslope and channel stabilization measures such as mulching and erosion barriers (Nunes et al. 2018) as well as the establishment of riparian buffer zones alongside rivers and around shoreline of lakes are proven methods (Canning & Ryan 2020). On catchments affected by extreme fires (large area burned at high burn severity), establishing long-term monitoring programmes for increased erosion, surface runoff and to prevent landslides on burned slopes may be necessary.

Measurement networks of water and air quality could be integrated with ad-hoc measurements of contaminants released or produced by fires, especially in proximity to drinking water reservoirs and/or potential pollutants sources. The EU Drinking Water Directive (EU) 2020/2184 sets limits for contaminants including PAHs which, for example, should not exceed 0.10 µg l-1 (European Parliament and Council 2020). If not systematically measured by the network, pollutants such as PAHs, and PCBs could be monitored in the immediate post-fire with ad-hoc and event-driven sampling programs of rivers, lakes and reservoirs. Such contaminants can be removed using advanced water treatment techniques to prevent potential effects on human health. For trace metals such Fe, Mn, As, Cr, Al, Ba, and Pb water treatment by coagulation and filtration may be required. The effectiveness of water treatment after a fire will depend on the availability of conventional treatments as well as additional procedures resulting in higher operational costs. Where water treatment capacity is exceeded, the capacity to switching to alternative sources provides contingency. Restoration of burned ecosystems (e.g. seeding, planting) might be necessary over the medium and long term to mitigate against the lasting impacts of wildfires. Some of these measures already form part of catchment management in the EU in some of the more fire-prone areas. However, the rising risk of larger and more severe wildfires also in previously less fire-prone regions, will necessitate a more wide-spread application and augmented adoption of measures.

References

Bodí, M.B.; Martin, D.; Santín, C.; Doerr, S.H.; Balfour, V.N.; Pereira, P.; Mataix-Solera, J.; Cerdà, A. (2014). Wildland fire ash: production, composition and eco-hydro-geomorphic effects. Earth-Science Reviews 30:103-127, https://doi.org/10.1016/j.earscirev.2013.12.007.

Copyright © FirEUrisk Consortium. All rights reserved.

Canning, A.; Ryan G. (2020). National good practice operational guidelines for bushfire management for the Australian water industry. Water Services Association of Australia. https://www.wsaa.asn.au/publication/national-good-practice-operational-guidelines-bushfire-management-australian-water.

Cannon, S.H.; Gartner, J.E.; Wilson, R.C.; Bowers, J.C.; Laber, J.L. (2008). Storm Rainfall Conditions for Floods and Debris Flows from Recently Burned Areas in Southwestern Colorado and Southern California. Geomorphology 96: 250–269, https://doi.org/10.1016/j.geomorph.2007.03.019.

Carignan, R.; D'Arcy, P.; Lamontagne, S. (2000). Comparative Impacts of Fire and Forest Harvesting on Water Quality in Boreal Shield Lakes. Canadian Journal of Fisheries and Aquatic Sciences, 57:105–117, https://doi.org/10.1139/f00-125.

Caroni, R.; Pinardi, M.; Free, G.; Stroppiana, D.; Parigi, L.; Tellina, G.; Bresciani, M.; Albergel, C.; Giardino, C. (2024). Investigating the Impact of Wildfires on Lake Water Quality Using Earth Observation Satellites. Applied Science, 14: 2626, https://doi.org/10.3390/app14062626.

Council of the European Communities (2000). Directive 2000/60/EC of the European Parliament and of the Council of 23 October 2000 establishing a framework for community action in the field of water policy. L327: 72.

European Commission: Directorate-General for Environment (2024). River basin management in a changing climate – Common implementation strategy for the Water Framework Directive and the Floods Directive. Publications Office of the European Union.

European Parliament and Council (2020). Directive (EU) 2020/2184 of the European Parliament and of the Council of 16 December 2020 on the quality of water intended for human consumption (recast). https://eur-lex.europa.eu/legal-content/EN/LSU/?uri=CELEX:32020L2184.

Gorshkov, A. G.; Izosimova, O. N.; Kustova, O. V.; Marinaite, I. I.; Galachyants, Y. P.; Sinyukovich, V. N.; Khodzher T. V. (2021). Wildfires as a Source of PAHs in Surface Waters of Background Areas (Lake Baikal, Russia). Water Multidisciplinary Digital Publishing Institute 13: 2636, https://doi.org/10.3390/w13192636.

Holdgate, M. W. (1979). A perspective of environmental pollution. Cambridge University Press.

Lewis, T.L.; Lindberg, M.S.; Schmutz, J.A.; Bertram, M.R. (2014). Multi-trophic resilience of boreal lake ecosystems to forest fires. Ecology 95: 1253–1263, https://doi.org/10.1890/13-1170.1.

Malmon, D.V.; Reneau, S.L.; Katzman, D.; Lavine, A.; Lyman, J. (2007). Suspended Sediment Transport in an Ephemeral Stream Following Wildfire. Journal of Geophysical Research: Earth Surface, 112, https://doi.org/10.1029/2005JF000459.

Neris, J.; Santín, C.; Lee, R.; Robichaud, P.R.; Elliot, W.G.; Lewis, S.; Sheridan, G.; Rohlfs, A.M.; Ollivier, Q.; Oliveira, L.; Doerr, S.H. (2021). Designing tools to predict and mitigate impacts on water quality following the Australian 2019/2020 wildfires: insights from Sydney's largest water supply catchment. Integrated Environmental Assessment and Management, 17, 1151-1161, https://doi.org/10.1002/ieam.4406.

Nikolaidis, N.P.; Phillips, G.; Poikane, S.; Várbíró, G.; Bouraoui, F.; Malagó, A.; Lilli M.A. (2022). River and lake nutrient targets that support ecological status: European scale gap analysis and strategies for the implementation of the Water Framework Directive. Science of The Total Environment 813: 151898, https://doi.org/10.1016/j.scitotenv.2021.151898.

Copyright © FirEUrisk Consortium. All rights reserved.

Nunes, J.P.; Doerr, S.H.; Sheridan, G.; Neris, J.; Santín, C.; Emelko, M.B.; Silins, U.; Robichaud, P. R.; Elliot, W.J.; Keizer, J. (2018). Assessing water contamination risk from vegetation fires: Challenges, opportunities and a framework for progress. Hydrological Processes Wiley 32: 687–694, https://doi.org/10.1002/hyp.11434.

Pešić, V.; Kostianoy, A.G.; Soloviev, D.M. (2020). The impact of wildfires on the Lake Skadar/Shkodra environment. Ecologica Montenegrina, 37, 51-65, https://doi.org/10.37828/em.2020.37.7.

Robichaud, P.R.; Elliot, W.J.; Pierson, F.B.; Hall, D.E.; Moffet, C.A. (2007). Predicting postfire erosion and mitigation effectiveness with a web-based probabilistic erosion model. Catena 71, 229–241, https://doi.org/10.1016/j.catena.2007.03.003.

Robinne, F-N.; Hallema, D.W.; Bladon, K.D.; Flannigan, M.D.; Boisramé, G.; Bréthaut C.M.; Doerr, S.H.; Baldassarre, G.D.; Gallagher, L.; Hohner, A.K.; Khan, S.J.; Kinoshita, A.M.; Martin, D.; Mordecai, R.; Nunes, J.P.; Nyman., P.; Santín, C.; Sheridan, G.; Stoof, C.R.; Thompson, M.P.; Waddington, J.M.; Wei, Y. (2021). Scientists' warning on extreme wildfire risks to water. Hydrological Processes 35, e14086, https://doi.org/10.1002/hyp.14086.

Sanchez-Garcia, C.; Santín, C; Neris, J.; Sigmund, G; Otero, X.L.; Manley, J.; González-Rodríguez, G.; Belcher, C.; Cerdá, A.; Marcotte A. L. (2023). Chemical characteristics of wildfire ash across the globe and their environmental and socio-economic implications. Environment International 178: 108065, https://doi.org/10.1016/j.envint.2023.108065.

Smith, H.G.; Sheridan, G.J.; Lane, P.; Nyman, P.; Haydon, S. (2011). Wildfire effects on water quality in forest catchments: A review with implications for water supply. Journal of Hydrology 396: 170–192, https://doi.org/10.1016/j.jhydrol.2010.10.043.

Copyright © FirEUrisk Consortium. All rights reserved.